Electrical conductivity experiments on carbon-rich Karoo shales
&
Forward modelling of aeromagnetic data across the Beattie Anomaly

By

Thomas Branch

Submitted in fulfilment of the requirements for the degree of Masters in Science (MSc) to be awarded at the Nelson Mandela Metropolitan University

April 2013

Supervisor: Prof M.J. de Wit

DECLARATION

I, Thomas Cameron Branch (student Number: 198467730), hereby declare that the thesis for Masters Degree in Science (MSc) is my own work and that it has not previously been submitted for assessment or completion of any postgraduate qualification to another University or for another qualification.

_____

Thomas Cameron Branch
2nd April 2013

Official use:
In accordance with Rule G4.6.3,
4.6.3 A treatise/dissertation/thesis must be accompanied by a written declaration on the part of the candidate to the effect that it is his/her own work and that it has not previously been submitted for assessment to another University or for another qualification. However, material from publications by the candidate may be embodied in a treatise/dissertation/thesis.

Electrical conductivity experiments on carbon-rich Karoo shales
&
Forward modelling of aeromagnetic data across the Beattie Anomaly

For a

Masters in Geology

Nelson Mandela Metropolitan University

Prepared by

Thomas Branch

April 2013

Supported by:

Abstract

The Beattie Magnetic Anomaly is the world's longest terrestrial magnetic anomaly with a strike length of over 1000 km and a wavelength in excess of 100 km. Collinear with this is a large belt of elevated crustal conductivities called the Southern Cape Conductive Belt. Historical crustal interpretations proposed a common source of serpentinized ophiolite as an explanation for both the anomalous crustal magnetic susceptibility and electrical conductivities. Spreading between the Western and Eastern Cape of South Africa the mid- to lower crust that hosts these anomalies is obscured by the overlying Cape and Karoo Supergroups.

Between 2003 and 2006, three high resolution geophysical experiments were completed across the surface maximum of the Beattie Magnetic Anomaly (BMA) and the Southern Cape Conductive Belt (SCCB). These included a magnetotelluric (MT) survey and near vertical reflection and wide angle refraction seismic profiles. Within the MT inversion model the SCCB appeared as a composite anomaly, which included a mid-crustal conductor which is spatially associated with the BMA and a laterally continuous upper crustal conductor which is located at depths equivalent to the lower Karoo Supergroup. Subsequently; the upper crustal conductor was identified in northern and eastern extensions of the magnetotelluric profile; a distance in excess of 400 km.

Historical magnetometer and Schlumberger Sounding experiments have previously identified elevated conductivities in the Karoo sequences which were attributed to the Whitehill and Prince Albert formations. These carboniferous, transgressive sediments are known to be conductive from borehole conductivity surveys and direct measurements at surface. In order to constrain the conductive properties of these sediments, impedance spectroscopy (IS) experiments were completed on core samples collected from a historical borehole drilled near to the MT profile. Part One of this thesis presents the results of these experiments, which support the proposition that the Whitehill and Prince Albert Formations are responsible for the laterally continuous, sub-horizontal, upper crustal conductor visible in the MT inversion model. Vitrinite reflectance studies were performed on the same samples by the Montanuniversität, in Leoben, these results corroborate the proposition that elevated organic carbon, of meta-anthracite rank, is the primary conductive phase for the Whitehill and Prince Albert formations.

Part two of this thesis completed forward modelling exercises using historical aeromagnetic data previously collected across the Beattie Magnetic Anomaly. Preliminary models were unable to fit the geometry of any single magnetic model with conductors present in the MT inversion model discounting the proposition that the SCCB and BMA arise from a single crustal unit. Two constrained models were arrived at through an iterative process that sought a best fit between the measured data and the NVR crustal interpretations. The first model, proposes a largely resistive unit which incorporates portions of elevated crustal conductivity; these conductors are spatially correlated to crustal portions also characterised by high seismic reflectivity. The size of this modelled body suggest the likely host of the BMA is an intermediate plutonic terrane, analogous with the Natal sector of the Namaqua Natal Mobile Belt as well as the Heimefrontfjella in Dronning Maud Land, Antarctica, with magnetite hosted within shear zones. This is in agreement with previous studies.

The second model proposes a lower crustal sliver imaged in the NVR data at depths proximal to the Curie Isotherm for magnetite and hematite as the source of the BMA. At these depths geomagnetic properties such as burial magnetisation or thermo-viscous remanent magnetism (TVRM) can potentially be linked to regional scale tectonic processes and can theoretically elevate a body's net magnetic susceptibility. TVRM has been proposed for long wavelength crustal anomalies elsewhere.

Index

LIST OF FIGURES

LIST OF TABLES

Acknowledgements

- This project would not have been possible without the funding and support of the South African National Research Foundation and in particular the INKABA yeAfrica student program.
- I am most grateful to Maarten de Wit for his endless patience with me as well as Oliver Ritter and Ute Weckmann who are thanked for their mentorship. Without their support this project could not have been completed, especially considering the protracted timeframe that was taken.
- Reviews and comments by Jacek Stankiewicz were greatly valued for the earlier drafts of this thesis.
- Branko Corner provided insight and stimulation around the campfire and the Antarctic publications he supplied and advice he gave enriched the magnetic chapter greatly.
- Professor Frank Schilling is thanked for his guidance regarding the impedance spectroscopy at the GFZ.
- In 2005 Mr. David Motloi of the Council for Geoscience supplied coordinates for the southern Karoo boreholes located around the MT-1 survey. This assisted in the selection of borehole SA1/66 for sampling.
- Vitrinite reflectance on the core samples from SA1/66 completed for this thesis and the interpretation of these results was performed by Professor Reinhard Sachenhofer of the Montanuniversität, in Leoben, Austria in 2006. His interpretations and images from his 7 page report were incorporated into this thesis whereby they are quoted as 'Sachenhofer pers com'.
- The more recent modeling exercise completed in 2010 utilized the 2.5D MAG2DC program available as 'freeware' at ftp://ftp.cs.wits.ac.za/pub/general/geophys/. This software is unable to use the profile data generated by WinGLink. The raw data was re-gridded and extracted in a .csv format suitable for MAG2DC by Bravo Mukodzani of *Mineral Services* using available proprietary software; Geosoft, Oasis Montaj.

1. Summary and Introduction

1.1 The Beattie Magnetic Anomaly and the Southern Cape Conductive Belt

The Beattie Magnetic Anomaly (Beattie 1909) and the Southern Cape Conductive Belt (Gough et al. 1973) are two sub-continental scale geophysical anomalies that span the southern tip of South Africa. The sources for the two anomalies remain enigmatic as they are covered by a thick package of Cape and Karoo Supergroup sediments (de Beer & Gough 1980). They are buried at mid- to lower crustal depths in a terrane which is believed to be contemporaneous in age with the Proterozoic Namaqua Natal Mobile Belt (NNMB).

The main southern limb of the Beattie Magnetic Anomaly (BMA) is approximately 1000 km long and stretches between Port St. Jones in the east coast of South Africa (where the anomaly is truncated offshore by the Agulhas Fracture Zone) and in the west it disappears below the Western Branch of the Cape Fold Belt where it appears to split into a duplicated response (black square in Figure 5). With a wavelength in excess of 100 km in and residual field amplitudes of between 250 – 500 nT it is the largest continental magnetic anomaly on earth. Other large amplitude, long wavelength magnetic anomalies, north-east of the main limb of the BMA, share a parallel strike with major tectonostratigraphic terranes within the Natal sector of the Namaqua Natal Mobile Belt (de Beer & Gough 1980, Corner 1989). Collectively; these anomalies are referred to as the “Beattie Set” of magnetic anomalies (Du Plessis and Thomas 1991). The term “Beattie Set” of anomalies is cautiously used here the relationship of the other limbs to main limb is tentative; these anomalies are hosted in magnetically noisy crust, however they share similar geomagnetic character and strike. The surface maximum for the Beattie Set of anomalies and the outline of the Southern Cape Conductive Belt are shown in Figure 1. Interpreting these anomalies as a related set is hesitant

The Southern Cape Conductive Belt (SCCB) is an electrical crustal conductivity anomaly which was first identified by two regional magnetometer array experiments across the southern tip of South Africa (Gough et al. 1973, de Beer & Gough 1980). The magnetometer surveys identified a 150 to 300 km wide mid-crustal belt of high electrical conductivity that stretched between Elands Bay in the Western Cape and Port St. Johns in the Eastern Cape. This belt of anomalous conductivity is spatially correlated to the main limb of the Beattie Anomaly (Figure 1) with the collinear relationship suggesting a common source for both anomalies. In ophiolites, interconnected stringers of magnetite, can form during the transformation of olivine + pyroxene to serpentine + magnetite (Bowen & Tuttle 1949). However; both anomalies do not share a westerly limit, indicating either a different source, or destruction of one of the geophysical properties in the westerly region. Earlier crustal models for this portion of the crust; proposed an accretionary wedge of ophiolite within the mid-crust as a source for both anomalies (de Beer et al. 1982, Pitts et al. 1992, Hälbich et al. 1993).

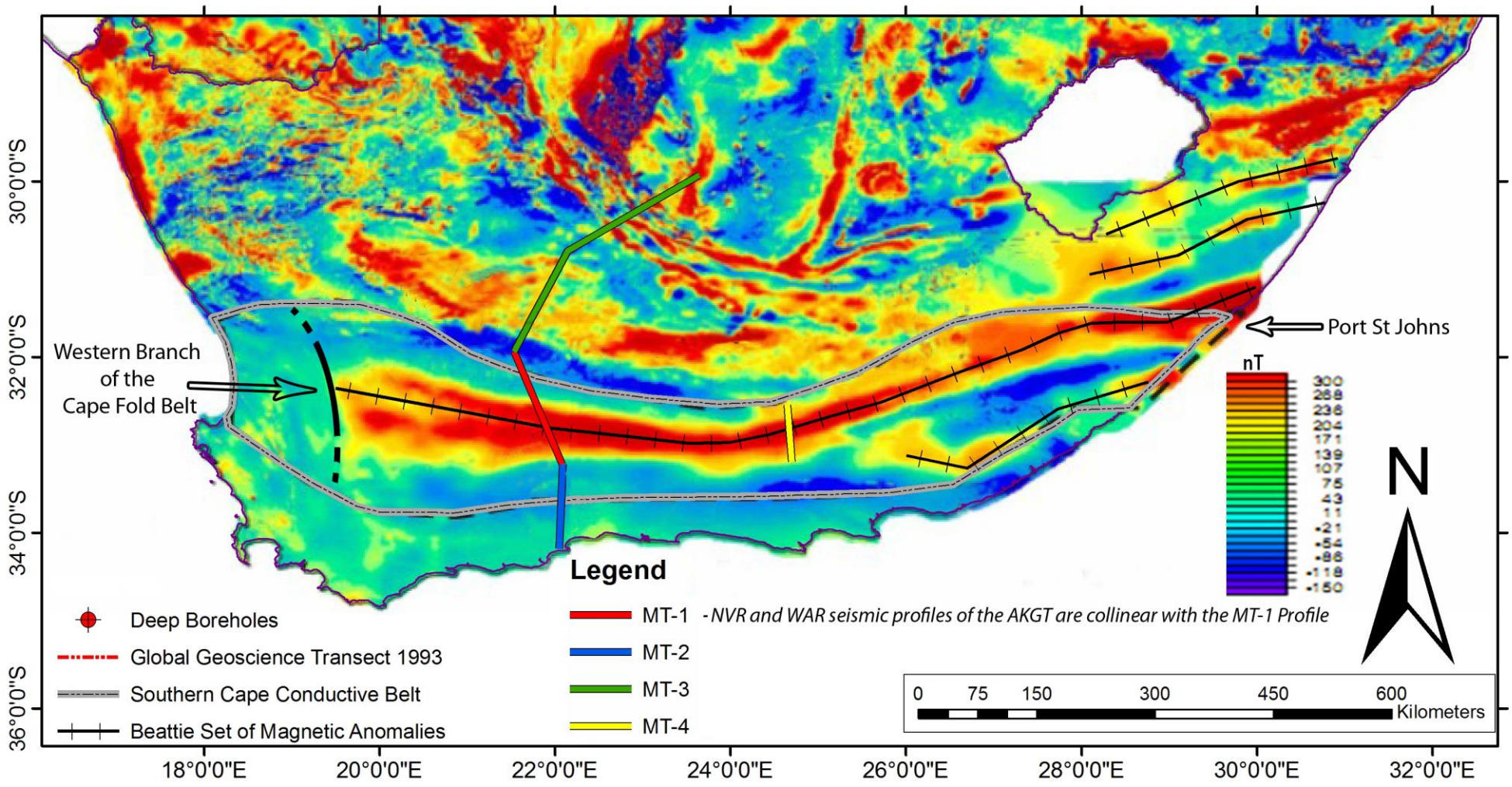

Figure 1: Residual, total-field aeromagnetic data across South Africa. The main limb of the Beattie Magnetic Anomaly is located between Port St. Johns in the east to the Western Branch of the Cape Fold Belt in the west (the Cape Syntaxis). The region of elevated crustal electrical conductivities described as the Southern Cape Conductive Belt as mapped by de Beer & Gough (1980) is outlined with a grey hatched line. The 'Beattie Set' of magnetic anomalies as described by Thomas et al. (1992) are also shown. Total Field magnetic map compiled by Anglo American Corp. Ltd. in the CIGCES database. Magnetic maximums are in red with minimums in blue. Magnetotelluric profiles (MT-1 to -4) of the Agulhas Karoo Geoscience Transect (AKGT) are shown.

1.2 The Agulhas Karoo Geoscience Transect and the BMA and SCCB

More recently; three high-resolution, crustal scale geophysical experiments were completed, between 2003 and 2006, along collinear traverses that crossed the surface maximums of both the SCCB and BMA. These geophysical surveys were part of the Agulhas Karoo Geoscience Transect (AKGT), a multidisciplinary research initiative funded by a South African and German geosciences collaboration called *Inkaba yeAfrica* (De Wit & Horsfied 2007, http://www.inkaba.org/). Work for this thesis was funded directly from the *Inkaba yeAfrica* program. Following publication of the results from the AKGT a revised crustal model, including for the BMA and the SCCB, has been published. This model incorporates new observations and interpretations afforded by the three geophysical experiments (Lindeque and de Wit 2009 and more recently Lindeque et al. 2011).

The three experiments employed across the BMA and the SCCB followed a collinear path with the MT-1 profile which is shown in Figure 1. The experiments were;

- a 150 km long high resolution magnetotelluric (MT-1) profile (Weckmann et al. 2007[a]) which provided an electrical conductivity model for the crust to a 30 km depth
- a 165 km long Wide Angle Reflection Refraction seismic profile (WRR) (Stankiewicz et al. 2007) which provided a seismic velocity model to 40 km depth
- a 100 km long Near Vertical Reflection (NVR) seismics (Lindeque et al. 2007) which provided a seismic reflectivity model to 50 km depth.

Work for this thesis first began with my involvement with Dr. Oliver Ritter and Dr. Ute Weckmann of the Magnetotellurics Deep Sounding group from the GeoForschungZentrum (GFZ) during the implementation of the MT-1 profile across the BMA. The data was collected from 82 stations installed across the profile during a 4 week field program in the Great Karoo semi-desert of the Western Cape in 2004. Inversion models generated from this data were published in 2007 and showed that the SCCB may be a composite anomaly representing potentially three crustal regions of elevated conductivity (Weckmann et al. 2007[a]).

The most laterally consistent conductor in the MT model was a thin, sub-horizontal conductor, located within the upper 5km of the crust. This conductor is shown with an undulating sub-horizontal dashed line between 1 and 5 km depth in Figure 2. These depths are known from historical oil exploration drilling programs by SOEKOR, to host the sediments of the Karoo Supergroup which are approximately subhorizontal and well exposed at surface along the MT-1 profile.

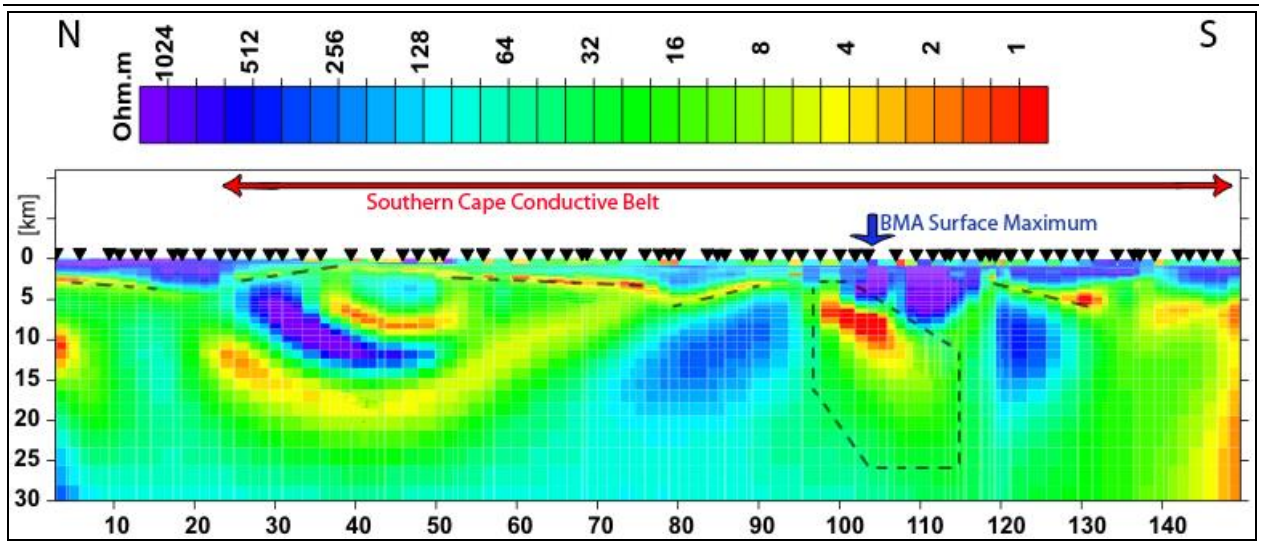

Figure 2: 2D inversion model showing electrical conductivity for the MT-1 magnetotelluric profile across the Beattie Magnetic Anomaly and the Southern Cape Conductive Belt (Image annotated from Weckmann et al. 2007$_a$).

The Karoo Supergroup in the Western Cape is dominated by terrestrial and marine sediments. The lower units are comprised of the carboniferous black shales of the Prince Albert and Whitehill Formations. Due to the elevated total organic carbon content (TOC) these formations were targeted by SOEKOR's oil exploration program in the early 1970's. Resistivity logs from holes drilled during this exploration program identified elevated electrical conductivities within these formations and show them as being located at depths that correlate to the sub-horizontal conductor present in the MT-1 inversion model.

The initial correlation between resistivity results for the Whitehill and Prince Albert Formations from the SOEKOR drilling and the conductor in the MT-1 profile was made by Prof. Maarten de Wit in 2004 following release of preliminary models from the inversion of the MT data. To investigate the electrical properties of the Whitehill and Prince Albert formations and to test the interpretation that they could be responsible for the upper crustal conductor visible in the MT model, I collected representative core samples from the Council for Geoscience Core Library in Pretoria, South Africa. To constrain their electrical conductivity and dielectric properties; impedance spectroscopy was performed on these samples at the GeoForschungZentrum (GFZ), in Potsdam, Germany, under the supervision of Prof. Frank Schilling. Vitrinite reflectance analyses were completed for the same samples by Prof. R.J. Sachenhofer, Montanuniversität, Leoben Austria to obtain further information regarding the rank and physical properties of the organic carbon within the samples. The reflectance data supports the interpretation that organic carbon is the primary conducting phase in the samples with pyrite an accessory phase to charge transport. The most carboniferous of the samples had sufficiently elevated electrical conductivities to explain the upper crustal conductor within the MT-1 model (Branch et al. 2007). Section One of this thesis presents the results from this work.

Section Two of this thesis targeted another conductor present at mid-crustal depths in the MT-1 model. The conductor is shown in Figure 2 as enclosed in a dashed polygon between 5 and 25 km depths in the southern portion of the MT-1 inversion model located beneath the surface maximum of the BMA. This portion of the crust is known from previous aeromagnetic modelling exercises published for the BMA as the crustal terrane most likely to host the BMA (Pitts et al. 1992). In contrast to the upper crustal conductor located within the Karoo, no borehole drilling exists at these depths and since the BMA is covered entirely by younger stratigraphy, its interpretation is restricted to geophysical methods such as the experiments of the AKGT. To complement the results from the MT-1 magnetotelluric inversion model; aeromagnetic data was obtained for this thesis along the same profile as that traversed by the MT-1, WRR and NVR surveys. 2D Modelling of the total field aeromagnetic data is a non-unique forward modelling method, whereby a theoretically infinite number of models can reproduce a measured field. However; modelling of the aeromagnetic data was able to be constrained by the interpreted crustal sections generated from the three AKGT geophysical experiments. During this exercise the supposition that the BMA and the SCCB have a common source was tested. Additionally; basic inferences were made regarding potential geometries such as length and volumes required to fit the 100 km wavelength of the BMA. These modelling exercises are presented and discussed in Section Two of this thesis.

2. The Regional Geology of the Agulhas Karoo Geoscience Transect

Geographically, the southern limit of the magnetotelluric profile, MT-1, is located 110 km inland of the Atlantic coastal town of Mossel Bay (Figure 3). The profile starts at the inland base of the Cape Fold Belt (CFB) and strikes NNW in the rain shadow of the CFB through the relatively flat semi-desert of the Great Karoo and across the surface maximum of the BMA. Approximately 130km north of Prince Albert the profile climbs the Great Escarpment of South Africa and ends 20km further north outside the town of Fraserburg, with a total distance of 150km.

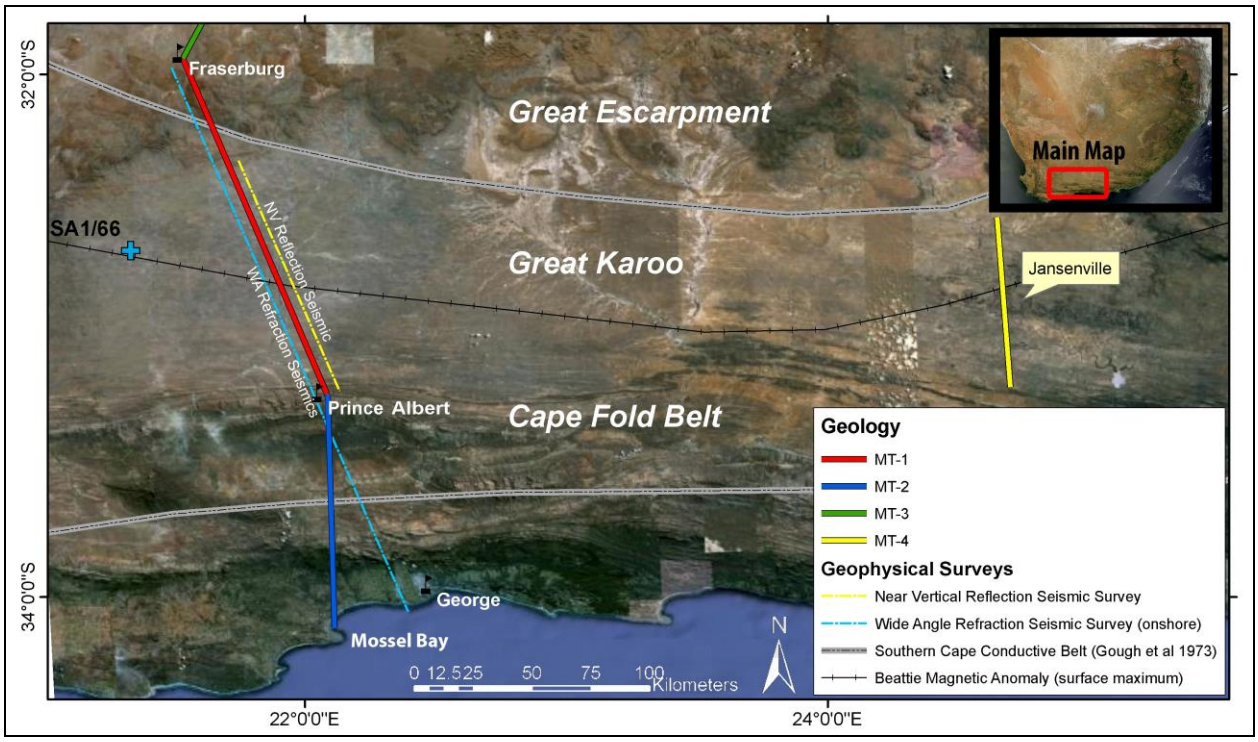

Figure 3: Location of the onshore geophysical surveys of the Agulhas Karoo Geoscience Transect (Image from Google Earth).

The local geology that influences the MT-1 profile can broadly be divided between:

1) The Palaeozoic to Mesozoic Cape and Karoo Supergroups that are well exposed at surface along the entire length of the profile, and
2) The unexposed basement that underlies these Supergroups and inferred to be Proterozoic in age and part of the Namaqua Natal Mobile Belt (NNMB).

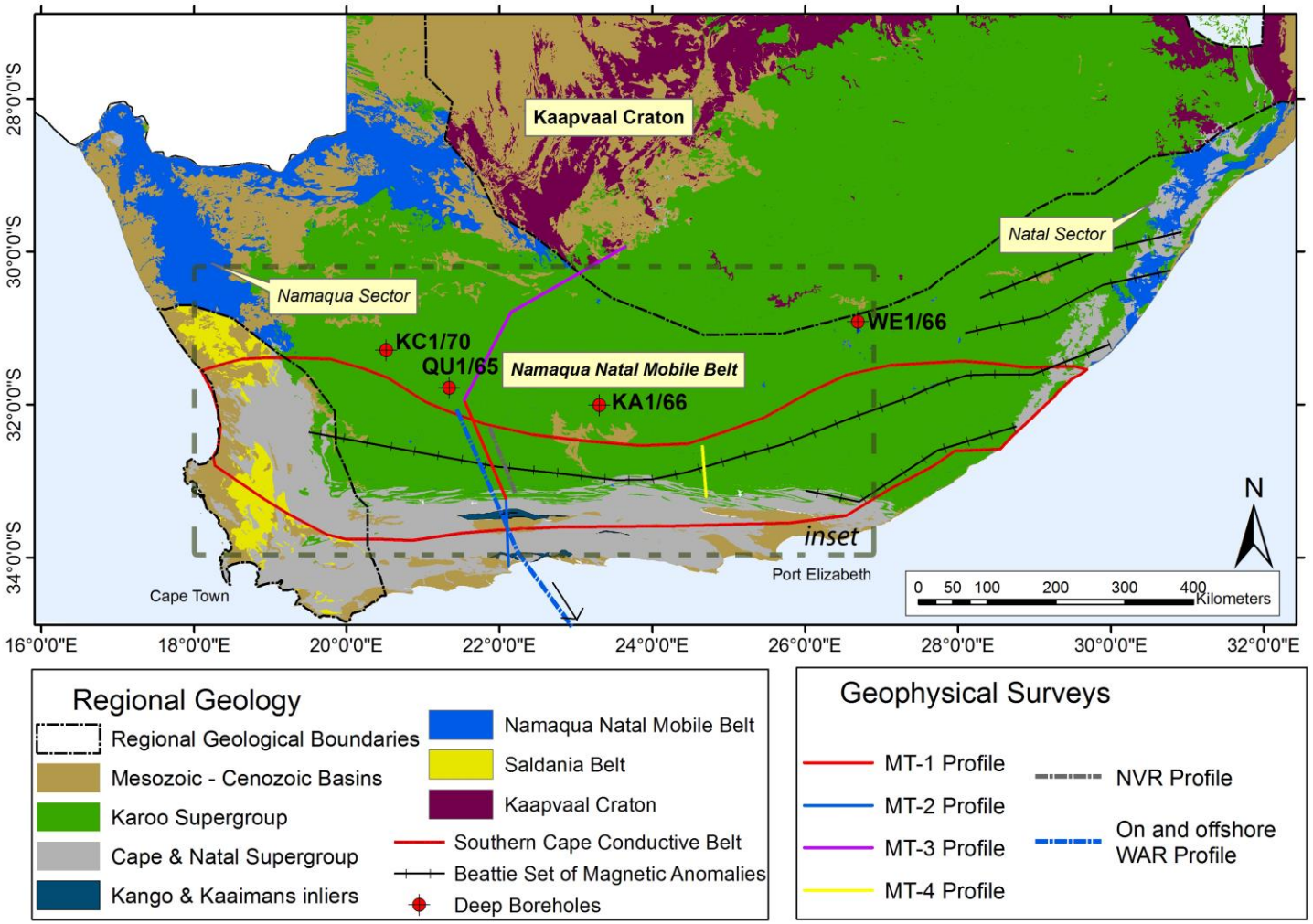

Figure 4: Approximate regional geological boundaries for the onshore portion of the Agulhas Geoscience Transect. All three geophysical experiments were approximately collinear across the BMA and the SCCB. They are displayed above as separate for clarity. Deep boreholes analysed by Eglington & Armstrong (2003) are annotated with red circles. Map generated from 1:1 000 000 South African Geology shapefile, with Regional Geological Boundaries adapted from Eglington (2006).

2.1 Inferred Geology of the Basement: Proterozoic Namaqua Natal

The basement hosting the BMA is interpreted regionally as being contemporaneous with the Proterozoic-aged Namaqua Natal Mobile Belt (NNMB) which spans the breadth of South Africa. The NNMB is well exposed at its western (Namaqua) and eastern (Natal) sectors, however these lie approximately 400 km to north-west and 1000 km to north-east of the MT-1 profile (Figure 2).

However; the nearest direct evidence for the NNMB below the MT-1 profile are granitic samples collected from historical borehole (QU1/65) at a depth of 2493 m. This hole is located approximately 30 km to the north-west of the profile, and along with three other holes (KC1/70, KA1/66, WE1/66) have penetrated the Cape and Karoo cover and intersected rocks equivalent in age with the NNMB (Eglington & Armstrong 2003). The locations for these boreholes are shown in Figure 4.

Whole rock Sm-Nd model dates for the granitic samples from these holes were between 2.4 and 1.2 Ga. These ages contrast those of the Natal Sector of the NNMB where Palaeoproterozoic ages are entirely absent. As a result Eglington & Armstrong (2003) interpret the samples from these holes as contemporaneous with the Namaqua sector of the NNMB and identified isotopic similarities with the Bushmanland Sub-Province of Namaqualand. Summary details for these samples are tabulated below in Table 2-1.

Table 2-1: Summary details for whole rock samples collected from boreholes studied by Eglington & Armstrong (2003).

Borehole	QU 1/65	QU 1/65	KA 1/66	KC 1/70	WE 1/66
Depth (m)	2493	2993	2579	6005	3735
Lithology	Megacrystic Granite	Biotite granodiorite gneiss	Dark grey microporphyry	Granitoid gneiss	Biotite gneiss
Model Age (Ma)	1199 ±116	2326 ±87	2427 ±96	1162 ±130	2307 ±126

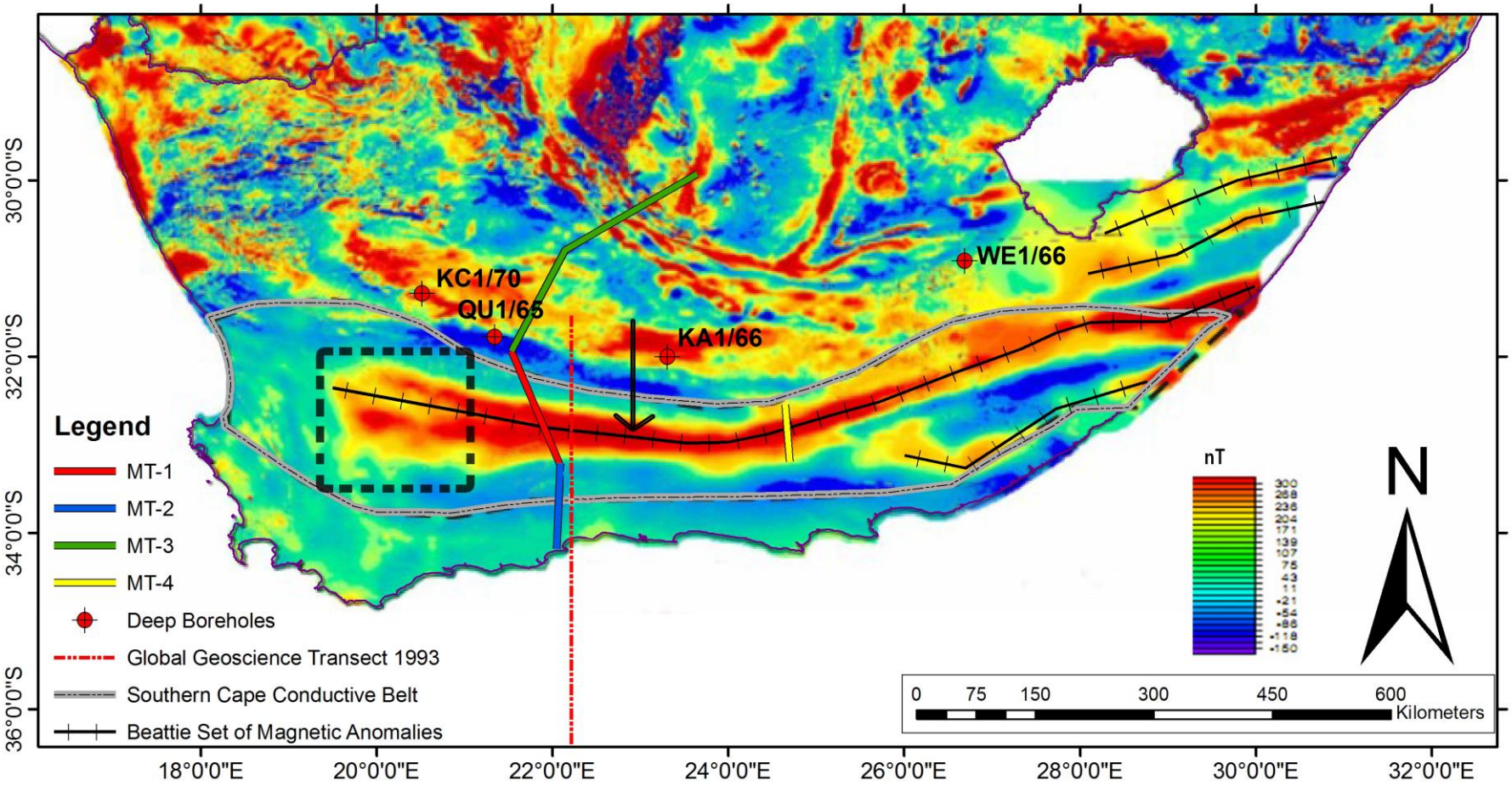

Figure 5: Regional aeromagnetic data (residual total field) for South Africa. Black arrow indicates surface maximum for the main limb of the BMA with location of deep boreholes analysed by Eglington & Armstrong (2003) annotated with red circles. All boreholes lie north of the BMA and north of their inferred terrane boundary that must separate the Natal and Namaqua sectors of the NNMB. Additional NE-SW striking collinear long wavelength anomalies as described by Thomas et al. (1992) are shown (Beattie set of anomalies). Total Field magnetic map compiled by Anglo American Corp. Ltd. from the CIGCES database. Magnetic maximums in red with minimums in blue.

Previously; the most comprehensive regional interpretation for the crustal basement hosting the BMA and the SCCB in the vicinity of the MT-1 profile was the Global Geoscience Transect. This crustal model proposed a suite of southerly dipping mid-crustal units. Within the mid-crust, dipping between 10 and 30 km depth and with a horizontal extent over 70 km in length a serpentinized, ophiolitic wedge was proposed as the source of the BMA and SCCB located within a Neoproterozoic suture zone (Pitts et al. 1992, Hälbich et al. 1993). However; this crustal interpretation for the mid-crust, which hosts the BMA, interpreted the crustal fabric as southerly dipping (Lindeque et al. 2011).

Both the Natal and Namaqua sectors of the NNMB have experienced a common Kibaran tectonothermal history, however they are formed from the accretion of isotopically distinct terranes. These terranes were accreted against the western and southern margins of the Kaapvaal craton during a period of oblique collision (Nicolaysen and Burger 1965, Jacobs et al. 1993, Thomas et al. 1994). This orogeny took place along a 1400 km long and 400 km wide arcuate orogenic belt, commencing at the Kaapvaal's western cratonic margin and wrapping around to its south-eastern boundary between ± 1200 to 1000 Ma (Jacobs and Thomas 1994, Cornel et al. 2006).

The Namaqua sector of the NNMB is a polymetamorphic complex, composed of five main stratigraphic units (Cornel et al. 2006) comprised of:

1. The Richtersveld Subprovince:- which consists of 2.0 – 1.8 Ga high grade supracrustals, represented by a small remanent of Kheisian crust intruded by granites at 1.0 Ga, but without a pervasive Namaquan-aged fabric.
2. The Bushmanland Terrane:- consists of 2.0 – 1.8 Ga high grade metasediments and intercalated mafic and felsic metavolcanics with 2.0 Ga granitic gneisses and 1.2 Ga to 1.6 Ga high grade supracrustals. These are intruded by 1.0 Ga Namaquan syntectonic granitoids with associated tectonic fabrics regionally. The paragneisses of the Bushmanland Terrane are well known as they contain world-class stratabound base metal ore deposits (Thomas et al. 1994).
3. The Kakamas Terrane:- consists of 2.0 Ga supracrustals and Namaquan-aged granitoids and associated tectonic fabrics.
4. The Areachap Terrane:- consists of juvenile, arc-related 1.3 Ga supracrustal amphibolites and calc-silicate rich rocks. The terrane has a pervasive Namaquan fabric and is intruded by ubiquitous granitoids.
5. The Kaaien Terrane:- consists of Keisian metaquartzites and early volcano-sedimentary rocks with some high temperature and low pressure bimodal metavolcanics.

The Natal sector of the NNMB comprises three major tectono-stratigraphic units which were obducted against the Kaapvaal craton during a period of subhorizontal, compressional tectonics and crustal thickening. These units are:

1. The mafic to ultramafic Tugela Terrane which is the northernmost terrane of the Natal Belt and is interpreted to be an oceanic crust/island arc sequence. It is thrust forward onto the southern flank of the Kaapvaal Craton and consists of layered amphibolites, serpentinites and quartzo-feldspathic gneisses aged at 1200 Ma. Plagiogranites and ultramafic complexes intruded into these sequences at 1050 Ma (Jacobs et al. 1993).
2. The Mzumbe Terrane and the 3) Margate Terrane are interpreted as magmatic arc packages. They consist of supracrustal gneisses and felsic to mafic metavolcanic gneisses and paragneisses (Jacobs et al. 1993). Again these are intruded by significant volumes of syntectonic granitoids, charnockites and quartz monzonites between 1050 to 1110 Ma (Eglington 2006).

2.2 The Geology of the Cape and Karoo Supergroups

In contrast to the inferred basement of the MT-1 profile, the Carboniferous-Jurassic Karroo sediments are well exposed at surface for the entire 150km length of the profile (Figure 6). In the north portion of the profile, the Karoo Supergroup is known from borehole data to directly overly the NNMB basement (Eglington & Armstrong 2003) and is approximately 3-4 km thick. However; towards the south of the profile the Karoo is firstly underlain by the Cape Supergroup (SOEKOR log CR 1/68). Here, the Cape Supergroup is shown by Hälbich et al. (1993) to lie disconformably over the basement. This interpretation is based on results from a single SOEKOR seismic profile shot near to the MT-1 profile (Fatti and du Toit, 1970). In the southern portion of the MT-1 profile the Cape and Karoo sequences are known from borehole data to become increasingly thicker, deeper and from surface mapping are more deformed as they approach the exposed Cape Fold Belt mountain range. Adjacent to the belt, the Cape and Karoo sequences are incorporated in a series of northward direct trusts and overfolds (Newton 1992) associated with the Cape Orogeny which began at 250 Ma (Cole 1992). Immediately south of the MT-1 profile the Cape Supergroup continues to be well exposed throughout the Cape Fold Belt mountain range from west to east between Cape Town and Port Elizabeth respectively, a distance of nearly 1000 km.

Prior to their involvement in the Cape Orogeny, the argillaceous sediments of the Cape Supergroup were deposited within the Cape Basin during the Palaeozoic. The basal units are represented by the cratonic sheet sandstones of the Table Mountain Group. These are overlain by the deltaic and fossiliferous shales and feldspathic sandstones of the Bokkeveld Group. Towards the end of the Cape Basin's evolution the predominantly subfeldspathic and sublithic arenites, orthozquartzites and mudrocks of the Witteberg Group represent both marine and freshwater environments (Broquet 1992). The exact lithostratigraphy, thicknesses and ages of the sedimentary units of the Cape Supergroup are poorly constrained. This is due to a distinct lack of fossils in the quartzites, and the elimination of pelitic marker-bed during thrusting and tectonism as

well as duplication of units during the Cape Orogeny between 278 and 230 Ma (Shone and Booth 2005).

The Cape Basin is superseded by the Karoo retroarc foreland basin in the Late Carboniferous. The initial Karoo Basin occupied much of southwestern Gondwana (Visser 1987) and its southern portion is thought to have developed ahead of the advancing Cape orogenic front from the present-south (Cole 1992). The basal sediments of the Dwyka Group were deposited disconformably over the Cape Supergroup and are represented by glacial diamictites, debris-flows and marine suspended muds and silts.

The Dwyka Group was then followed by the Lower Ecca Group's Prince Albert and Whitehill Formations. These are represented by marine transgressive and lacustrine, carboniferous to graphitic shales with interbedded cherty bands. The shales likely formed by suspension load settling within a predominantly reducing, anoxic environment between 280 and 270 Ma (Catuneananu 2004, Cole & McLachlan 1994). The shales are relatively iron-rich, with pyritic stringers reportedly common particularly within the Whitehill Formation (SOEKOR CR1/68). In outcrop; the Whitehilll Formation (previously known as the White Band) weathers white due to the oxidation of this pyrite to gypsum sulphate (Cole & McLachlan 1994).

Due to the anoxic nature of their deposition, the mudstones have elevated contents of Total Organic Carbon (TOC). TOC values for these shales range between 5.1 and 14.8 % and the southern facies of the Whitehill and Prince Albert Formations (in the vicinity of the MT-1 profile) typically have a 3 % higher average TOC, due to the lack of gasification effects associated with the Jurassic-aged dolerite swarm that intruded the Karoo north of the Great Escarpment (Cole & McLachlan 1994). The Prince Albert and Whitehill Formation are synchronous with the Vryheid and Volksrust Formations further north. These northern facies contain world class coking coal reserves which have been economically extracted since the 1920's (Cole & McLachlan 1994).

Overall the metamorphic grade is low for both the Prince Albert and Whitehill Formations (prehnite-pumpellyite to greenschist facies), however a prolonged thermal overprint and lack of reservoir porosity within the overlying quartzitic units inhibited the formation of oil reserves economically exploitable in the 1970's and SOEKOR ceased their exploration program.

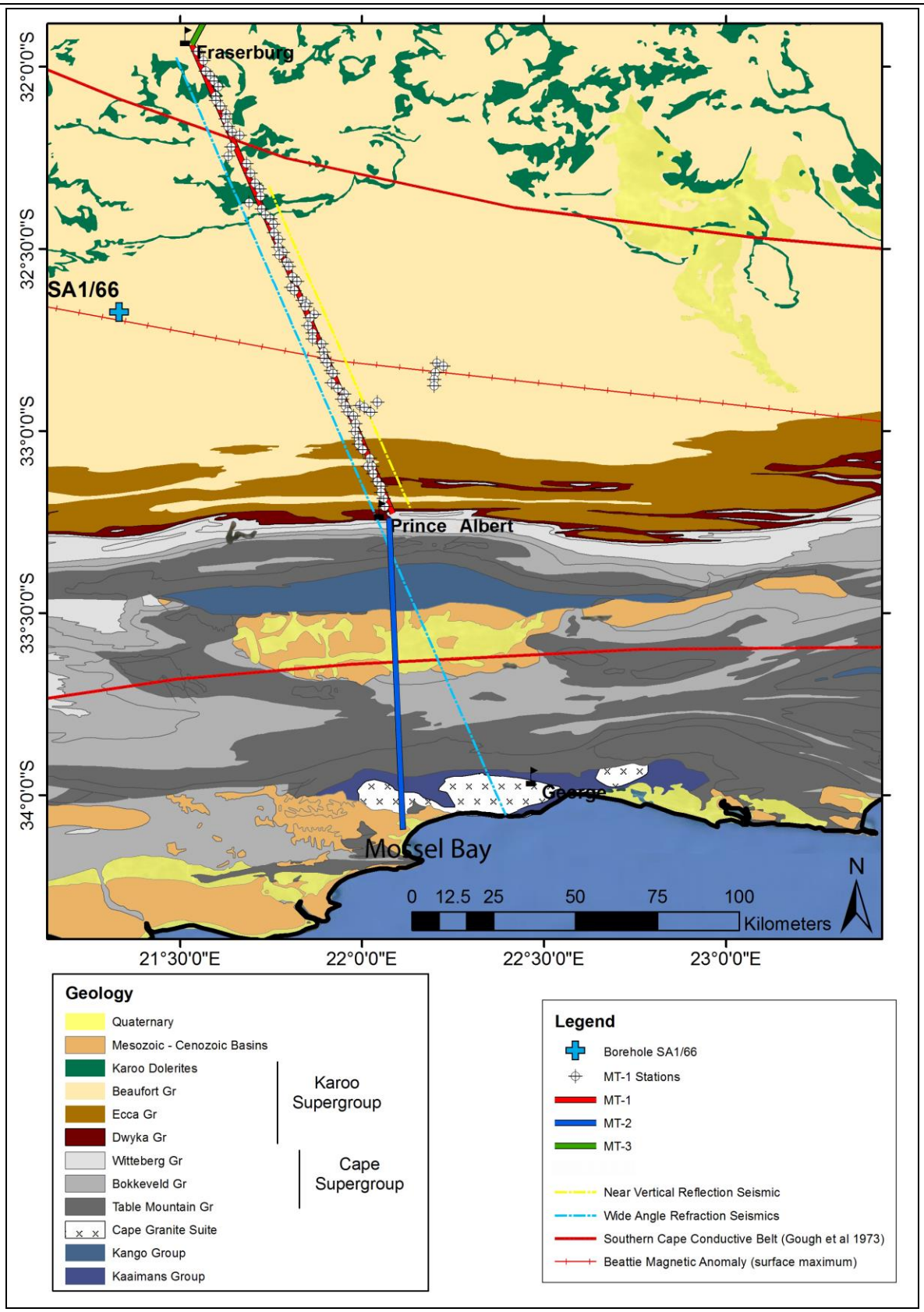

Figure 6: Detailed geological map for the MT-1 portion of the AKGT profile. The map was generated in GIS software package using a Council for Geoscience shape file.

Moving upwards in the stratigraphic column, the Upper Ecca is dominated by fluvio-deltaic sands in the north-eastern part of the basin while in the south of the basin these become submarine fans and turbiditic sandstones, deposited from the south into the

southern portion of the Karoo Basin. By the Late Permian and Triassic, the environment of the Karoo Basin becomes dominated by the channel and lacustrine sediments of the Beaufort Group, Molteno and Elliot Formation exposed in northern and eastern South Africa. Subsequent desertification resulted in the fine-grained Aeolian sands of the Clarens Formation during the early Jurassic. The Karoo Supergroup ends with the outpouring of the continental Drakensberg Group flood basalts and ubiquitous doleritic intrusions (Johnson et al. 1997); a precursor to the breakup of Gondwana.

A stratigraphic column is presented below in Table 2-2 using average thicknesses for the South Western Province (west of 24°). These thicknesses are taken from Cloetingh et al. (1992) and references therein.

Table 2-2. Summary stratigraphy for the Cape and Karoo Supergroups for the the South Western Province (west of 24°). Stratigraphic location of Whitehill and Prince Albert Formations shown. Thicknesses are taken from Cloetingh et al. (1992) and references therein. Unit thicknesses are approximately to scale.

Age	Supergroup	Group	Thickness (m)	Formation/ Subgroup	Thickness (m)
	Karoo Supergroup	Beaufourt Group	3390	Teekloof Fm.	1030
				Abrahamskraal Fm.	1280
230 Ma					
		Ecca Group		Waterford Fm.	180
275 Ma				Fort Brown Fm.	500
				Laingsburg Fm.	400
270 Ma			300	Vischkuil Fm	300
295 Ma					
		Dwyka Group	660	Elandsvlei Fm.	660
300 Ma					
360 Ma	Cape Supergroup	Witteberg Group	1100	Lake Menz Sub-Grp.	500
375 Ma				Weltevrede Sub-grp.	600
		Bokkeveld Group	1165	Bidouw Sub-Grp	540
				Ceres Sub-Grp.	625
438 Ma		Table Mountain Group	3345	Nardouw Sub-Grp.	555
				Peninsula Fm.	1550
				Graafwater Fm.	440
500 Ma				Piekenierskloof Fm.	800

Collingham Fm. (30m)
Whitehill Fm. (50m)
Prince Albert Fm. (180m)
Cederberg Fm. (120)
Pakhuis Fm (40m)

Intercalated sandstones, mudstones and shales

Carbon-rich mudstones

Glacial sediments, diamictites and mudstones

Dominated by argillaceous sandstones with intercalated shales

3. Agulhas Karoo Geoscience Transect: Results and Discussion

The three onshore AKGT geophysical experiments are the most integrated, multidisciplinary crustal survey completed across the BMA and the SCCB. All publications for these and other *Inkaba yeAfrica* studies are available online at *www.inkaba.org.* The three sectional models for the MT-1, NVR and WRR seismic profiles are displayed in Figure 7. Based on the results from the AKGT an updated crustal section interpretation was published by Lindeque and de Wit (2009) and more recently by Lindeque et al. (2011) which incorporated dominant reflector geometries in the Near Vertical Reflection (NVR) profile.

Within the Near Vertical Reflection Seimic profile (Figure 7ii), Lindeque et al. (2007) interpret a mid-crust dominated by south verging, reflectors dipping north at approximately 20 degrees (points **A** – **C)**. This is significant as it is in contrast to previous crustal model interpretations which consisted of a mid-crust composed of south dipping units (Hälbich et al. 1993). Below the surface maximum of the BMA, Lindeque et al. (2011) identified an approximately 10 km wide mid crustal unit of high reflectivity located between the depths of 7-15 km (**B**). This unit correlates with a zone of contrasting high and low seismic velocities in the Wide Angle Refraction seismic profile model published by Stankiewicz et al. (2007); annotated **F** and **G** respectively in Figure 7iii. This portion of the magnetotelluric profile hosted a unit of elevated electrical conductivities annotated by **H** in Figure 7i. This mid-crustal conductor identified in the MT-1 model dips southwards between 5 and 15km depth, below which it becomes poorly resolved (Weckmann et al. 2007[a]), The width of this structure is only a few (+/- 2km) and is mainly controlled by the regularisation of the inversion algorithm. The anomaly's dip is well constrained by the inversion but the exact shape and depth is less well constrained. Additionally the diffuse conductor annotated by **J** is believed to be a boundary effect in the inversion model, where the conductive metasediments of the Kango and Kaaimans group inliers to the south of the MT-1 profile are 'sensed' at longer periods by the its stations and are attempted to be fitted in the vertical section inversion model (Weckmann pers comm).

Initial magnetic models for this thesis were generated in 2007 (Weckmann & Branch 2007, Weckmann et al. 2007[b]) and assumed a southerly-dipping mid-crustal fabric as published by Hälbich et al. (1993). However; following the publication of the NVR crustal model, new magnetic modelling exercises for this thesis were completed to incorporate a northerly dipping crustal fabric and are presented in Section two of this thesis.

Shallower structures identified in the AKGT profiles include a distinct seismic unconformity at the base of the Cape and Karoo Supergroups visible in the NVR model (**C** in Figure 7iii). This is interpreted by Lindeque et al. (2007) as an erosional peneplain

separating the Cape sequences with the NNMB basement (Lindeque et al. 2011). Above this, the Cape and Karoo Supergroups are seen dipping gently south in the northern part of the NVR model but deformation intensity visibly increases towards south in agreement with structural outcrop studies near Prince Albert (Newton 1992). In the NVR data the Karoo units are disrupted by low angle thrusts, rooted in local decollements located within the lower Ecca Group (Lindeque et al. 2011): (**D** in Figure 7i).

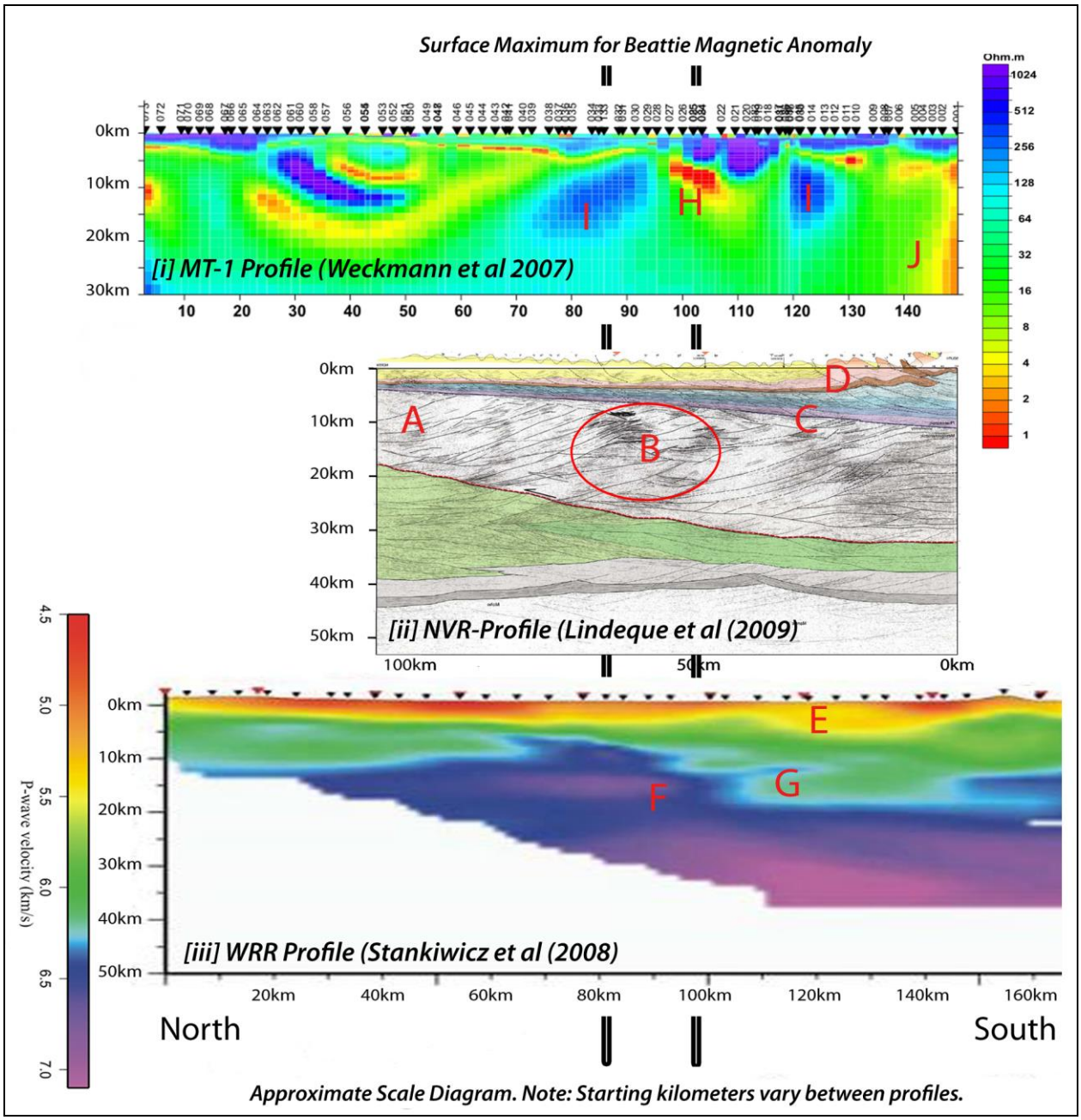

Figure 7: Aligned AKGT geophysical experimental results across the BMA and the SCCB. i) MT-1 geoelectric model (Weckmann et al. 2007[b]). ii) NVR seismic reflection model with proposed crustal divisions from Lindeque & de Wit (2009), iii) WRR P-wave velocity model (Stankiewicz et al. 2008). Surface locations of BMA maximums shown at top of image.

The Cape and Karoo sediments are also visible within the P-wave velocity model as a clearly defined thin upper crustal layer <7 km thick of low seismic velocities between 4.6

- 5.3 km/s (**E** in Figure 7iv). A Vp/Vs model derived from a tomographic inversion of the 'first breaks' provided a velocity model for the upper 1 km that accurately correlated with the Karoo lithologies as mapped at surface (Bräuer et al. 2007).

The increase in depth and structural complexity in the Cape and Karoo sequences in the south of the profile is also evident in the MT-1 inversion model. This is exemplified by the laterally continuous, sub-horizontal conductor (proposed to be the basal, carboniferous lower Karoo units). In the south of the MT-1 profile this conductor becomes partly discontinuous, increasing in depth and dipping more steeply to the south.

In 2006, a northern extension of the MT-1 profile (profile MT-3) of approximately 300 km and in 2005 an eastern MT profile across the BMA of approximately 50 km (profile MT-4) were completed. Inversion models for the upper crust from these additional MT profiles were compiled together in a single image (Figure 8) and showed the lateral continuity of the inferred Karoo conductor (Branch et al. 2007). This conductor was located at depths that equated to the Lower Karoo Supergroup as inferred from regional borehole data (Weckmann et al. 2007[a], Branch et al. 2007).

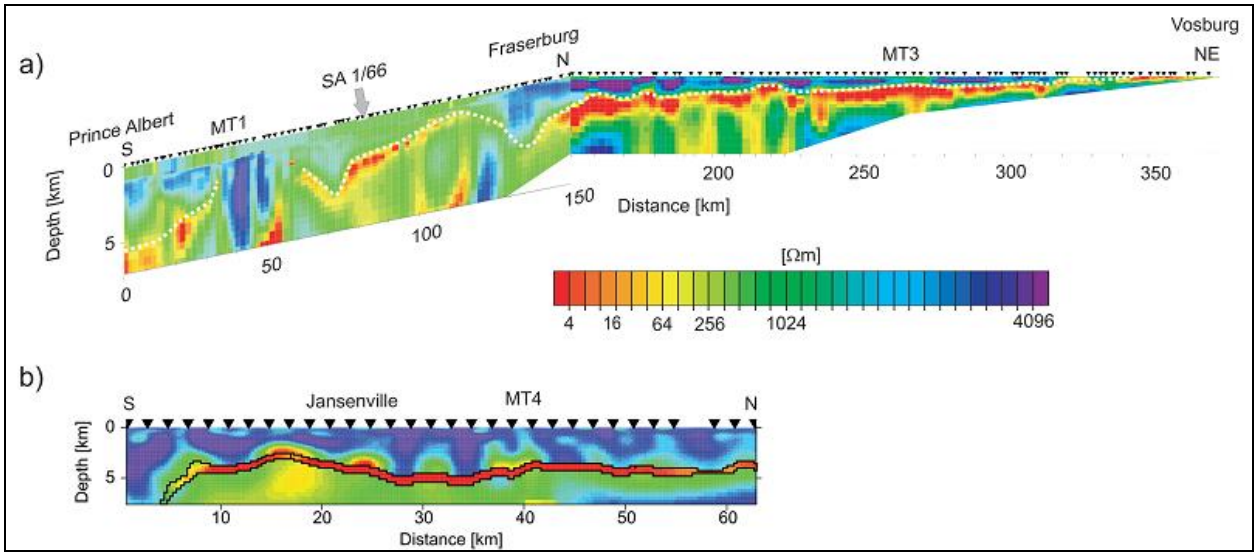

Figure 8: Lateral continuity of a subhorizontal upper crustal conductor within MT profiles 1, 3 and 4 (image from Branch et al. 2007).

More recently a comparison of borehole log depths for the Whitehill Formation was made with both archive seismic data collected by SOEKOR and with the NVR results Lindeque et al. (2011). In the SOEKOR exploration reports the Whitehill Formation's consistent seismic reflectivity lead it to being referred to as 'Old Faithfull' (Fatti and du Toit 1970). The comparison undertaken by Lindeque et al. (2011) showed strong correlations between prominent reflectors in the NVR data and the transition between the Whitehill Formation and the Dwyka Group and also corresponds with the conductor present in the MT-1 profile (Lindeque et al. 2011).

4. SECTION ONE – Impedance Spectroscopy for Lower Karoo, Permo-Carboniferous shales

4.1 Introduction

High electrical conductivities in the Whitehill and Prince Albert Formations were first identified from down-hole resistivity surveys collected from boreholes drilled by SOEKOR. These elevated conductivities were also supported by measurements take at outcrop along the Meiringspoort national road near Beaufort West (SOEKOR Log KW1/67). Subsequent to this, the influence of these formations to the regional crustal conductivities identified by the magnetometer surveys of Gough et al. (1973) and de Beer & Gough (1980) was described based on results from Schlumberger sounding experiments undertaken by van Zijl (1979) which identified the Whitehill and Prince Albert Formations as regionally persistent conductors. Following this a review of old DC electrical sounding data by Van Zijl (2006) constrained the bulk resistivities in Whitehill Formation to values approaching 1 Ωm. In the inversion model completed by Weckmann et al. (2007[a]) elevated conductivities in the upper crust were modelled at depths varying between 8 km depth (adjacent to the Cape Fold Belt) to between 5 and 2.5 km depth in the mid and north of the profile.

In order to test whether the Whitehill and Prince Albert Formations could be responsible for this conductor, core from SOEKOR boreholes drilled near profile MT-1 was located at the National Core Library operated by the South African Council for Geoscience's (CGS) in Donkershoek, Pretoria (www.geoscience.org.za). Collar locations and summary logs were checked prior to sampling (Table 4-1) and borehole SA1/66 chosen due to its proximity to the MT-1 profile, and as it contained a full intersection of the carboniferous Whitehill and Prince Albert shales at depths that correlated to the conductor in the MT inversion model. The collar coordinates for this borehole are E21.333, S32.674 (WGS1984, decimal degree).

In late 2004, the core from SA1/66 was laid out at the CGS warehouse and shale samples selected between 2789 and 2874 meters depth. Sampling targeted units with visibly elevated TOC and/or with evidence of alternative conducting phases such as pyrite. These samples were split onsite and packaged for transportation to the GeoForschungZentrum (GFZ), Potsdam.

At the GFZ, four samples were chosen to represent the typical carbonaceous, lower Karoo units visible in the core. Brief descriptions for each sample are presented in Table 4-2 along with photographs for each sample in Figure 9. More detailed petrographic descriptions are given for each sample in a vitrinite reflectance study that was commissioned for this thesis. The detailed petrographic descriptions and images are included within the Appendix 1.

Table 4-1: Summary logs for boreholes intersecting the Whitehill and Prince Albert Formations near the MT-1 study area (taken from SOEKOR logs).

SA 1/66		
From	To	Lithology
0	457	Beaufort
457	1280	Upper Ecca
1280	2743	Lower Ecca
2743	2842	Whitehill Formation
2842	3100	Dwyka Tillite (to EOH)

KA 1/66		
From	To	Lithology
0	884	Beaufort
884	1545	Upper Ecca
1545	2083	Lower Ecca
2083	2155	Whitehill Formation
2155	2531	Dwyka Tillite
2531	2601	Basement Gneiss (to EOH)

KW 1/67		
From	To	Lithology
0	2885	Beaufort
2855	3676	Upper Ecca
3676	4360	Lower Ecca
4360	4543	Whitehill Formation
4543	5555	Dwyka Tillite (to EOH)

CR 1/68		
From	To	Lithology
0	1295	Upper Beaufort
1295	2118	Lower Beaufort
2118	3658	Ecca
3658	3780	Whitehill Formation
3780	4267	Dwyka Tillite
4267	4542	Bokkeveld
4542	4877	Table Mountain (to EOH)

KL 1/65		
From	To	Lithology
0	3292	Beaufort & Ecca
3292	3429	Whitehill Formation
3429	?	Dwyka (no complete log)

Table 4-2: Summary descriptions for core samples collected from borehole SA1/66 (SOEKOR SA1/66)

Sample	Depth (m)	Formation	Lithology
Sample 1	2789	Whitehill Formation	Laminated, fragile, carbonaceous black shale. Trace pyrite and possible limonite relics visible as iron oxidation.
Sample 2	2817	Prince Albert Formation	Laminated black shale with pervasive and irregular calcite veins.
Sample 3	2863	Prince Albert Formation	Massive grey-black mudstone. Single layer with a high proportion (>30 modal %) disseminated pyrite.
Sample 4	2874	Prince Albert Formation	Homogeneous, massive black siliceous mudstone.

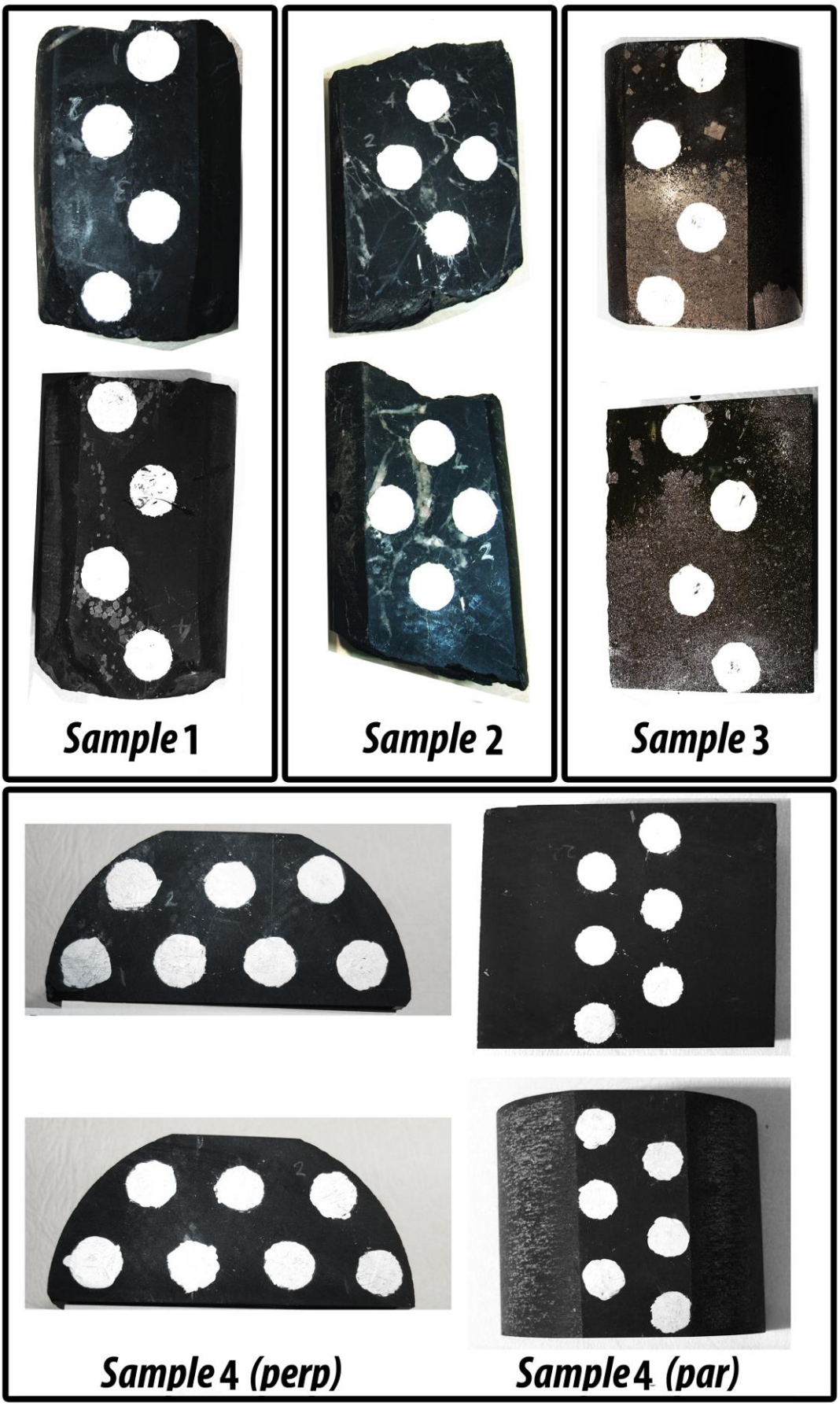

Figure 9: Selected photos of Samples 1 to Samples 4. White platinum circle painted on surface are 0.8 cm in diameter. Platinum paint conductive circles are 8 mm in diameter.

4.2 Vitrinite Reflectance and Organic Petrology

The Vitrinite Reflectance (VR) and organic petrology was carried out on Samples 1 to 4 by Mr. R.J. Sachsenhofer, from the Montanuniversität, Leoben, Austria. The aim of the study was to identify the thermal history of the samples by describing the maturation index of the organic carbon present. Vitrinite is fossilized herbaceous material, predominantly composed of plant polymers, cellulose and lignin and is abundant in kerogens and thus typically common in carboniferous shales. Vitrinite is an anistropic polymer and an increase carbon maturity corresponds with an increase in this anisotropy and their ability to reflect light. Vitrinite reflectance is a simple analytical method which measures the percentage of light reflected off these polymers, exposed at a polished sample surface (Dow 1977). Values are reported as a maximum (Rmax) and minimum (Rmin) reflectance (Davis 1978) and measurements are taken perpendicular to the grain axis. As the organic carbon increases in rank, approaching graphite, so does its anisotropy and reflectivity, with bedding/grain parallel Rmax values increasing with a corresponding decrease in Rmin values.

Polished blocks were prepared for samples along axes parallel and perpendicular to the borehole drill axis and values were measured using a Leitz MPV microscope and presented as ranges following established procedures (e.g. Stach et al., 1982). In addition to the reflectance values, organic petrology was completed which provided a summary description of the major compositional elements of the samples and the distribution and textural nature of the organic carbon present within each sample. The results for the VR study are presented in Figure 10 with complete results presented in the Appendix 1.

In summary; the carbon in the shales from SA1/66 are classified as metaanthracite based on their Rmax % values. Some grains do approach graphitic classification and the Rmin % values are unusually high. Overall, the carbon within the four samples displays a variety of rank. This coexistence of kerogen with several ranges of carbon rank and maturity can be attributed to the initial heterogeneity of the organic matter (Kribek et al. 1994). This variability of carbon rank corresponds with results from Tmax Rock-Eval experiments also for the Whitehill Formation published by Cole and McClachlan (1994) for borehole KL1/65. The variability in this borehole was considered by Cole and McClachlan (1994) to be due to the presence of recycled organic material which could be associated with reworking of younger Karoo sediments within the basin, particularly in the southern portion of the basin, adjacent to the orogenic front of the Cape Fold Belt. This would have provided organic material of various oxidation ranges and herbaceous origin to the Prince Albert and Whitehill Formations.

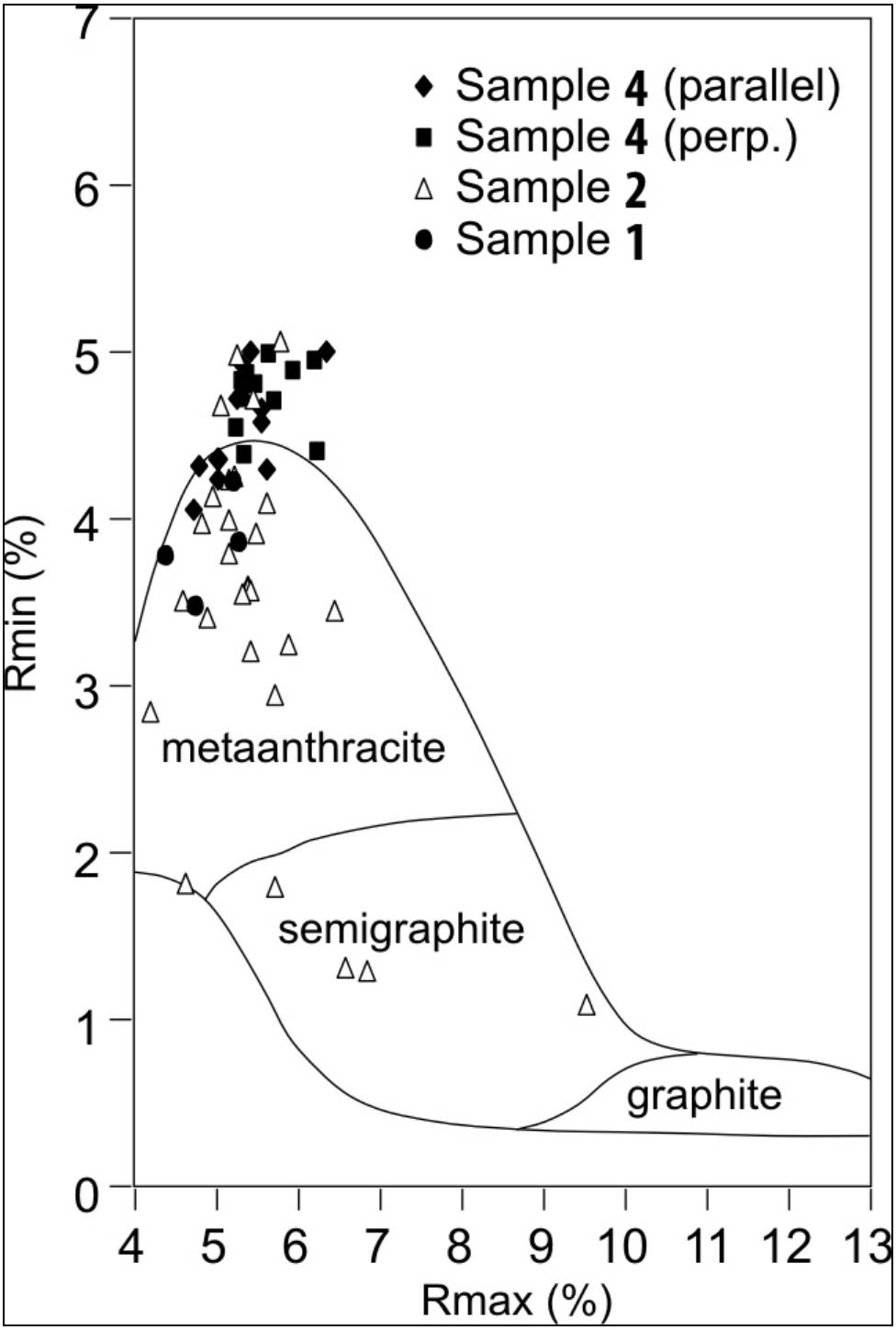

Figure 10: Reflectance of organic matter in borehole SA1/66. The outlined fields correspond to the reflectance of metamorphosed vitrinite according to Teichmüller et al. (1979) (graph from Sachsenhofer pers comms)

4.3 Electrical Conductivity and Impedance Spectroscopy (IS)

To obtain the electrical conductivity properties of the samples, Impedance Spectroscopy (IS) was performed on the four lower Karoo samples. IS obtains the bulk electrical conductivity across portions of a sample. Electrical conductivity (σ) is defined by a material's ability to support electron movement through it. This is defined by the proportional relationship between the vectors of current density ($\overline{J}$) passing through the sample and the applied electric field ($\overline{E}$) that drives the current. This is Ohm's Law:

$$\overline{J} = \sigma \overline{E} \qquad 1$$

For magnetotellurics, Maxwell's equations form the foundation of classical electrodynamics and describe how this moving charge results in time-varying electric and magnetic fields and vice versa. The Maxwell-Faraday equation (Eq 2) shows how a time-varying magnetic field induces an electric field while Amperes Law (equation 3) shows the converse relationship; how moving charge, or a changing electric field, induces a magnetic field:

$$-\frac{\partial \overline{B}}{\partial t} = \nabla \times \overline{E} \qquad 2$$

$$\nabla \times \overline{B} = \mu_o \overline{j} = \mu_o \sigma \overline{E} \qquad 3$$

(Vozoff 1991)

Where $\frac{\partial \overline{B}}{\partial t}$ is the partial derivative of $\overline{B}$ with respect to time

And $\nabla \times$ is the curl operator

Magnetotellurics utilizes these relationships and measures electric currents coupled with magnetic fields using electrodes and magnetometers installed at stations at varying intervals across a profile. From these measured fields passing through the earth, information relating to the conductive properties through which they travel can be obtained. The predominant sources that drive these electric currents are two-fold: fields with high oscillatory frequency are induced mainly by thunderstorm activity (10^3 - 1 Hz) largely around the equator, while long period fluctuations are generated by diurnal/nocturnal variations in solar plasma and their interaction with the earth's terrestrial magnetopause (1 – 10^{-4} Hz). These electric currents are transmitted through the earth with diffusion equations describing the dispersion of their energy as they propagate through the conductive subsurface. High frequency waves are attenuated more rapidly than the short frequency waves and so convey geoelectric information from shallower and deeper depths respectively (Skin-effect); in this respect the angular

frequency of the EM field variations measured at the surface is a non-linear proxy for depth (Vozoff 1991).

Magnetotellurics is, however, limited in its precision and ability to constrain the true dimensions of the conductors that are modelled by the inversion of the data. The inversion process seeks a smoothest, least structured model and as a result modelled features can have dimensions and boundaries that are poorly defined. Ultimately, as with all geophysical techniques the ideal is to test the inversion model by direct observations, for example testing samples of diamond drilled core.

Rocks consist of a variety of minerals and grains that are interconnected at variable microscopic and macroscopic scales, these boundaries impede the movement of electric charge through them. If the electric field responsible for the movement of charge is oscillatory, then this impedance is related to the frequency of field and is defined by the substance's dielectric permittivity (ε). In a slowly alternating current the polarization of bound charge is able to remain in phase with the applied field however as the frequency increases the relaxation times for these bound charges begin to affect their polarization, resulting in disequilibrium. This disequilibrium is therefore frequency dependant and is represented by a phase shift occurring between the applied and measured electric fields. This disequilibrium is additive and will increase proportional to the increase in frequency (Barsoukov & MacDonald 2005). The use of complex numbers allows for the incorporation of this frequency dependence as an imaginary number ($\overline{Z}^{i}$) while the purely conductive properties are defined and defined ($\overline{Z}^{r}$), this is termed the 'complex impedance' ($\overline{Z}$).

The standard approach to obtaining the complex impedance is by applying an oscillating current across a sample across a bandwidth of frequencies. By measuring the phase shift, across the chosen bandwidth, the sample's complex impedance is obtained. To achieve this and measure $\overline{Z}$ there are commercially available systems that perform IS analyses, such as the *BAS-Zahner IM6* located at the GeoForschungZentrum, used for this thesis (http://www.zahner.de/imp/im6e.htm). These instruments are generally easy to use and produce rapid results. The BAS-Zahner IM6 uses an alternating potential difference, transmitted across a frequency spectrum. This is done by utilizing a potentiostat together with a spectrum/frequency response analyser (FRA). The potentiostat is connected to the sample with four electrodes (terminals) and applies a constant voltage (V) using a control loop. This allows the FRA to analyse the complex impedance, $\overline{Z}$ at each frequency.

During the experimental process, a sample's conductivity (σ), and electrical permittivity (ε) is modelled as a resistor (R) and a capacitor (C), connected in parallel within an electrical circuit. The total current (I_{tot}) that moves through this sample is defined by:

$$I_{tot} = I_R + I_C \qquad 4$$

Where the current moving through the resistor is defined by I_R where I_R is:

$$I_R = \frac{V}{R} \qquad 5$$

And the current moving through the capacitor is defined by:

$$I_C = C\frac{dV}{dt} = i\omega CV \qquad 6$$

Where ωt is the frequency of alternating of the alternating current with respect to time

Combining equations 5 and 6 the total current within the experimental circuit would thus take the form of:

$$\bar{I}_{tot} = V(\frac{1}{R} + i\omega C) \qquad 7$$

Where

$$Z = \frac{V}{I} = Z' + iZ'' = 1/(\frac{1}{R} + i\omega C) \qquad 8$$

By solving for the real (Z^r) and imaginary (Z^i) parts of Z we obtain:

$$Z^r = \frac{R}{1+(RC\omega)^2} \qquad 9$$

$$Z^i = \frac{R^2 C\omega}{1+(RC\omega)^2} \qquad 10$$

This is the general form of the complex impedance (Z) (Barsoukov & MacDonald 2005).

Diagrammatically, the data recorded is presented in a "Cole-Cole" plot with Z^r on the x-axis and $-Z^i$ (negative) on the y-axis respectively. In theory, a semi-circle is obtained where the purely resistive properties are obtained at Z^i=0, and the dielectric properties of the sample increase proportionally with an increase of frequency.

From equations 9 and 10 it can be shown that:

1) At a resonant/critical frequency, $-Z^i$ is at a maximum and indicates the maximum dielectric energy loss when $\omega\tau = 1$ and $\tau = RC$.
2) As the angular frequency of the applied field tends towards zero the dielectric properties of the sample ($RC\omega$ and therefore Z^i) approach zero too and $\overline{Z}$ is defined solely by Z^r and exhibits zero phase shift and conduction is not influenced by any dielectric properties.

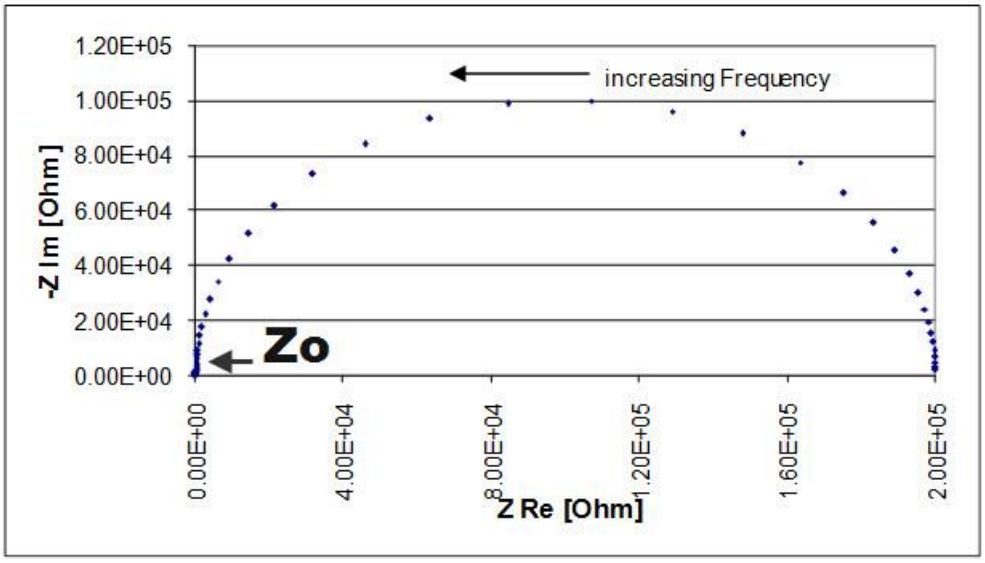

Figure 11: The ideal Cole-Cole plot showing Real (x-axis) and Imaginary (y-axis) components of Impedance (Barsoukov & MacDonald 2005).

4.4 IS Methodology

The experiments were carried out at the GeoForschungZentrum (GFZ) in Potsdam using a BAS Zahner IMP6. An alternating current was provided across the sample with a two electrode configuration. The counter electrode (CE_{in}) applied the current while the output was measured by the working electrode (WE_{out}). Two additional reference electrodes were used to measure the potential between the applied and output current The input resistance of the potentiostat and the capacitance are greater than 50 GOhm and less than 50 pF respectively, making their contribution to the system negligible.

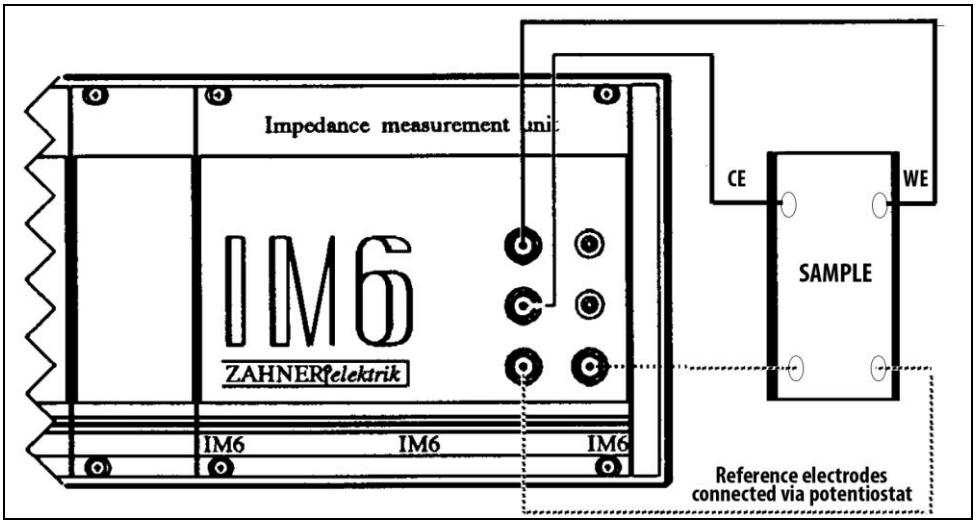

Figure 12. Experimental setup showing connection of CE and WE electrodes across the sample and reference electrodes connected (via a potentiostat).

Prior to analysis the system was run through a test menu with the electrodes connected to an industrially manufactured resistor and capacitor connected in parallel. A single frequency (1 x10^6 Hz) at a voltage of 20 mV, was set for the potentiostat and the output impedance was recorded and checked with the known resistance of the circuit. This tested the accuracy/precision of the experimental setup.

Flat, parallel faces were prepared on each side of all the samples using a core cutter at the GFZ. This was done a month prior to the experiment to provide sufficient time for the samples to dry naturally. Circular patches of platinum paint were applied to the sample's parallel surfaces to facilitate charge transfer between the electrodes and the sample and to minimize the capacitive effects of the electrode-sample interface. A stencil of 0.8 cm in diameter with a 0.5 cm spacing between each disk was used and a minimum of 4 measuring locations were prepared for each sample. Electrodes were connected via a rubber pressure clamp to their corresponding sites on either side of the samples, to form opposite poles.

Each sample was analysed by recording a spectral range of 1 MHz to 5 Hz increasing at a constant of 1/20 Hz. A proprietary software package (*Thales*) analysed the data and using the measured current and phase shift of the potential difference across the sample obtained the real and complex components of the sample's impedance at each frequency.

Each sample location was analysed twice to ensure reproducibility of the results. Duplicate readings, for example of reading '3.1' (the first reading from Sample 3) are presented with a suffix of 'b' (for example '3.1b'). This raw data is plotted for each sample on the '*Data*' graphs presented in the Appendix 2 (see Figure 37, Figure 39, Figure 41, Figure 44 and Figure 46).

IS results are in reality do not produce the ideal semi-circular dielectric arc as shown in the experimental analogy (Figure 11). Rather incomplete curves are typically obtained as samples are often dominated by either their capacitive or conductive properties. Additionally, samples with relatively high impedance, experience electrode effects that commonly distort measurements particularly at low frequencies. As a result Z_o is not in phase with the potential difference as it tends towards a direct current.

A theoretical 'fitted curve' is fitted to the measured curve to duplicate the Cole-Cole plot shown in Figure 11. The X and Y values for the 'fitted curve' (Z^r and Z^i) are calculated using equations 9 and 10 and allow for the calculation of R at Z_o and from R the sample's *bulk resistivity* can be calculated (Barsoukov & MacDonald 2005). This is a function of the volume across through which the measurement was taken, namely:

$$\frac{(Z_o)(Area)}{length} = \rho[\Omega m] \qquad 11$$

Length is taken for the thickness of the sample while the area is constant and calculated from the diameter of platinum disks painted onto the samples (0.8 cm).

In summary; two sets of graphs are displayed for each sample. '*Data'* graphs display the true measured data for both initial and repeat readings. The '*Model'* graphs display the idealized Cole-Cole plots that are fitted to the measured data.

In the case of a recording site producing some shift between initial and duplicate readings an average was obtained at each frequency and the ideal curve was fitted to this average in the corresponding Model graph. For example; recordings 3.1 and 3.1b (Figure 41) differed significantly. For this the average was calculated at each frequency, this was plotted for the complete spectrum on the data graph 3.1_avr, and from this the model graph was obtained "3.1z_avr" (Figure 42).

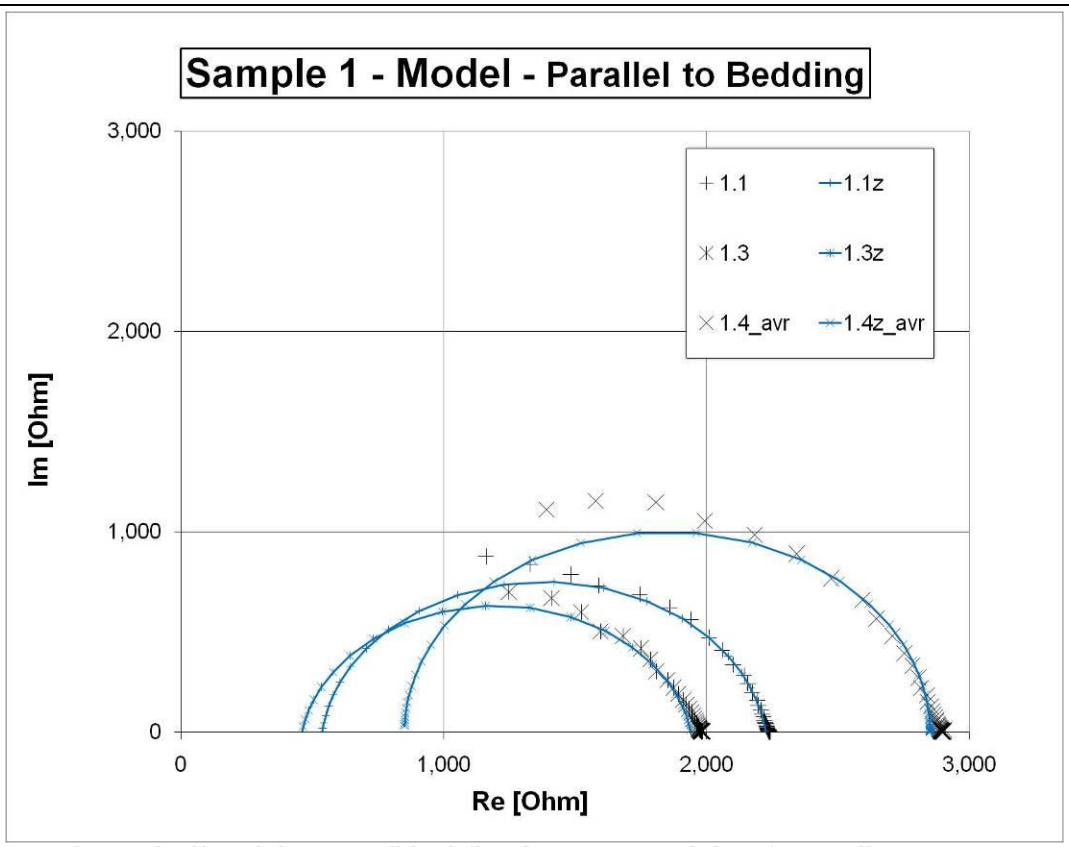

Figure 13: Theoretical/model curves (blue) fitted to measured data for readings 1_1, 1_3 and 1_4.

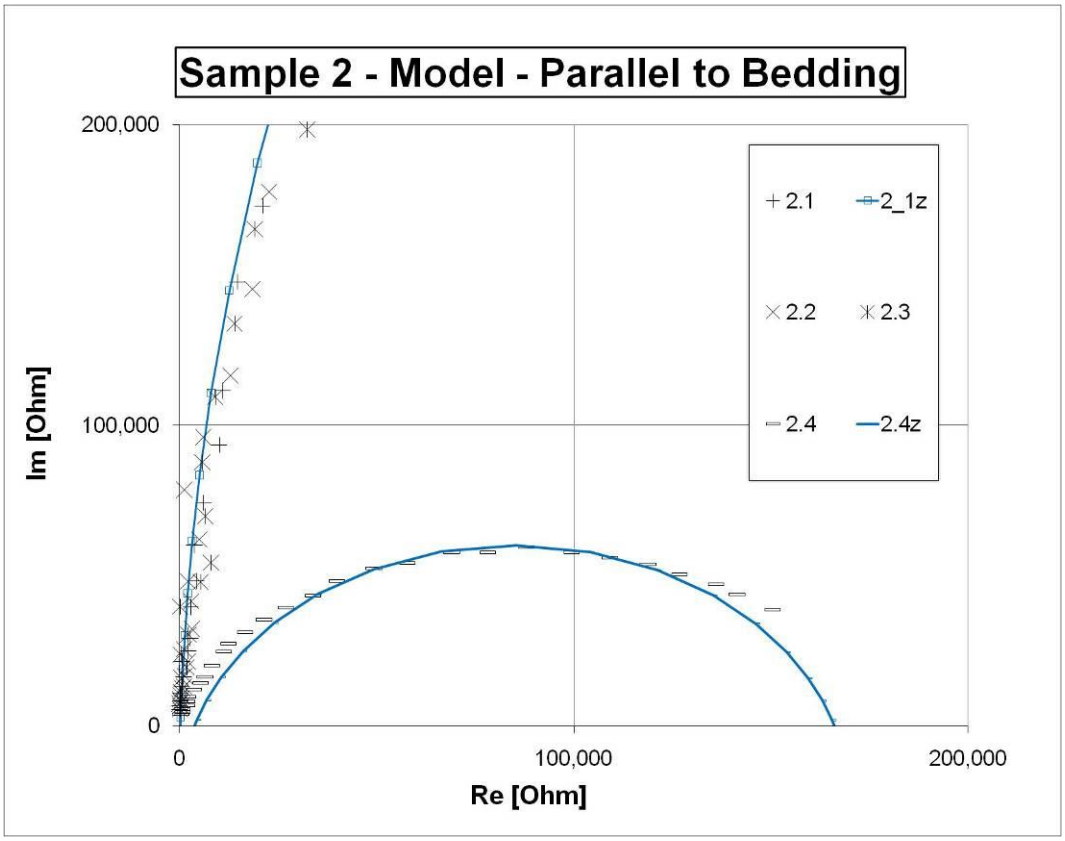

Figure 14: Theoretical/model curves (blue) fitted to measured data for Sample 2.

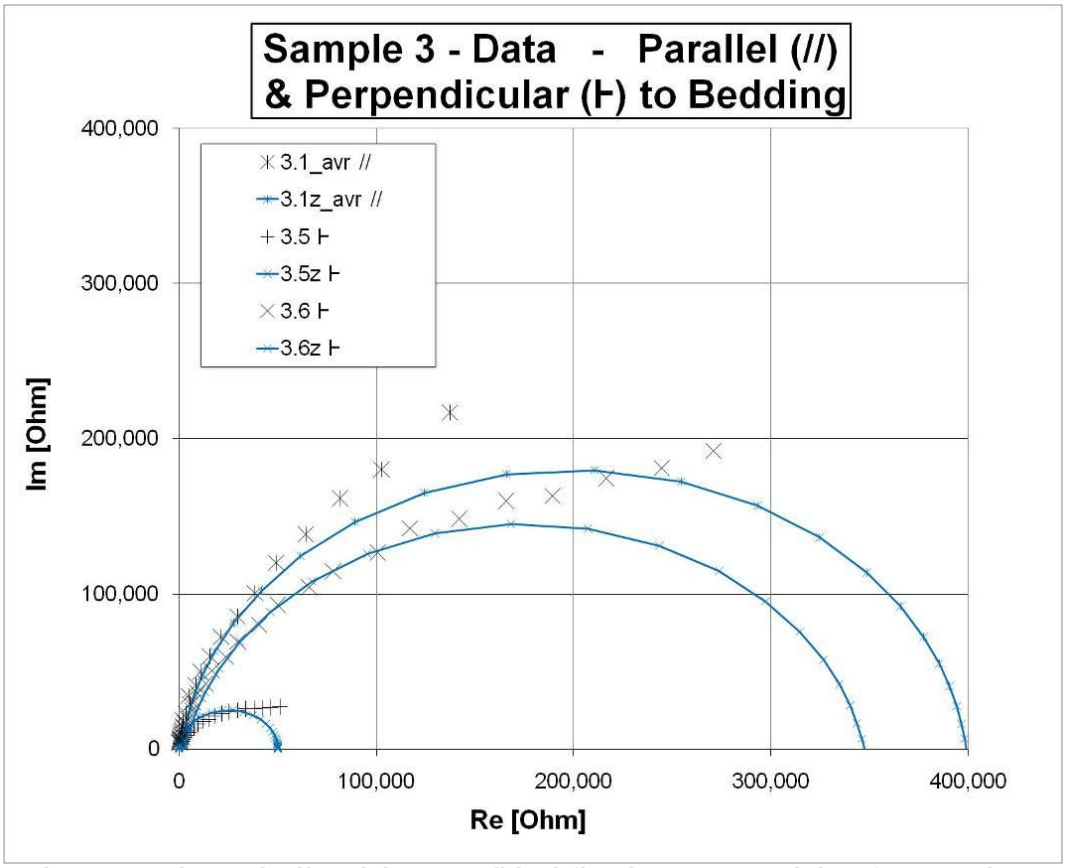

Figure 15: Theoretical/model curves (blue) fitted to measured data for Sample 3.

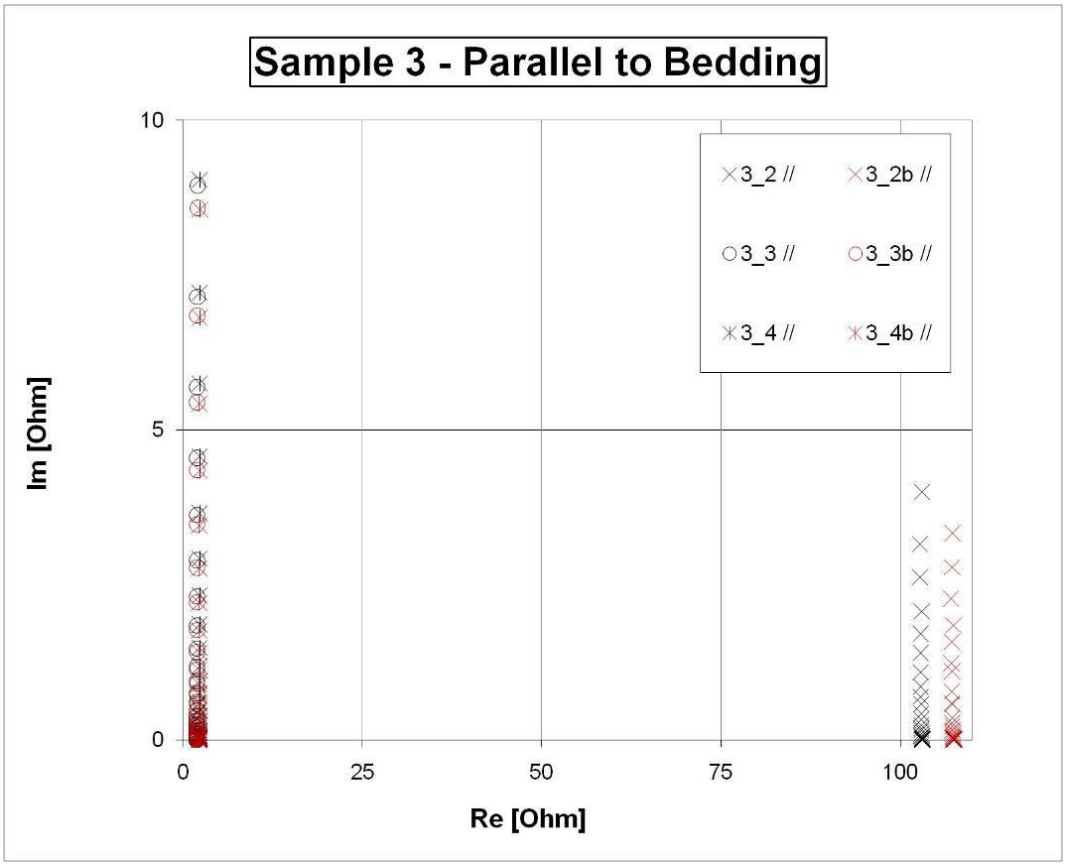

Figure 16: Measured curves for low resistivity sites on Sample 3, recorded parallel to bedding. Note dominance of quasi-metallic conduction and therfore lack of capacitive (dielectric) influence of Z_{Im} on the value of Z_{Re}.

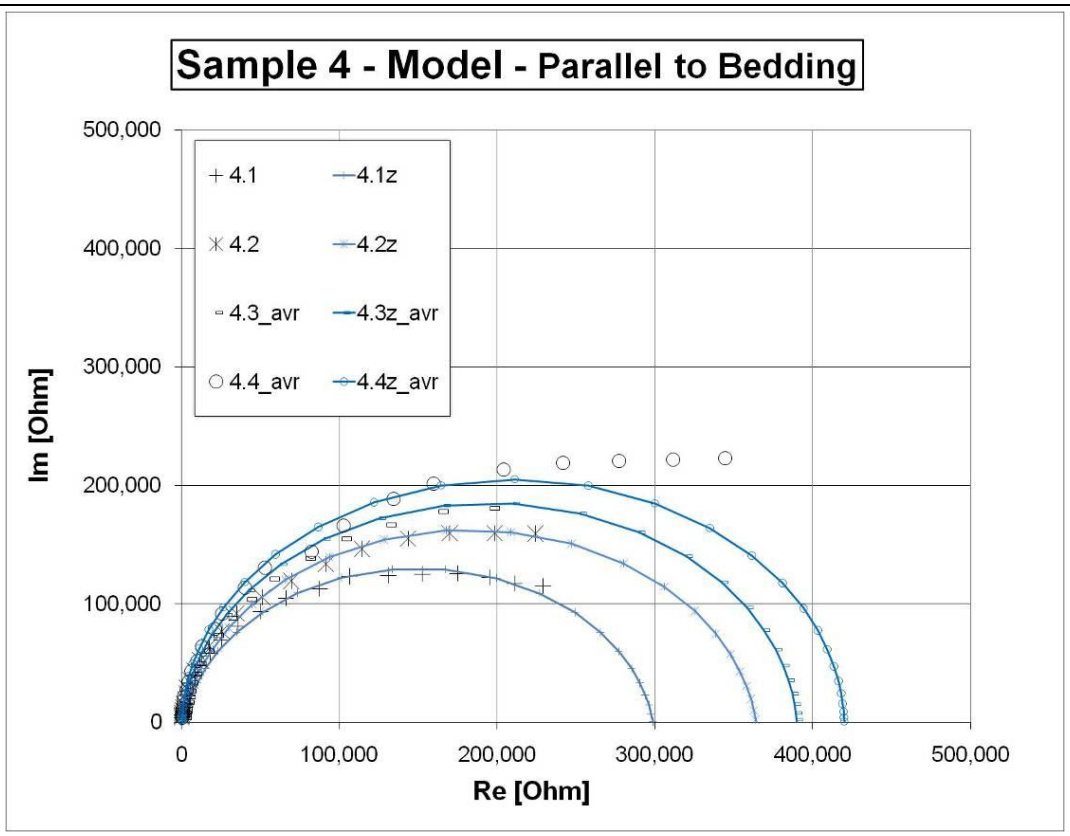

Figure 17: Theoretical/model curves (blue) fitted to the measured data for Sample 4, parallel to bedding.

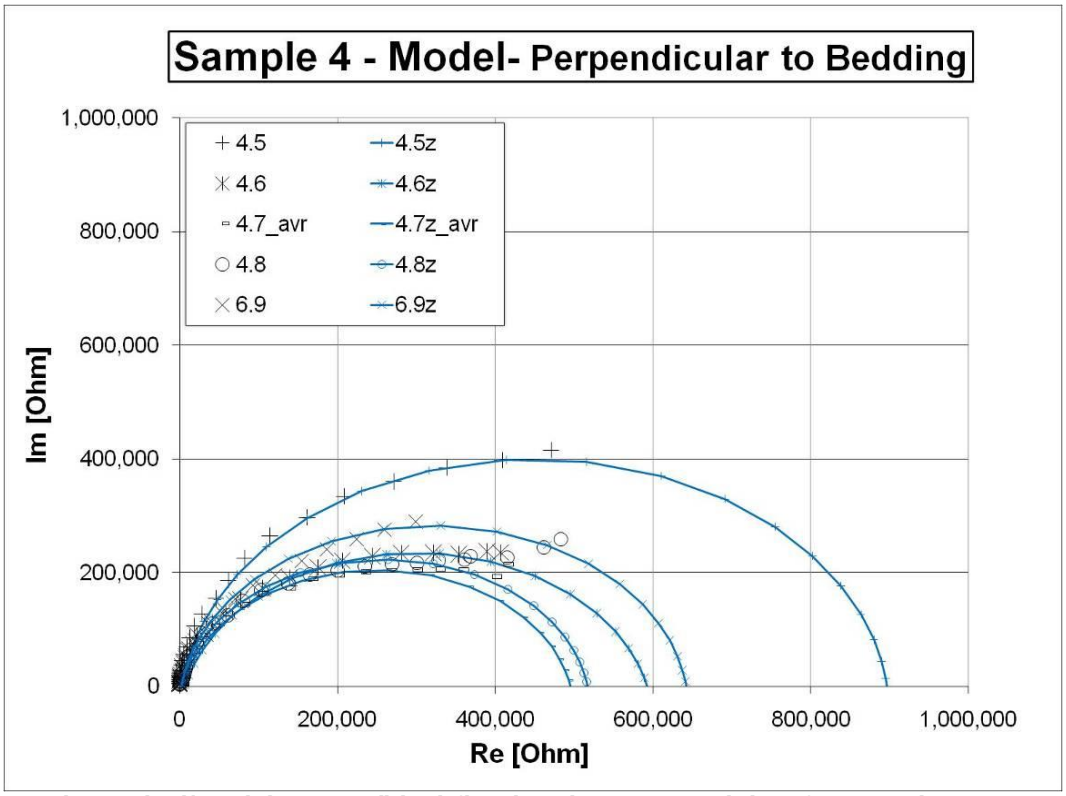

Figure 18: Theoretical/model curves (blue) fitted to the measured data for Sample 4, perpendicular to bedding.

4.5 Results

A total 23 individual points on Samples 1 to 4 were analysed. For each point the resistance was calculated by using the modelled curves at Z_o from which the bulk resistivity was calculated. These results are summarised in Table 4-3 and Table 4-4 and modelled curves shown in Figure 13 to Figure 18.

During the preparation of the sample's parallel sides prior to analysis a single large crack was sealed with epoxy to keep the sample intact. Along this crack reading 1.2 and 1.2b measured exceptionally high resistivities, these results are ignored.

In summary; significant variability was recorded, with resistivities spanning six orders of magnitude, from 0.01 to 4,916 Ω.m indicating significant differences regarding the dielectric properties of these samples, regardless of the fact that they are all logged as carbon-rich black mudstones. Sample 2 along had a calculated difference of 4,553 Ω.m between its maximum and minimum value. Sample 1, from the Whitehill Formation, returned the most consistent values, with a standard deviation of only 1 across all impedance measurements for the sample.

Higher conductivities were recorded for Sample 3; however the variance of measured conductivities ranges between very high (1309 Ω.m) to exceptionally low verging on quasi-metallic (0.01 Ω.m). This is likely a function of its pyrite content, which within Sample 3 is located in a band parallel to lamination, in the lower half of the sample and is estimated at > 20 modal %. Three recording sites (3.2, 3.3 and 3.4) were located directly on the pyrite band (See Figure 9) recording 0.4 and 0.01 and 0.01 Ω.m resulting in a short cut. As a result no ideal impedance curve was obtained for these readings (See Figure 43). Z_{Re} remained constant with respect to the frequency of the applied voltage, with analyses forming a vertical line to the x-axis.

The significant variability within Sample 2 (between 363 and 4916 Ω.m) is also likely due to its visible compositional heterogeneity. Sample 2 is criss-crossed by irregular, calcite veins less than 2 mm in width. Readings 2.1, 2.2. and 2.3 all returned exceptionally high specific resistivities that approximated 4,900 Ω.m. Reading 2.4 returned only a moderately high bulk resistivity of 363 Ω.m. It is likely that the very high resistivity values for this sample are a result of the ubiquitous calcite veins in the sample impeding charge transport. These would generate strong Maxwell-Wagner effects, inhibiting the movement of charge and would result in its polarization at higher frequencies. A single analysis, # 2.4, appears to be located on a portion of sample that was visibly devoid of calcite veins.

Table 4-3: Summary of impedance and bulk resistivity results

	Reading	Orientation	Impedance (Z)	Resistivity (Ω.m)
Sample 1	1	Parallel to Bedding	2,250	5
Whitehill Formation, Carboniferous with Disseminated pyrite	2		∞	∞
	3		2,000	4
	4		2,900	6
Sample 2	1	Parallel to Bedding	2,300,000	4,916
Prince Albert Formation Carboniferous with calcite stringers	2		2,300,000	4,916
	3		2,300,000	4,916
	4		170,000	363
Sample 3	1	Parallel to Bedding	400,000	1,309
Prince Abert Formation Carboniferous with high % pyrite	2		103	0
	3		2	0
	4		2	0
	5	Perpendicular to bedding	50,000	46
	6		350,000	321
Sample 4	1	Parallel to Bedding	300,000	481
Prince Albert Formation Silaceous mudstone, Massive	2		365,000	585
	3		390,000	625
	4		420,000	673
	5	Perpendicular to Bedding	900,000	805
	6		600,000	537
	7		500,000	447
	8		520,000	465
	9		645,000	577

Table 4-4: Summary bulk resistivity statistics (all values are in Ω.m)

	Sample 1	Sample 2	Sample 3		Sample 4	
Orientation	**Parallel**	**Parallel**	**Parallel**	**Perpendicular**	**Parallel**	**Perpendicular**
Average (Ω.m)	5.1	3778	327	183	591	566
Max (Ω.m)	6.2	4916	1309	321	673	805
Min (Ω.m)	4.3	363	0.01	46	481	447
Standard Dev.	1.0	2276.5	654.4	194.3	81.8	143.6

However; Samples 1 and Samples 4 appeared to return relatively consistent values of resistivity within each sample, a testimony to their visibly homogenous composition. Sample 4 is massive in structure, with no visible sedimentary laminations. It is also the most siliceous and hardest of the four samples and this corresponds with high values of resistivity, with analyses both parallel and perpendicular to bedding averaging between 591 and 566 Ω.m, respectively.

Sample 1, from the Whitehill Formation, is also relatively homogenous. The sample is visibly carboniferous, is soft and friable to the touch, and does have a strong cleavage, parallel to the bedding plane. There is very finely disseminated pyrite but it is highly

unlikely to be sufficiently interconnected to support charge transport. Due to the sample's lack of an alternative conductive phase; and organic particles that are visibly aligned parallel to the sedimentary laminations; and that kerogen has been identified as forming a network throughout portions of the sample, it appears likely that organic carbon is the major contributor to the sample's low resistivity, which averages 5.1 Ω.m (See Figure 38 and Table 4-4).

4.6 Discussion

The ability of organic carbon to form an interconnected network is a function of the carbon's rank, thermal maturation path and metamorphic history (Duba et al. 1988). During lithification, and within increasing rank, complex kerogens and hydrocarbon molecules are reduced to chemically simpler carbon chains. With the irreversible and progressive aromatization of the kerogen there is an associated loss of aliphatic chains, hydrogen and other 'impurities'. For the meta-anthracite stage (between 200 to 450°C) pyrolisis of these impurities and aromatics can result in the deposition of a sub-microscopic network of bitumite along grain boundaries, often concentrated along foliation planes, and so providing pathways for electron transfer. This deposition in relatively porous sedimentary units such as highly carboniferous units or shear zones is aided by the low density and relative mobility of hydrocarbons. This network of kerogen at grain boundaries is however difficult to locate without SEM elemental analysis.

The interpretation that organic carbon in Sample 1 is the primary conducting phase is equivalent to the findings of Duba et al. (1988). These authors studied the role of carbon as a conducting phase in black shales from Munsterland, Germany which were very similar in composition to those incorporated within this study. Low resistivities of approximately 3 Ω.m were reported for their meta-anthracite, oil-rich shale samples which contained approximately 5-8 % organic carbon and 10% pyrite. In comparison; Cole and McLachlan (1994) reported TOC values in hole SA1/66 of 4.9 % (number of readings = 12) and 4.6% (number of readings = 3) for the Whitehill and Prince Albert Formation, respectively. The low resistivities for the oil shales of Duba et al. (1988) were attributed to amorphous, marceral bitumite which formed a sub-microscopic matrix between the mineral grains. No graphite was detected during an X-ray study of the samples however; step-wise heating of the rocks indicated that carbon of a lower rank was the dominant conductive phase. This was supported by heating the samples at 150°C for three hours; this improved their conductivity, following which an order of magnitude decrease in conductivity was exhibited when the temperature increased to 320°C. Conductivity continued to decrease by a further three orders of magnitude following 24 hours of sustained heat at 420°C. Since pyrite is stable at these temperatures the decrease in conductivity was attributed to the pyrolysis and oxidation of carbon within the sample (Duba et al. 1988).

While carbon was considered the primary conductive phase in the samples studied by Duba et al. (1988), the pyrite was considered an accessory to charge transport, by further assisting the interconnectedness of the graphite. This was also recorded for pyrite hosted in higher grade gneisses and amphibolites by Duba et al. (1994). As discussed previously, pyrite is known to be common, even abundant within the carboniferous units of the Prince Albert and Whitehill Formation and it is clearly capable of affecting the bulk resistivity of its host as seen in Sample 3. However; it is unlikely that pyrite is sufficiently interconnected on a regional scale and is therefore unlikely to be responsible for a conductivity anomaly laterally continuous for over 400 km as seen in the MT profiles (Figure 8).

An additional factor that is likely to play at least a supporting role to electrical conduction in the Prince Albert and Whitehill Formations are dissolvable salts within groundwaters stored by these formations. Electrolytic conduction is a dominant source of charge transport in the crust and TDS values in these formations are approximately 1500mg/L (de Beers pers comms). However; elevated conductivities from dry outcrops of these formations (SOEKOR Log KW1/67) as well as the IS results presented here support the model that solid state conductors, such as carbon, may also be a primary mode of charge transport.

In the absence of other conductive phases (apart from pyrite) within Sample 1 it appears that the rank and proportion of organic carbon is sufficient to be highly conductive. In conjunction with this the contribution of pyrite to the bulk resistivity for Samples 1 and 3 are consistent with the results of previous publications (Duba et al. 1994). In the absence of downhole induction probe measurements to rule out electrolytic conductors as the main contributor to the Whitehill and Prince Albers anomalous conductivity carbon is proposed as the primary conductive phase. This elevated TOC is a regional feature of the Whitehill and Prince Albert Formations and its temporal equivalents further north in the Karoo Basin supporting their role as the primary conducting rocks visible in the upper 5 kms of the MT-1, MT-3 and MT-4 inversion models (Branch et al. 2007).

5. SECTION TWO - Magnetic Modelling for the Beattie Magnetic Anomaly

5.1 Introduction

In the absence of borehole data, the mid-crust hosting the BMA and the SCCB can only be investigated through the use of geophysical techniques which indirectly probe their geophysical properties. Forward modelling of aeromagnetic data is one such potential field method. The modeller seeks to fit the magnetic field calculated from a model against real data measured across a geological terrane. The measured data is historical aeromagnetic total field data collected across the BMA in the 1980's and available from the Council for Geoscience, South Africa. This data was modelled in *Mag2DC,* a forward magnetic modelling software package available from Wits University.

Forward modelling is non-unique; meaning, a variety of models can be made to fit the measured data. However; models generated for this thesis were tested against crustal interpretations as published for the MT, NVR and WRR experiments of the AKGT. By comparing the MT-1 crustal electrical model the potential for the BMA and the SCCB to arise from a single crustal source is assessed.

Structures that appear resolved in more than one geophysical experiment may be considered more robust; however different properties are merely resolved by differing geophysical methods. Two constrained forward models were generated through an iterative process that sought to arrive at a best fit with crustal blocks identified in the NVR crustal model. These models are then compared with equivalent crustal portions within the WRR and MT profiles. The two models differ with respect to their regional tectonic significance and the results are then discussed.

5.2 Magnetic Theory

The aim of aeromagnetic surveys is to measure the response of magnetic minerals in the earth's crust within the internal field generated by the earth. This magnetic field, termed the magnetosphere, approximates an axial geocentric dipole that extends several thousand kilometres into space. Although there are external contributors to this field, for example solar wind (the source for MT surveys), the majority of its strength is presumed to be derived from electrical currents generated by the mass flow of iron within the earth's liquid outer core. The self-perpetuating nature of this convection is described by the dynamo theory whereby centripetal spin initiated by the Coriolis Effect couples with convecting molten iron (Buffett 2000). Fluctuations in these outer core currents keep the earth's magnetic field in a constant state of flux. Additionally; its strength varies across the earth's surface relative to the distance away from the earth's magnetic poles. As a result the earth's magnetic field is relatively well defined

mathematically and from historical measurements at the earth's surface (Macmillan & Maus 2005). These models are available online from the American National Oceanic and Atmospheric Agency (NOAA) for any location between the years 1900 and 2015 (http://www.ngdc.noaa.gov/geomag/).

Within the vicinity of earth the magnetic flux flows from the north to the south pole. The magnetic force ($\overline{F}$) between any two magnetic poles of strengths m_1 and m_2 is

$$\overline{F} = \frac{\mu_0 m_1 m_2}{4\pi\mu_r r^2}\bar{r} \qquad 12$$

Where the magnetic permeability of a vacuum is a constant: $\mu_o = 4\pi 10^{-7}$ Vs/Am
And r is the vector distance between the two poles

From this the magnetic induction fields ($\overline{B}$ in Vs/m^2 or Tesla T) is expressed as the force on a unitary pole m_1 by the pole m:

$$\overline{B} = \frac{\overline{F}}{m_1} \qquad 13$$

Magnetic materials placed within this field have their elementary dipoles aligned in the direction of the applied field. This induces a secondary magnetic field ($\overline{J}$). The strength of this induced magnetisation is defined by the magnetic moment ($\overline{M}$) per unit volume and is expressed in A/m:

$$\overline{J} = \frac{\overline{M}}{v} \qquad 14$$

From this the magnetic susceptibility (k) is dimensionless quantity which describes a material's ability to be magnetized and is a function of $\overline{J}$ and $\overline{H}$:

$$k = \frac{\overline{J}}{\overline{H}} \qquad 15$$

Where $\overline{H}$ describes how $\overline{B}$ (the total field) is modified by the secondary field where:

$$\overline{B} = \mu_o \overline{H} + \mu_o \overline{J} \qquad 16$$

(Source: Telford et al 1990, www.tomoquest.com)

This total field is targeted during aeromagnetic surveys and measured using magnetometers. For the purpose of most forward modeling exercises, the component of

the total field attributed to the secondary induced lithological fields can be obtained by simply subtracting the components of the regional field (as modeled for example by the NOAA) from the data being collected across a profile (Nabighian et al. 2005).

The response of lithological sources to the earth's regional field is a function of their magnetic susceptibility. In minerals, magnetic susceptibility is a function of their atomic make-up and is determined by the spin and orbital paths of unpaired electrons around atomic nuclei forming magnetic moments. In an applied field these magnetic moments align parallel to the applied field with positive and negative poles accumulating at the opposite ends of the grain forming a dipole. This is exemplified in Figure 19(b) which shows three bodies with calculated responses for two external fields with differing inclinations of + and -66.2°, a declination of -25.9° and total field intensity of 28,358 nT, equivalent to that along the MT-1 profile (-66.2 inclination) .

Broadly; there are five main classes of magnetic materials:

1) *Diamagnetic* minerals (e.g. carbon): which have completely filled outer electron orbits and zero magnetic susceptibility.
2) *Paramagnetic* minerals (e.g. tungsten): which have permanent magnetic dipoles arising from unpaired electrons within the outer atomic orbits. These become only partially aligned in a magnetic field and result in weak magnetic susceptibilities.
3) *Antiferromagnetic* minerals (e.g. hematite): which are essentially paramagnetic but can retain a net magnetisation only through secondary crystal lattice defects within the mineral structure.
4) *Ferromagnetic* (e.g. iron) and *Ferrimagnetic* (e.g. magnetite) minerals: which exhibit strong exchange interactions between partially filled outer electron orbits; resulting in the parallel alignment of magnetic moments within crystallographic structures forming large magnetic domains. The result is a large magnetic susceptibility (Dunlop 1995).

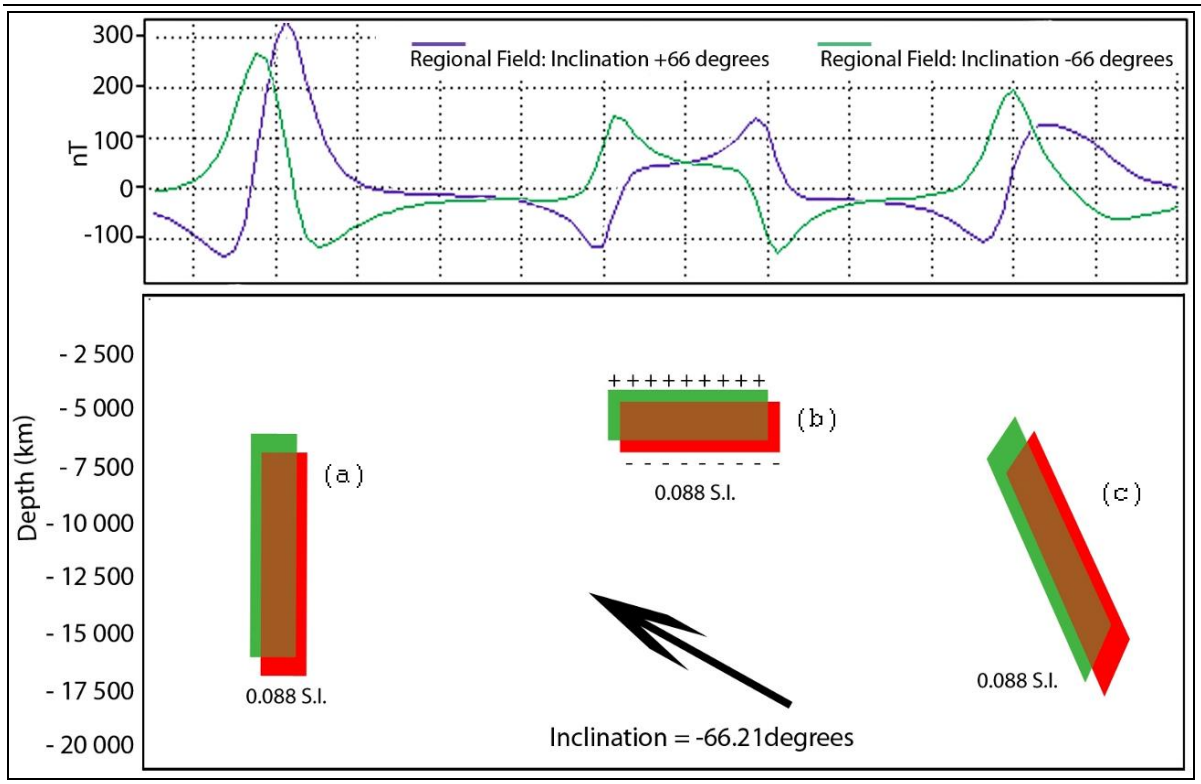

Figure 19: Magnetic models showing influence of a regional field (inclined of -66.21˚) on homogeneously magnetised bodies. Green portions of the model exemplify the concentration of positive monopoles (green) at the boundaries of each model. The calculated field is shown above each model in green, blue calculated response is for +66.21˚. 2D models generated using WinGlink ®.

Table 5-1: Magnetic Susceptibility for selected minerals. All values are x10^{-6} S.I. (Modified from Hunt et al. 1995)

Mineral	Min	Max
Iron Sulphides		
Pyrrhotite	1,200	3,200,000
Pyrite	35	5,000
Iron-Titanium Oxides		
Hematite	500	40,000
Maghemite	2,000,000	2,500,000
Ilmenite	2,200	3,800,000
Magnetite	1,000,000	5,700,000
Titanomagnetite	130,000	620,000
Ulvospinel	4,800	

Within geophysical surveys; ferrimagnetic compounds and elements are the most common sources of large susceptibility minerals (Hunt et al. 1995). Of these there are two dominant geochemical groups:

1) the iron-titanium-oxygen solid solution with magnetite (Fe_3O_4) and ulvospinel (Fe_2TiO_4) as end members and
2) the iron-sulphur group which provides the magnetic mineral pyrrhotite ($Fe_{(1-x)}S$ where x = 0 to 0.2).

Of these; magnetite is the most widespread (Harrison et al. 2002) as well as the most magnetic, being 3 to 4 orders of magnitude more magnetic than hematite and other ferromagnetic silicates (Hunt et al. 1995). As a result, magnetite is generally considered the main source of induced mid- and upper crustal magnetic anomalies (Williams et al. 1985, Shive & Fountain 1988, Nabighian et al. 2005). Lists of magnetic susceptibility ranges for important minerals and rock types are presented in Table 5-1 and Table 5-2.

Table 5-2: Magnetic Susceptibility for selected rocks. All values are x10^{-6} S.I. (Modified from Hunt et al. 1995). Note the extreme variability of magnetic susceptibility within the same rock type.

Rock Type	Range			Average
Igneous Rocks				
Andesite	17,000			17,000
Basalt	250	-	180,000	90,125
Gabbro	1,000	-	90,000	45,500
Granite	0	-	50,000	25,000
Peridote	96,000	-	200,000	148,000
Porphyry	250	-	210,000	106,000
Pyroxenite	130,000			130,000
Rhyolite	250	-	38,000	20,000
Average Igneous Rocks	2,700	-	270,000	140,000
Average Acid Igneous Rocks	38	-	82,000	41,000
Average Basic Igneous Rocks	550	-	120,000	60,000
Sedimentary Rocks				
Clay	170	-	250	210
Coal	25			25
Dolomite	-10	-	940	465
Limestone	2	-	25,000	12,500
Sandstone	0	-	20,900	10,500
Shale	63	-	18,600	9,500
Average Sedimentary Rocks	0	-	50,000	25,000
Metamorphic Rocks				
Amphibolite	750			750
Gneiss	0	-	25,000	12,500
Granulite facie lower crustals	3,000	-	30,000	16,500
Phyllite	1,600			1,600
Quartzite	4,400			4,400
Schist	26	-	3,000	1,500
Serpentine	3,100	-	18,000	2,500
Slate	0	-	38,000	19,000
Average Metamorphic Rocks	0	-	73,000	36,500

5.3 Remanent Magnetism

In contrast to induced magnetisation, remanent magnetisation is a permanent alignment of magnetic moments which can exist in the absence of an external field. These magnetic moments can be aligned in directions other than the earth's regional field and complicate the dimensionality of a total field response measured at the earth's surface. Geologically there are three fundamental processes by which remanent magnetisation can be acquired. These are:

1) *Thermo remanent magnetism* (TRM)*:* occurs when ferrimagnetic minerals cool through the *Curie Temperature* (see below) at which point the magnetic moments remain aligned to the applied field at that time. An example of this would be magnetite crystallizing from a magmatic fluid or uplift and cooling of a deeply buried crustal block.
2) *Chemo remanent magnetism* (CRM): occurs when new ferrimagnetic minerals are grown, for example through metamorphic fluid rock interactions such as the transformation: olivine + pyroxene → serpentine + magnetite.
3) *Viscous remanent magnetism (VRM)*: occurs from the nucleation of magnetic domains towards a local energy minimum. This occurs within a magnetic field applied over geologically long periods (Dunlop 1995).

Remanent magnetisation is affected by the magnetic domain state of the magnetic moments and is inversely proportional to grain size. A general rule is that plutonic rocks or metamorphic rocks with coarse multi-domain magnetite generally resist remanent magnetisation. In contrast to this; rapidly cooled extrusive rocks, with fine grained magnetic domains are prone to retaining remanent magnetisation (Clark 1997).

2D forward modeling exercises typically assume that the remanent component of the total field measured is zero or parallel to the applied field since it is difficult to quantify without direct observations made from samples of the lithology being modeled. Regardless, detailed studies have shown that remanent magnetisation can be a significant contributor to total field data (Pullaiha et al. 1975).

5.4 Curie Temperature

Both remanen and induced magnetisation exhibit an inverse relationship with temperature. As temperatures increase; the distances between individual magnetic moments also increase, disordering their domain state. At very high temperatures the inter-atomic distances exceed the zone of influence of electronic exchange forces and the aligned magnetic moments become randomized; preventing and/or destroying any magnetisation. The temperature at which randomization occurs is termed the *Curie*

Temperature, and is specific to a mineral's composition. Using geothermal gradients, Curie Isotherms are calculated so as to estimate at what depths crustal temperatures increase beyond Curie. These are typically based on the unblocking of magnetite, which occurs between 578 to 585 °C; however hematite-ilmenite intergrowths can play a key role at lower crustal depths and retain magnetism at depths that exceed magnetite (McEnroe et al. 2004). Table 5-3 lists the Curie temperatures for common magnetic minerals.

Table 5-3: Curie Temperatures for common ferri/antiferromagnetic minerals (Hunt et al. 1995)

Oxides		
Hematite	Canted antiferromagnetic	675 C°
Ilmenite	Antiferromagnetic	600 C°
Magnetite	Ferromagnetic	578-585 C°
Ulvöspinel	Antiferromagnetic	-153 C°
Troilite	Antiferromagnetic	305 C°
Sulphides		
Pyrrhotite	Ferromagnetic	320 C°
Greigite	Ferromagnetic	333 C°
Oxyhydroxides		
Goethite	Antiferromagnetic	120 C°
Native Metals		
Cobalt	Ferromagnetic	1131 C°
Iron	Ferromagnetic	770 C°
Nickel	Ferromagnetic	358 C°

5.5 Methodology

5.5.1 Data Processing

High resolution total field aeromagnetic data across the BMA was obtained under a personal, non-exclusive, non-transferable license from the Council for Geoscience (CGS), South Africa in 2005. The CGS retains copyright and intellectual property in respect of the data. The aeromagnetic data forms part of a regional scale geophysical dataset available from CGS as required by the State's initiative for the Promotion to Access Information Act (Act 2/2000). The data necessary to form a complete coverage of the MT-1 magnetotelluric profile of the Beattie Magnetic Anomaly was sourced by Mrs. M. Havenga of the CGS. In total 10 files comprising eight north-south and two east-west profiles were provided in XYZ format.txt files totaling approximately 215 MB of data. Coordinates were provided in latitude and longitude (WGS 1984, decimal degree).

The locations for these profiles are listed in Table 5-4 and displayed in Figure 20 and utilize the original profile numbering as supplied by the Council for Geoscience.

Table 5-4: Summary details for aeromagnetic profiles received by CGS. Coordinates are decimal degrees, WGS 1984.

Survey	kb size	Position Lat Begin	Position Long Begin	Position Lat End	Position Long End
Kar 2c	20,088	-31.98608	20.0116	-33.51383	20.21647
Kar 2f	21,103	-31.98637	21.06023	-33.51354	21.21259
Kar 2i	11,312	-32.00209	19.99072	-33.49492	22.01671
Kar 3a	27,705	-30.994228	18.99436	-31.338155	20.011268
Kar 4c	25,222	-29.99332	20.00048	-32.00673	20.15656
Kar 4f	23,135	-29.98726	21.63827	-32.01342	21.20277
Kar 5c	24,666	-29398649	22.00668	-32.01066	22.18267
Kar 5f	27,224	-29.98697	23.05514	-32.07396	23.22465
Kar 6c E	18,935	-31.9932	22.99506	-33.50681	23.04592
Kar 6c W	21,778	-31.99354	22.00136	-33.51077	22.16233
Kar 6f	21,778	-31.9932	22.99506	-33.5066	23.22186

The aeromagnetic surveys were flown during the early 1980's and recorded total field magnetic intensity, flight altitude and geographic position approximately every 70 m. Flight altitudes varied between 80 m to over 500 m due to large topographic differences within the study region, with higher altitudes apparently necessary over the mountainous Cape Fold Belt. Three adjacent profiles (surveys kar-5C, 5F and 6C) exhibited a datum shift of approximately 112 *nT*, the cause for this shift could not be identified, but was likely either the use of different instruments or different dates of data capture. The average datum shift was identified along portions of surveys that overlapped and the value subtracted from the total field values. The corrected data

gridded satisfactorily with a visible correlation across the overlapping profiles. However one major failing of the dataset supplied by the council was the lack of survey data down to the coast. Any magnetic response is bipolar with the negative field an intrinsic part of the whole. It can be seen that the Pitts (et al) 1992 modeling profile extended sufficiently south to include this. To address this in these modeling exercises the fit of the magnetic data to the southern portion of the measured response was given a high priority and fits were compared against the dataset used by Pitts et al. (1992).

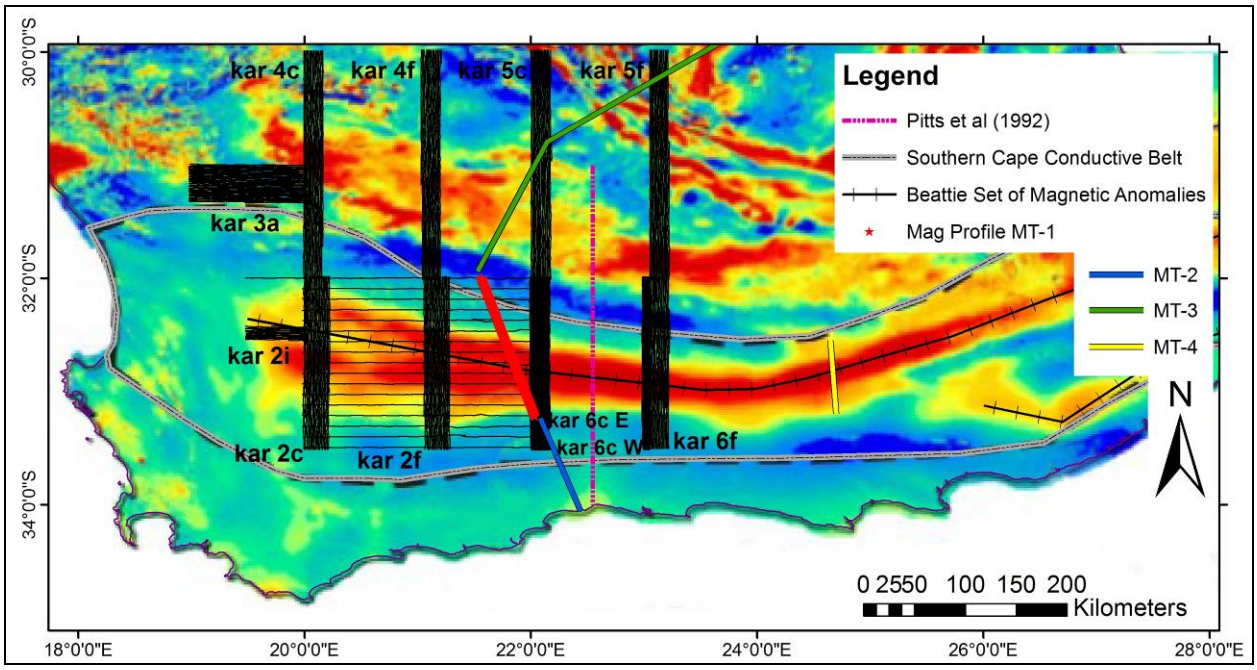

Figure 20: Location of 10 data profiles supplied by the South African Council for Geoscience. The data was gridded and the modeled profile was extracted along the same orientation as the MT-1 profile.

In an effort to identify any significant variance between the maximum and minimum flight altitudes registered in the data the residual field was extracted along a profile using a constant flight altitude of 50 and of 500 m and the results were compared (See Figure 21). No significant effect was found and the final dataset was gridded at an altitude of 100 m.

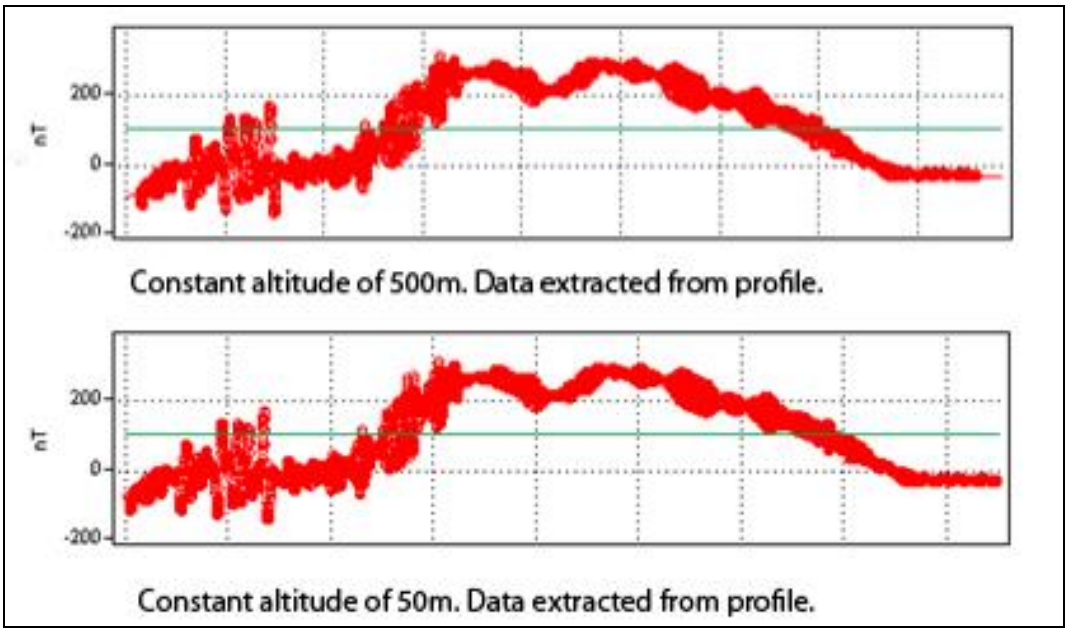

Figure 21: Comparison between 500 m vs 50 m constant altitude extrapolation in WinGLink. North is to the left.

Prior to initial modeling exercises the external field was removed within the WinGLink mapping component using the International Geomagnetic Reference Field (IGRF) for the year 1982. The components used for the IGRF were at the center of the MT-1 profile and are 28,358 nT with an inclination of -66.2° and a declination of -25.9°.

An interpolation radius of 5 km and a spline weight of 5 provided sufficient model smoothness and continuousness between points while maintaining adequate resolution in the final image. The gridded image for all data supplied by the Council for Geoscience is presented in Figure 22. Of the 10 surveys received only one was necessary to form a complete coverage of the MT-1 profile (east-west survey Kar 2i).

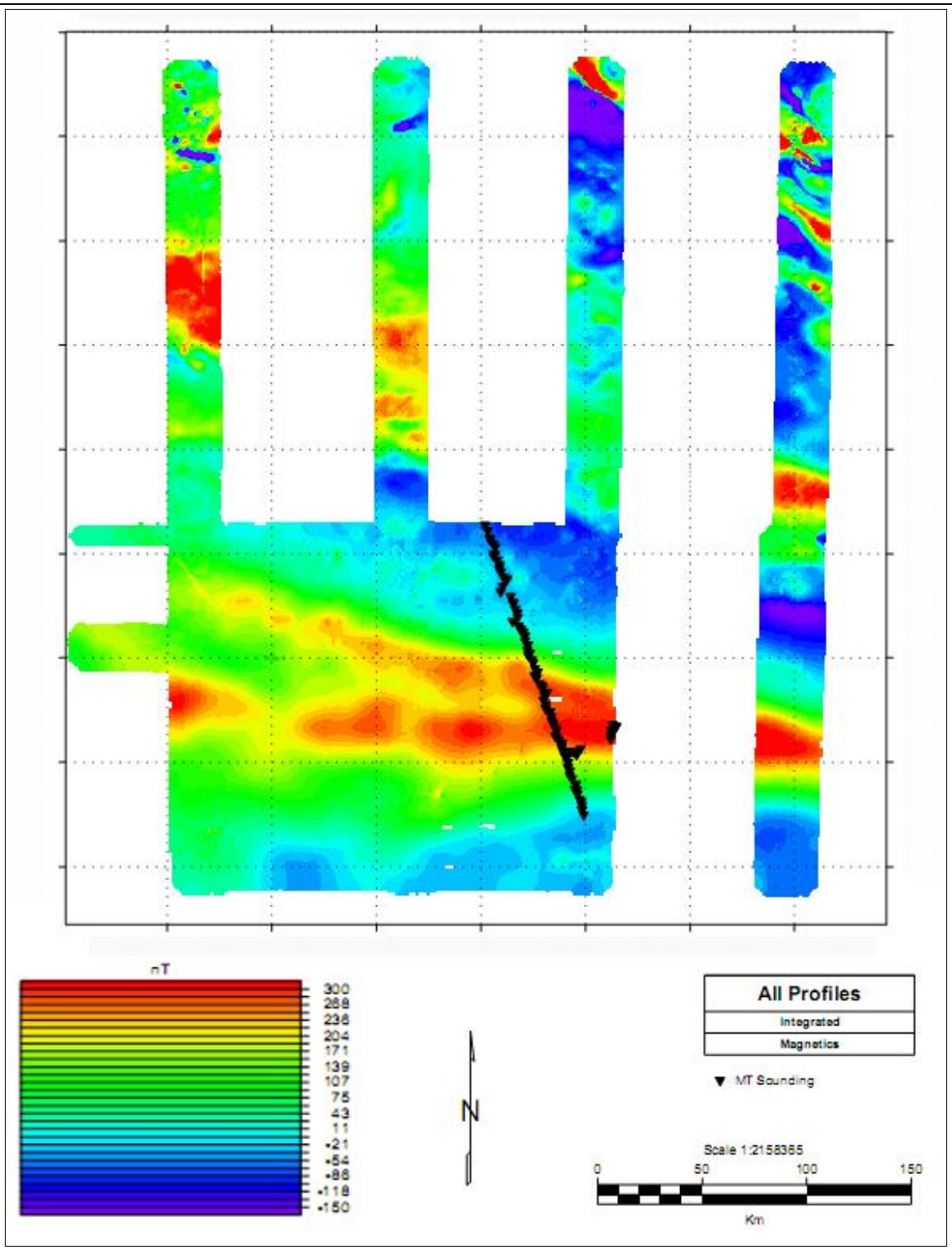

Figure 22: High resolution aeromagnetic residual field image gridded within the WinGLink modelling component. The NW-SE line of black triangles indicates the MT-1 stations.

Forward modelling was completed during two periods. An initial model was generated for this thesis in 2005 and was published by Weckmann et al. (2007)[b]. This model was created using the software package *WinGLink* available at the Geophysical Deep Sounding Section at the *GeoForschungZentrum*, in Potsdam. The more recent modeling exercise completed in 2011 utilizes the 2.5D MAG2DC program, developed and published by Prof G.R.J. Cooper of the Witwatersrand University and available as freeware at ftp://ftp.cs.wits.ac.za/pub/general/geophys/. MAG2DC only allows the

removal of the IGRF and forward modeling exercises, but is unable to map and grid data. As the WinGLink profile file format used in 2006 was compatible with MAG2DC another profile was kindly extracted for this thesis by Bravo Mukodzani using identical gridding parameters with the proprietary software; Geosoft, Oasis Montaj.

Both WinGLink and MAG2DC allow for comparison of the measured data with a forward model. Both programs use the algorithms of Rasmussen & Pedersen (1979) to calculate the induced field arising from the forward model. The dimensions and susceptibility of the forward model and its orientation within the regional field is controlled by the modeler within these programs. MAG2DC has the benefit of allowing the calculation of a body's response assuming both induced and remanent magnetism, and then calculates an integral difference between the measured and calculated fields. This allows the modeler to seek a mathematical minimum of error. For a theoretical and operational description of the software, see Cooper (1997).

5.5.2 MT, NVR and WRR Forward Model Rationale

Potential field modelling exercises are essentially non-unique and as a result an effectively infinite number of models can be generated to fit a measured response. This is exemplified by the simple model shown in Figure 23 where the combined magnetic field response of two bodies of lower magnetic susceptibilities is the fit the magnetic field response of a single body of greater susceptibility.

As a result the ability to compare theoretical models with other geophysical models along the same profile is invaluable and allows the modeller to test particular crustal geometries as supported by other geophysical methods. In this respect forward modelling was strongly influenced by the crustal sections as exposed by the NVR-, MT-1 and WRR experiments. Initial forward modelling exercises sought portions of the MT-1 and WRR geophysical sections which displayed crustal units of homogenous electrical conductivity and seismic velocity respectively. For the NVR section; modelling followed structural blocks as interpreted by Lindeque & de Wit (2009) from dominant reflector dips.

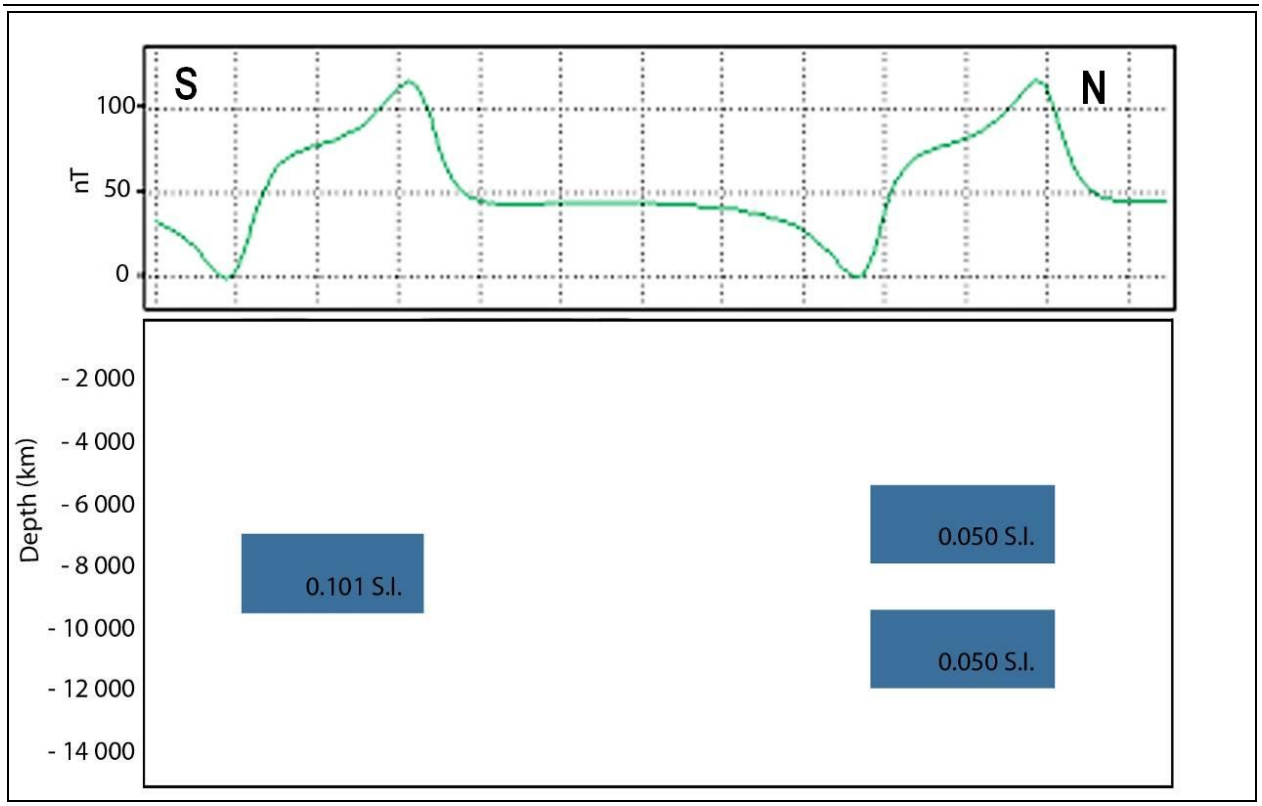

Figure 23: Magnetic model showing inherent non-uniqueness of total field modelling. The calculated field arising from the crustal block located on the left is duplicated by two blocks of lesser susceptibility. Susceptibility is in S.I. units; the regional field is inclined at -66.21˚, north is to the right. Forward 2D model generated using WinGlink ®.

Each of the forward models was generated separately within a MAG2DC half space; by a simple process of keying in each corner's depth and lateral position along the profile and its depth. These coordinates were measured physically from the scaled images published by each author and the relative position projected on the magnetic profile. Where reasonable; modelled magnetic units were extended past the boundaries of their geophysical sections (see modelled unit NVR-b in Figure 24), this is necessary to prevent artificial edge effects in the calculated magnetic response.

Each sub-unit was assigned an infinite strike length, no remanent magnetism and a volume magnetic susceptibility that would best fit the amplitude of the BMA. Its calculated response was saved along with the relative error/misfit with the BMA's measured response. All modelling excluded the upper crustal Cape and Karoo sequences as inferred by the authors. The bottom limit for modelling was 40 km depth. De Beer et al. (1982) calculated a Curie Isotherm (based on the unblocking of magnetite) at between 20-35 km based on observed surface heat flows of approximately 60 mW/m.

The rationale explaining the chosen geometries for each forward model are summarized in Table 5-5. The models are presented in Figure 24 over their corresponding geophysical crustal sections. Figure 24i shows the position of the measured residual

field magnetic response across the BMA. In total 15 crustal units were used as forward models. These are:

- **MT-a** to **MT-e**, totalling 5 units based on the MT-1 geophysical section
- **NVR-a** to **MVR-d**, totalling 4 units based on the NVT geophysical section
- **WAR-a** to **WAR-f**, totalling 6 units based on the WRR geophysical section

The calculated responses from these models are collected in Figure 25 to Figure 27. For clarity of presentation, results were combined within Photoshop into a single image for each of the geophysical surveys. These results are discussed in the following section and summarized in Table 5-6. Additionally results are summarised within figure captions for Figure 25 to Figure 27.

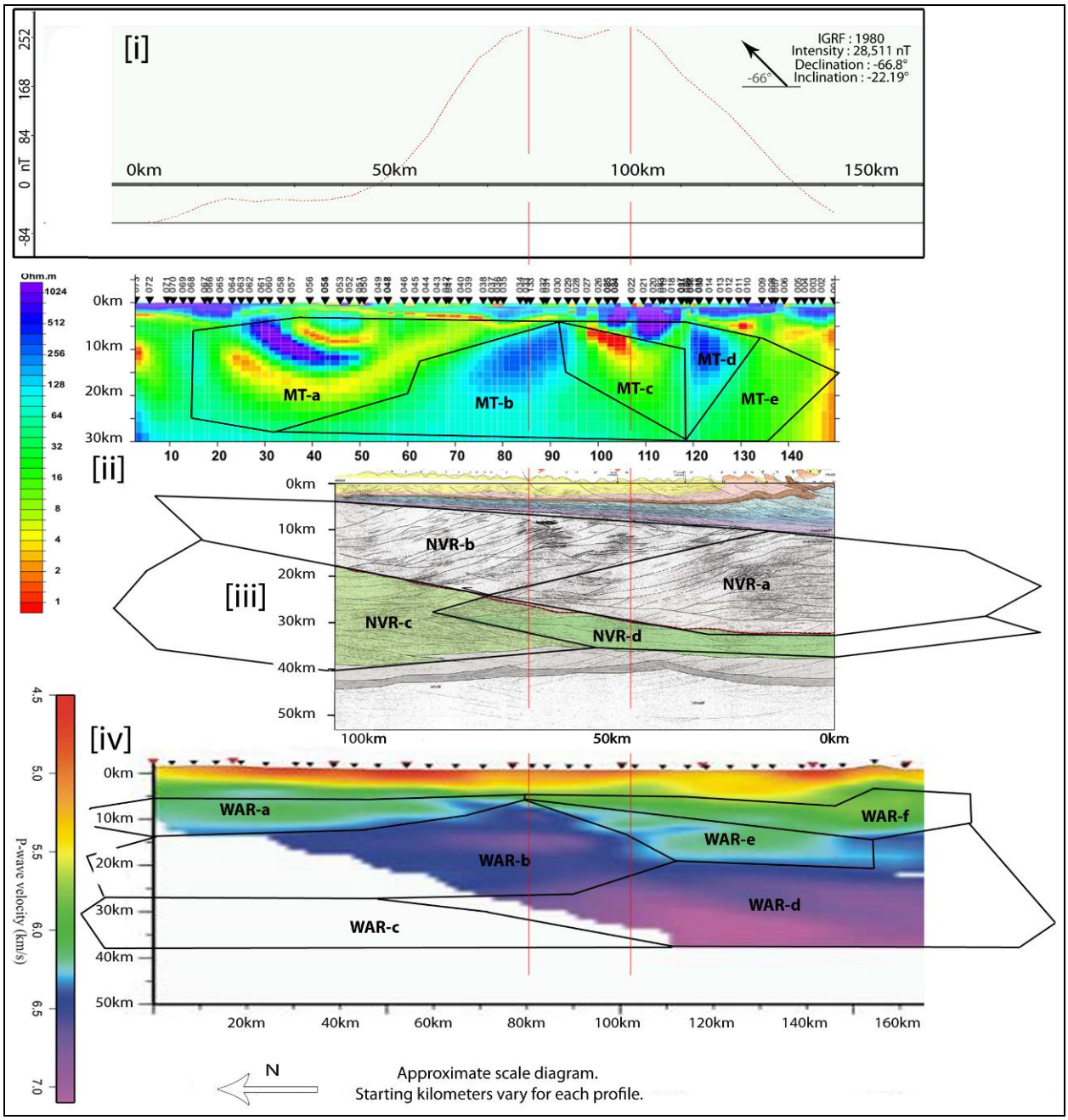

Figure 24 : The crustal sub-units used as magnetic forward models within MAG2DC. Results for each geophysical traverse are presented in Figure 25 to Figure 27.

Table 5-5: Forward models used within MAG2DC magnetic modelling.

Geophysical Profile	Forward model	Model Rationale
MT-1	MT-a	Incorporates two synformal conductors that exhibit a similar structural character
	MT-b	Mid to lower crustal unit of high electrical resistivity
	MT-c	Mid to lower crustal unit of low electrical resistivity
	MT-d	Irregular mid crustal unit of high electrical resistivity
	MT-e	Mid to lower crustal unit below the Cape Fold Belt of intermediate electrical resistivity
	MT-b-e	Combining forward models b,c,d,e
WAR eastern profile	WAR-a	Upper crustal unit of lower seismic velocity
	WAR-b	Large mid to lower crustal unit of high seismic velocities
	WAR-c	Lower crustal sliver, located within region of now WAR data
	WAR-d	Large mid to lower crustal unit of very high seismic velocities
	WAR-e	Thin mid-crustal unit of irregular low seismic velocities
	WAR-f	Low seismic velocity sliver, likely located within root of Cape Fold Belt (Stankiewicz et al. 2009)
NVR	NVR-a	Mid-crustal unit composed of northerly dipping reflectors. Interpreted as Mesoproterozoic equivalent of Bushmanland Terrane (NNMB), Lindeque et al. (2009)
	NVR-c	Mid-crustal unit composed of northerly dipping reflectors. Interpreted as Mesoproterozoic equivalent of Bushmanland Terrane (NNMB), Lindeque et al. (2009).
	NVR-d	Lower-crustal unit. Interpreted as slivers of Namaqua Natal Mobile Belt, Lindeque et al. (2009).
	NVR-e	Lower-crustal unit. Interpreted as slivers of Namaqua Natal Mobile Belt, Lindeque et al. (2009).

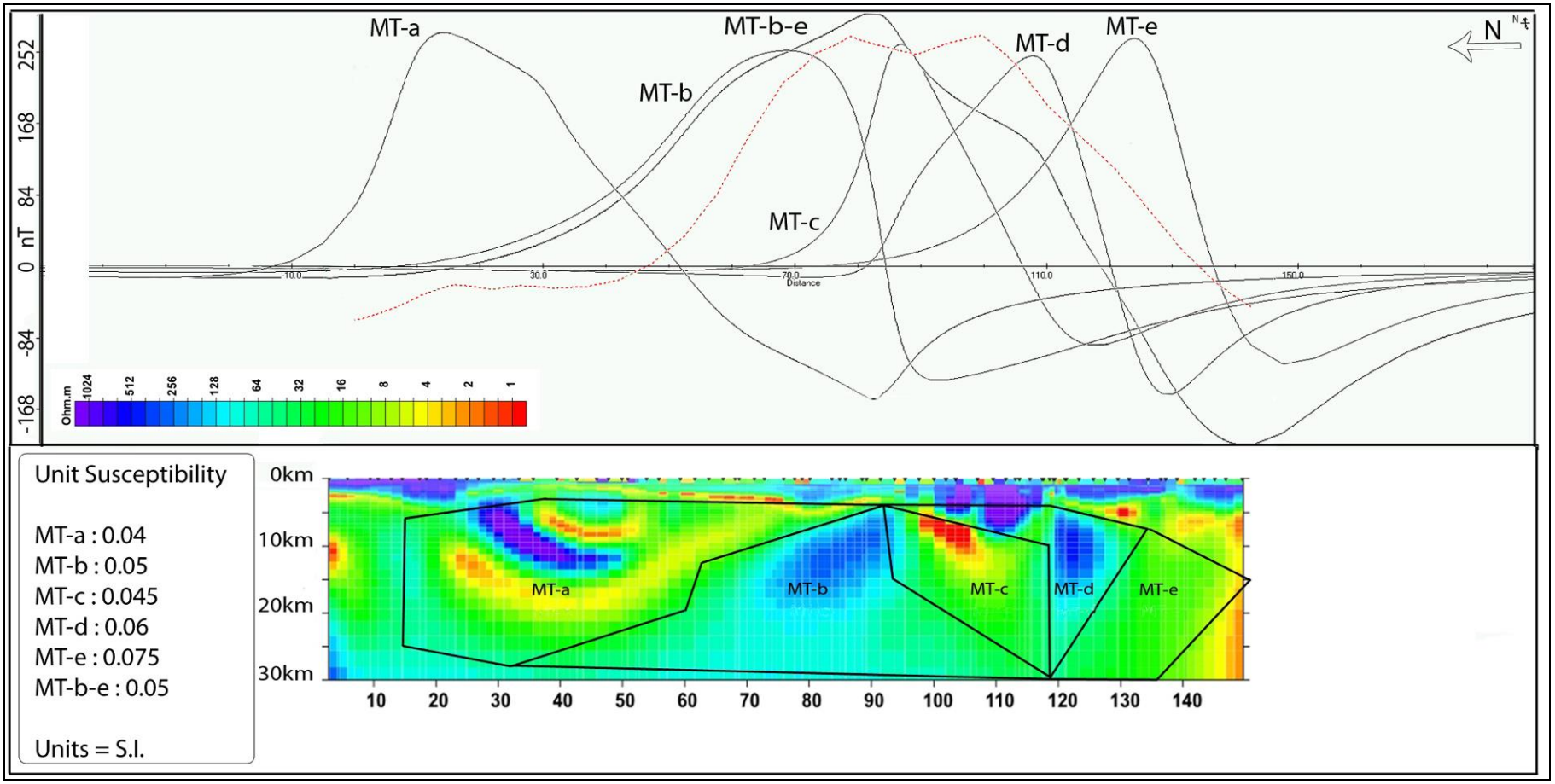

Figure 25: Magnetic forward model responses based on MT-1. The profile was divided into 5 units. Calculated responses from MT-c and MT-d are situated within the BMA's measured response indicating that they are located within the correct lateral position along the profile. The least error of misfit (r) was found with an average magnetic susceptibility of 0.05 S.I. assigned to a composite of units b, c, d and e (MT-b-e). In the north this closely approximates the initial magnetic model published for this thesis by Weckmann et al. (2007)[b]. The large negative anomaly located in the south of the response from MT-b-e shows edge effects arising from the cessation of MT-e in the south.

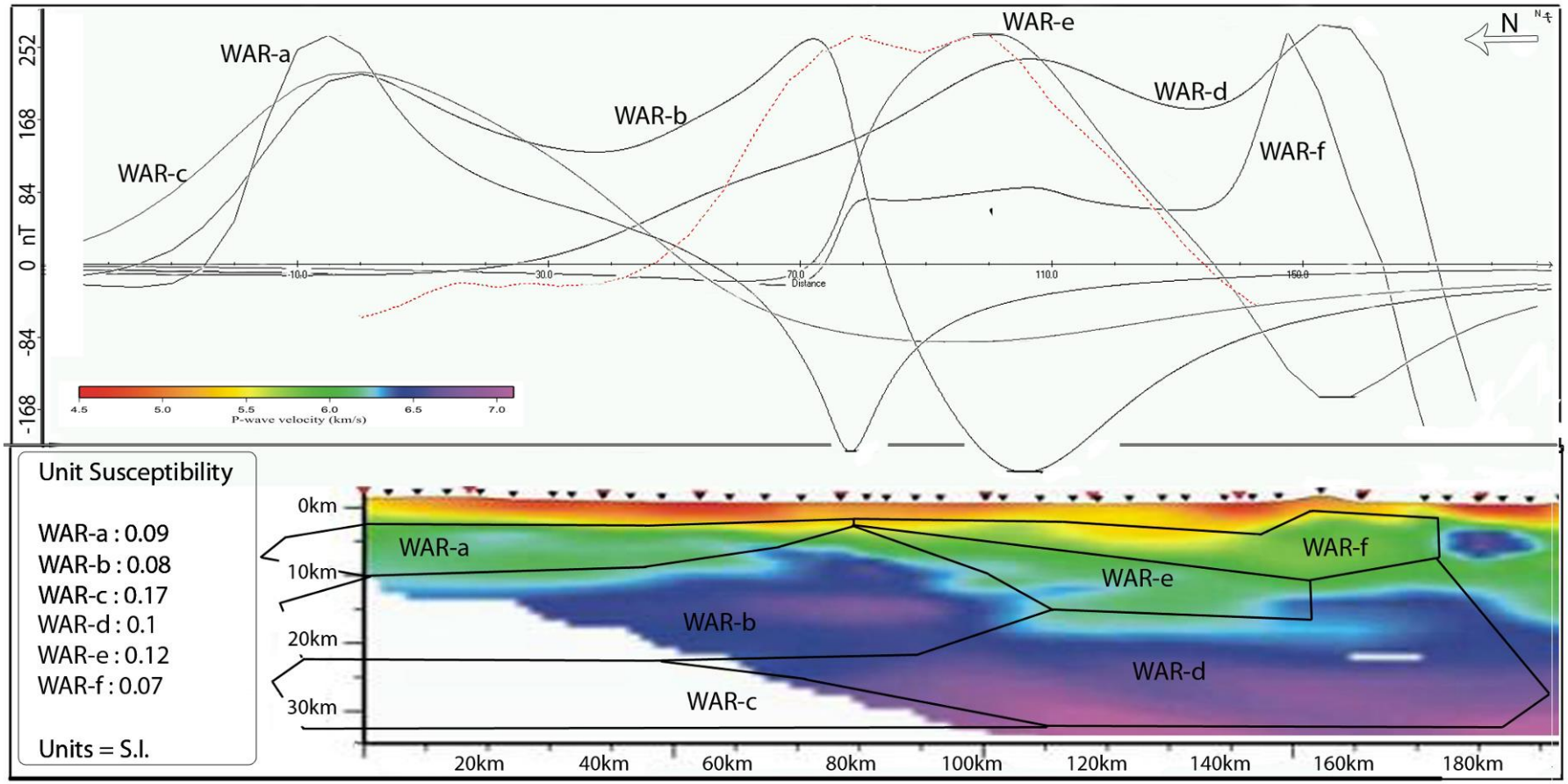

Figure 26 : Magnetic model based on WRR Profile (Stankiewicz et al. 2008). A total of 6 magnetic units were interpreted from the WRR section. Although the mid-crust in the north and the lower crust in the south are largely homogeneous with respect to p-wave velocity their units were separated for this modelling purpose. The calculated magnetic responses from WAR-a, c, d and f all fall either side of the BMA maximum. However; the southern portion of the response from WAR-b and WAR-e indicate a close proximity towards the causative source.

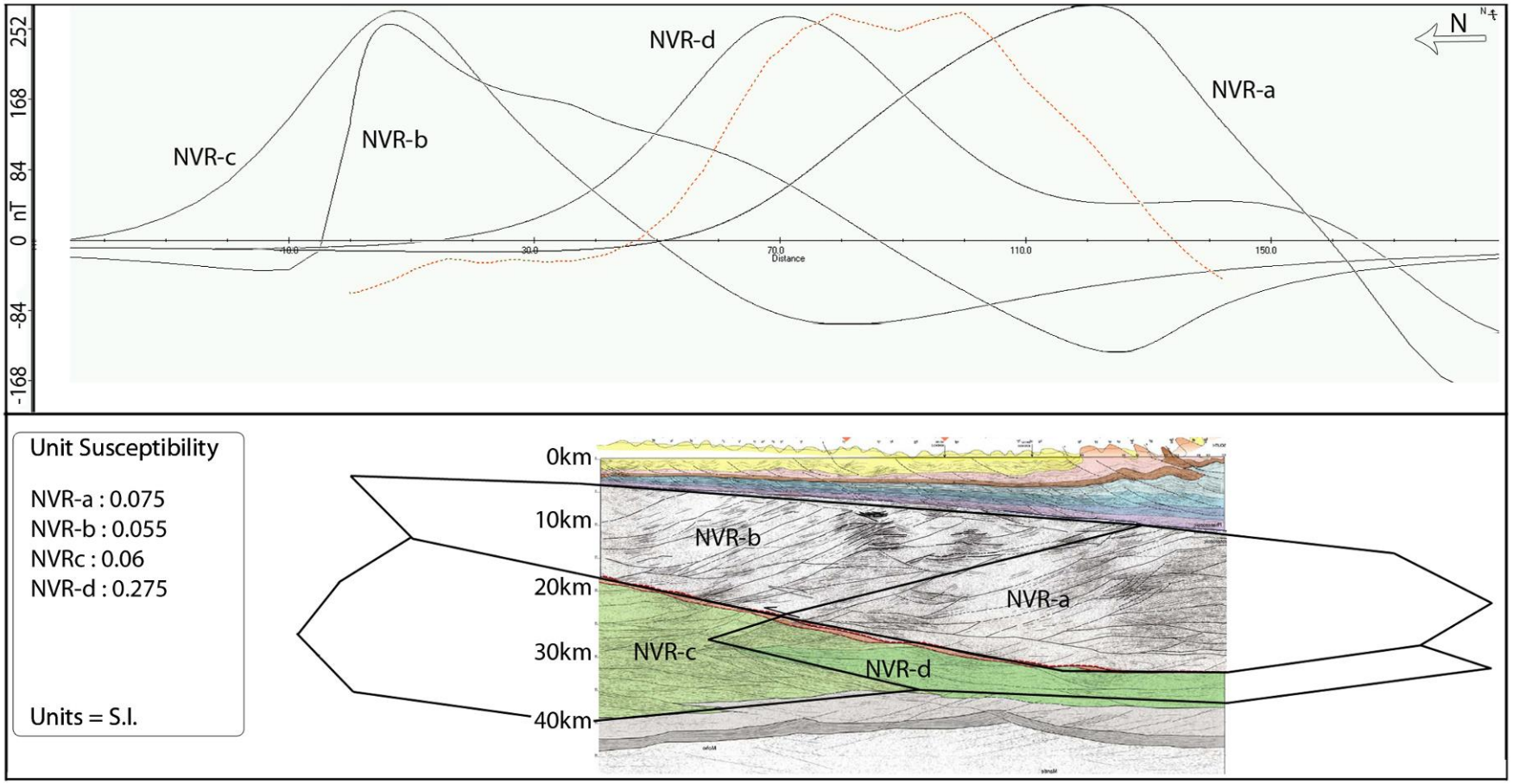

Figure 27 : Magnetic model based on NVR Profile and the crustal interpretations of Lindeque & de Wit (2009). The NVR body was divided into 4 potential sub-units. The lower crustal units proposed as 'mafic under-platting' were not incorporated within the forward modelling exercises as they exceed the published Curie Isotherm for the region. Immediately it can be seen that the larger bodies (relative to the magnetic units used within MT-1) approximate the breadth of the BMA more closely. While NVR-b and NVR-c are located too far north to be responsible for the BMA. The calculated responses from NVR-a and NVR-d show the least misfit errors of r = 1110.51 and 817.53, respectively. However; these units appear to fall either side of the measured BMA response.

Table 5-6: Summarized results from forward models used within MAG2DC magnetic modelling.

Geophysical Profile	Forward model	Result & Interpretation	Magnetic Susceptibility (S.I.)	Error Misfit (r)
MT-1	MT-a	Calculated response is approximately 100 km further north than the measured response	0.04	2,438.7
	MT-b	Calculated response is approximately 30 km further north than the measured response	0.05	1,847.4
	MT-c	Calculated response is located within the centre of BMA's measured response however it is too narrow in N-S to be solely responsible for the BMA	0.045	1,255.8
	MT-d	Calculated response is located within the centre of BMA's measured response however it is too narrow in N-S to be solely responsible for the BMA	0.06	1,252.2
	MT-e	Calculated response is approximately 40 km further south than the measured response	0.075	1,395.5
	MT-b-e	A combination of magnetic models b,c,d,e closely approximates the measured BMA magnetic response in both wavelength and amplitude	0.05	931.0
WAR eastern profile	WAR-a	Calculated response is >100 km further north than the measured response. A large negative anomaly in its south is related to the dipole shape of the body and its proximity to surface.	0.09	2,268.7
	WAR-b	Geometry of calculated response is too broad and it exhibits a double peak which is essentially >100 km further north than the measured response	0.08	2,518.5
	WAR-c	Geometry of calculated response exhibits a similar lateral extent to that of the measured BMA's response, however the calculated maximum is >100 km too far north.	0.17	2,427.7
	WAR-d	Geometry of calculated response is essentially too broad in wavelength and exhibits a massive negative anomaly and a double peak with a southern extent >100 km too far south	0.1	890.7
	WAR-e	Uniform geometry of calculated magnetic response is similar to BMA however lateral extent (wavelength) is too limited in the north.	0.12	840.1
	WAR-f	Irregular short wavelength geometry of calculated magnetic response is typical of shallow forward models and incongruous with the BMA	0.07	1,218.0
NVR	NVR-a	The calculated uniform, long wavelength anomaly is similar to BMA however the calculated maximum is approximately 30 km too far south	0.075	1,110.5
	NVR-b	The calculated response is located too far north, largely a factor of the artificially increased model limits used to prevent edge effects	0.055	2,153.6
	NVR-c	Calculated response is located too far north, largely a factor of the artificially increased model limits used to prevent edge effects	0.06	2,387.2
	NVR-d	Calculated magnetic response has a similar wavelength and amplitude to that of the measured BMA magnetic response, however the calculated maximum is < 30 km too far north	0.275	817.5

5.5.3 Results of Preliminary Modelling Exercises

The misfit errors (r) calculated by the MAG2DC software for each of the forward models in Table 5-7 represent an integral difference taken between the calculated and measured magnetic responses across the modelled profile. These constituted a quantitative constraint to what is essentially a qualitative process and assisted in identifying portions of the crust more likely to host the BMA. For example; forward models MT-b, -c and -d showed relatively low misfit errors and their calculated responses were located within the correct lateral position along the BMA maximum. However; the longitudinal dimensions were too small to individually explain the BMA's long wavelength.

A large proportion of the models are positioned too far north, resulting the magnetic maximum being located to far north and the influence of the bipolar negative portion of the response not influencing the models.

Subsequent modelling assigned an average susceptibility of 0.5 S.I. to all three units together and continued southwards underneath to CFB to include MT-e. The response from the four units combined (MT-b-e) more closely approximated both the amplitude and wavelength of the BMA. Essentially this replicates the original magnetic model derived for this thesis and published by Weckmann et al. (2007)[b].

Table 5-7: Relative error of misfit (r) calculated by MAG2DC between calculated and measured magnetic response

MT-1	
Model ID	Error (r)
MT-a	2,438.65
MT-b	1,847.37
MT-c	1,255.75
MT-c	1,252.17
MT-d	1,395.47
MT-b-e	931.02

NVR	
Model ID	Error (r)
NVR-a	1,110.51
NVR-b	2,153.59
NVR-c	2,387.18
NVR-d	817.53

WAR	
Model ID	Error (r)
WAR-a	2,268.71
WAR-b	2,518.48
WAR-c	2,427.66
WAR-d	890.66
WAR-e	840.05
WAR-f	1,217.95

In summary; results from these simple modelling tests allowed for first order observations that would inform the more constrained models presented in the following section. These observations were:

1. All forward models listed in Table 5-6 that attempted to constrain a crustal unit of homogeneous geophysical properties (e.g. P-wave velocity or conductivity) could not be solely responsible for the BMA. Thus the causative body must be heterogeneous with respect to either seismic velocity or electrical conductivity.

2. Certain domains within the geophysical models can be abolished as potential sources for the BMA. In particular; modelling constrained the lateral position of the source body along the profile and requires a body of at least 70 km wide to generate a calculated response that can equate the long wavelength of the BMA.

5.6 Constrained Forward Modelling

5.6.1 Model Rationale

Results from the preliminary modelling exercises constrained the lateral and vertical portions of the profile within which the BMA was most likely to be hosted. This portion of the crust was targeted for further modelling and the crustal geometry from the NVR profile was chosen to inform the geometry of more constrained models. From the NVR profile; mid-crustal and lower crustal units were identified that were similar to those interpreted by Lindeque and de Wit (2009), these units provided favourable geometries to duplicate the BMA's response closely. Based on this, two additional models were generated iteratively in order to achieve a minimum misfit with the measured data. Both models had a significantly low misfit error with the measured data and both correlate significantly well with the crustal geometry as interpreted by Lindeque and de Wit (2009). The mid-crustal model (MC-1) is presented in Figure 28 and the two lower crustal models (LC-1 and LC-2) are presented in Figure 29.

During the forward modeling of the LC-1, it was concluded that the calculated response would not accurately duplicate the measured response at the northern trough of the BMA, indicated by a dashed red arrow (in Figure 29). It was noted that the fit of the modeled response improved significantly if the geometry was slightly modified (Model LC-2) and a component of remanent magnetisation was applied (2000 nt with a declination of 115°). To display the baseline effect of the remanent magnetisation to the reader, it was applied to the LC-1 model, shown by LC-1r. Both LC-1 and LC-2 models are shown in Figure 29 to demonstrate that the BMA can be approximated with a lower crustal magnetic unit with or without remanent magnetisation. The inclination and magnitude of remanent magnetisation applied is however arbitrary and was chosen to merely improve the fit of the calculated response.

The geometries from the two NVR-constrained forward models (MC-1 and LC-1) are described in Table 5-8 and their results summarized in Table 5-9. The geomagnetic and tectonic relevance of each model is discussed individually in sections 5.7.1 and 5.7.2, respectively.

Table 5-8: Modelling rationale for constrained forward models based on crustal interpretation of NVR data (Lindeque and de Wit 2009).

Geophysical Profile	Forward model	Model Rationale
NVR	LC-1	A thin, 90 km long and 10 km thick, lower crustal model outlining an interpreted Palaeoproterozoic sliver of the NNMB (Lindeque & de Wit 2009). 100 % induced magnetisation.
	LC-1r	The same forward model as LC-1, with a calculated magnetic response utilizing a component of remnant magnetisation at 2000 nT with a declination of -115°.
	LC-2	A similar forward model to LC-1; however, it has been laterally shifted approximately 30 km northwards and has a component of remnant magnetisation of 2000 nT at a declination of -115°.
	MC-2	A large mid-crustal block, approximately 130 km long and 35 km thick. Interpreted as a Mesoproterozoic equivalent to the Bushmanland subprovince (Lindeque & de Wit 2009). Comprised of three units of similar magnetic susceptibility.

Table 5-9: Modelling results for constrained forward models based on crustal interpretation of NVR data (Lindeque and de Wit 2009).

Geophysical Profile	Forward model	Result & Interpretation	Magnetic Susceptibility (S.I.)	Error Misfit (r)
NVR	LC-1	The calculated response closely approximates both the amplitude and the wavelength of the BMA as well as outlines a lower crustal domain as interpreted by Lindeque & de Wit (2009) based on the tectonic fabric of the seismic reflectors.	0.45	367.5
	LC-1r	A component of remnant magnetisation was introduced merely to show a baseline effect for the remnance applied to LC-2.		547.0
	LC-2	Moving north to south, the gradient of increase towards the BMA maximum, as well as the gradient decrease after, is shallow and is more closely approximated with a component of remnant magnetisation applied to the calculated response.	0.4	234.7
	MC-1	The calculated response closely approximates both the amplitude and the wavelength of the BMA as well as outlines a mid-crustal domain interpreted by Lindeque & de Wit (2009). This forward model has the minimum misfit error of 185.31.	0.0367, 0.0786, 0.0649	185.31

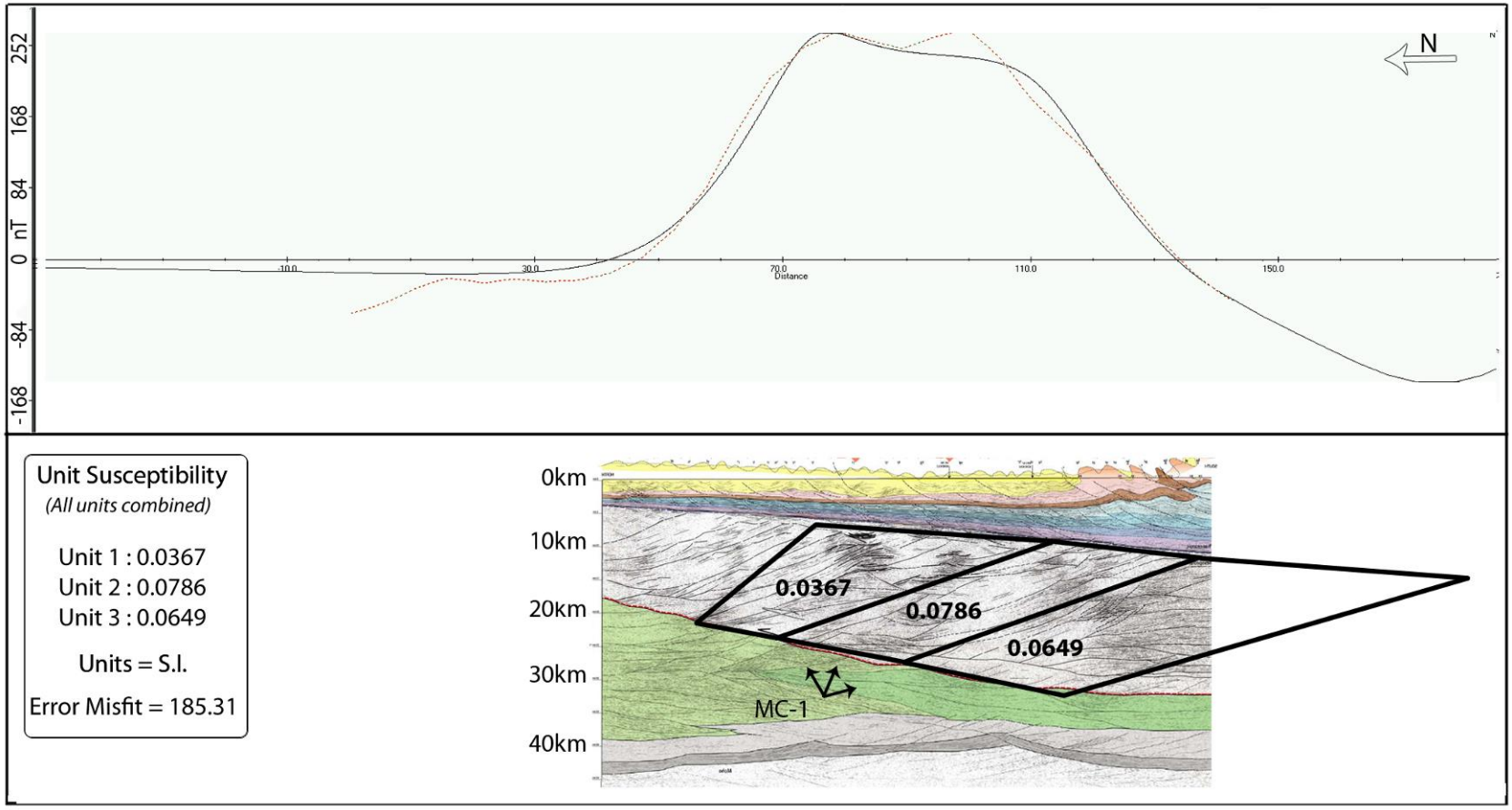

Figure 28 : Composite magnetic model (MC-1) correlated to the NVR section. The model achieves the least misfit error (r = 185.31) by assigning three different magnetic susceptibilities to each of the sub-units. Perhaps it is possible to interpret different reflectivity characters within each sub-unit. The southernmost unit appears to encompass a northward dipping mid-crustal zone of pervasive seismic reflectivity. No remanent magnetism was applied.

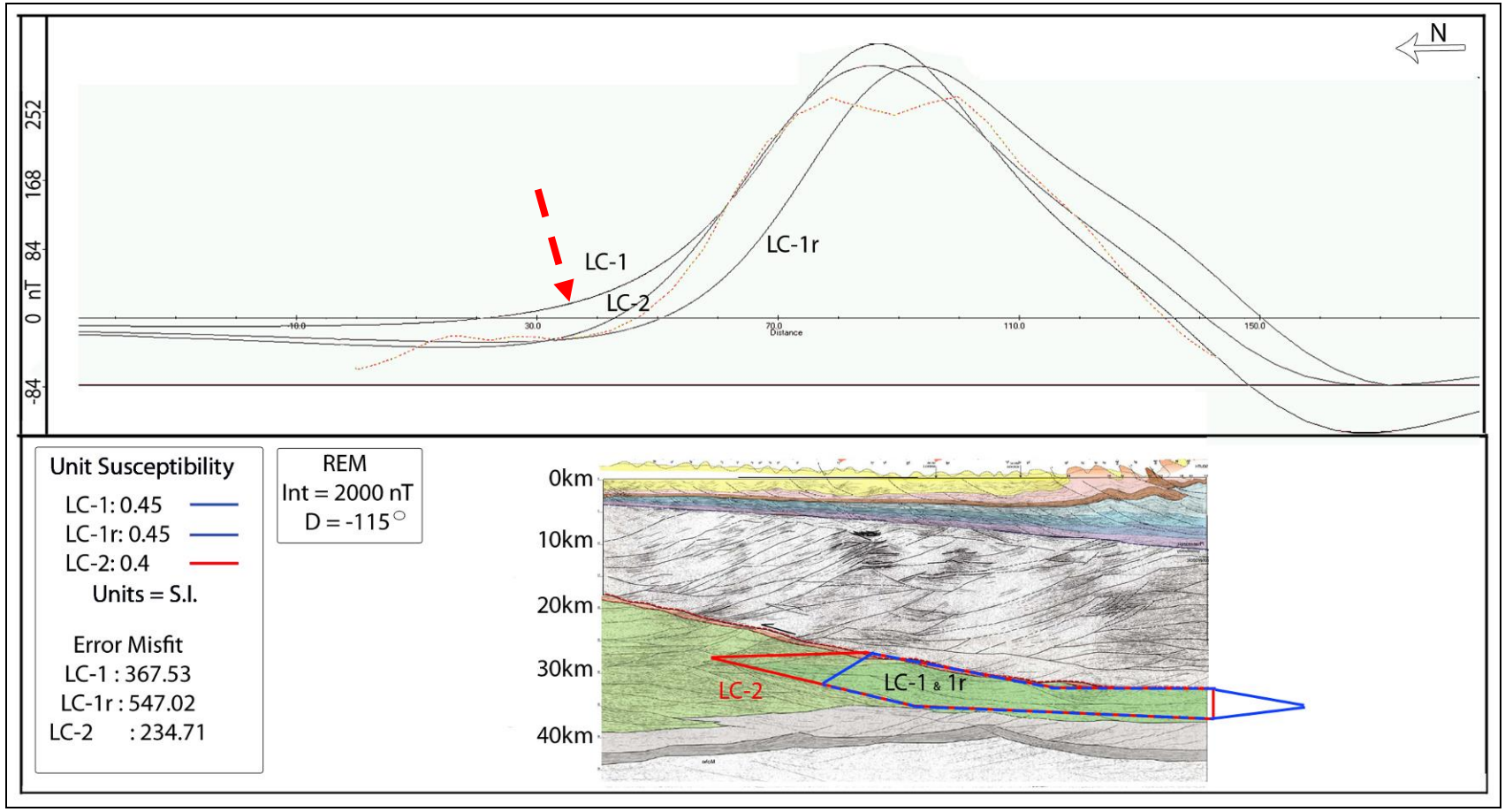

Figure 29 : Magnetic models (LC-1 and LC-2) correlated to the NVR section. The long wavelength response from magnetic model NVR-d inspired a more constrained lower crustal unit to fit the BMA's measured response. The generation of this model was in part biased by the research regarding lower crustal sources for long wavelength anomalies. The gradient increase and decrease of the magnetic maximum for LC-1 is too shallow, this is an intrinsic function of the model's orientation within the regional field. This was corrected by applying a component of remanent magnetisation (REM) to a model of similar geometry (LC-2).

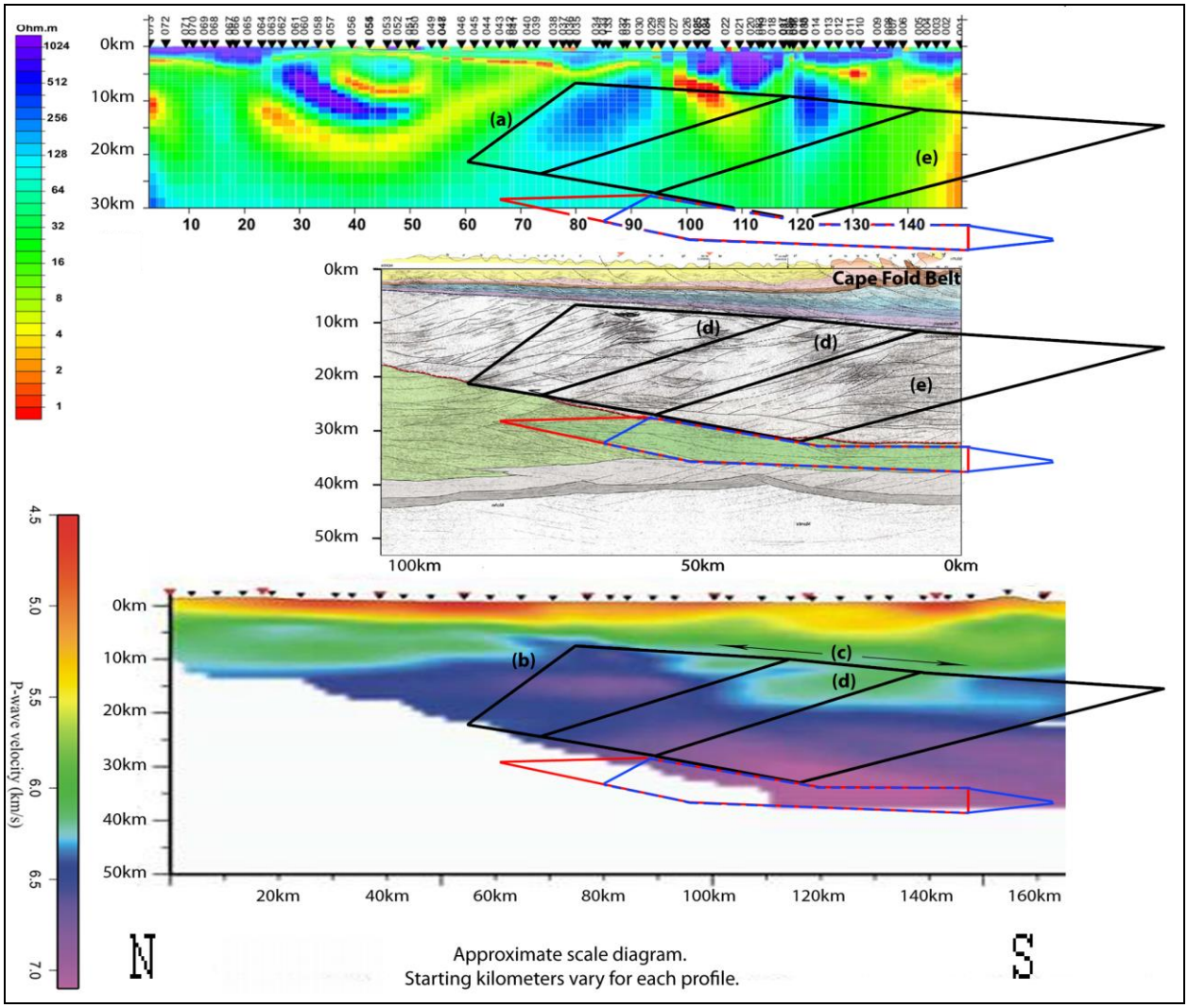

Figure 30: NVR correlated models LC-1 & -2 and MC-1 overlain on each geophysical traverse.

5.7 Discussion for Constrained Forward Models

5.7.1 Discussion: Forward Model MC-1

Model MC-1 is a simple rhomboid shape, nearly 100 km wide and over 20 km in thickness. Internally the body has been assigned three units of different magnetic susceptibilities. The choice of susceptibilities was purely to achieve a best fit with the measured response. Differences in magnetic susceptibilities could be explained by different proportions of magnetite within the host. The MC-1 model shares both the volume and the crustal fabric of the mid-crustal unit as delineated by Lindeque and de Wit (2009). In addition to this certain boundaries are shared with the MT and WRR data (See Figure 30). These are:

- The northern, northerly dipping face of the MC-1 body which correlates well with a division between high and low crustal conductivities, ('a' in Figure 30). This correlates with a discontinuity within the WRR seismic velocities within the mid-crust (**b**).
- The upper (shallowest) wall of MC-1 dips south beneath the Cape Fold Belt (CFB), this accurately matches an equivalent increase in depth between an upper and mid crustal velocity contrast (**c**) in the WRR model. This correlation is understood to represent the base of the CFB (Stankiewicz et al. 2008, Lindeque & de Wit 2009).
- The inconsistent p-wave velocities within the shallow, middle portion of MC-1 can perhaps be correlated to portions of elevated crustal reflectivity within the NVR section (**d**).
- The most southerly portion of the MC-1 magnetic model, located at mid-crustal levels beneath the CFB, is interesting in that it appears to be located within a zone of high p-wave velocities, but elevated reflectivity as well as elevated conductivity (**e**).

The overall magnetic susceptibility of the MC-1 model (0.075 S.I.) is approaching the upper average values for metamorphic rocks. Since Pitts et al. (1992) identified no significant gravity anomaly across the BMA, it is unlikely that a source of this size could be mafic. The source lithology proposed here is a chronological intermediate between the Namaqua and Natal portions of the NNMB, composed predominantly of high metamorphic grade, acidic to intermediate plutonic sequences.

Numerous geomagnetic studies from traverses crossing exposed mid- to lower-crustal terranes exposed at surface show that silicic plutonic rocks (which are typically poorer in iron than their mafic counterparts) could be responsible for large wavelength magnetic anomalies (Williams et al. 1985, Shive & Fountain 1988, Pilkington & Percival 1999). These studies showed that there was no correlation between iron content and magnetic

susceptibility. Explanations for this include the competition of paramagnetic ferrosilicates in the partitioning of iron, typically at the detriment of magnetite. In addition to this, sulphur is often ubiquitous in mafic and ultramafic rocks, favouring the formation of pyrrhotite over magnetite (Williams et al. 1985).

Proterozoic-aged, mylonitized granitic gneisses which are considered contemporaneous with the NNMB have been identified as highly magnetic in the Dronning Maud Land (DML) of Antarctica (Corner 1989). These rocks have been proposed as the source for the BMA, as they are considered the source for similar Proterozoic-aged craton-parallel, long wavelength (30-40 km) magnetic anomalies of between -300 to 500 nT (Corner 1989).

Reconstructions of Gondwana place the East Antarctic Grunehogna craton adjacent to the Kaapvaal (see Figure 31) and the continuity between the Grunehogna magnetic anomalies is consistent with the BMA set of anomalies (Corner 1989) as shown in Figure 31. This continuity has been used subsequently by numerous authors to support a pre-Gondwanan continental configuration (de Beer & Meyer 1983, Corner 1989, Jacobs et al. 1999, Groenewald et al. 1991, Golynsky & Jacobs 2001, Jacobs et al. 2003, Jokat et al. 2003, Bauer et al. 2003, Golynsky 2007).

In absence of any direct evidence indicating a definite source lithology for the BMA, magnetite bearing mylonitized granitic units such as those proposed by Corner 1989, in the shape approximated by the MC-1 model, are proposed as a plausible source for the BMA.

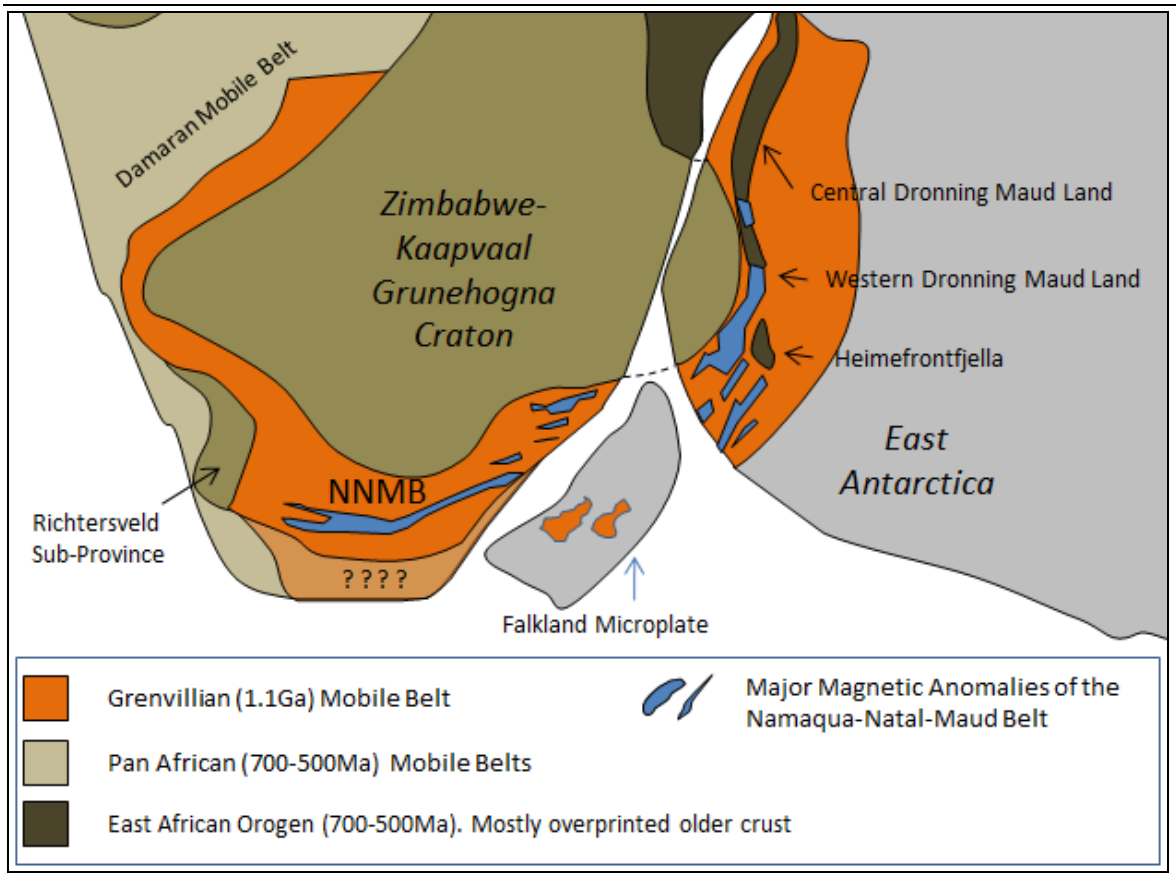

Figure 31: A Southern Gondwana reconstruction showing the spatial correlation of the crustal scale magnetic anomalies and the proposed Proterozoic Mobile Belt that flanks the Zimbabwe, Kaapvaal and Grunehogna cratons (simplified from Golynsky & Jacobs 2001).

5.7.1 Discussion: Forward Models LC-1 and LC-2

The BMA is the longest terrestrial magnetic anomaly on earth. It is unique in that it retains a relatively homogeneous magnetisation across a strike length of 1000 km. This fact alone should perhaps be the primary focus of future studies concerning the anomaly, i.e. what singular event or lithological source could result in relatively homogeneous magnetisation at this scale?

The portion of the crust traversed by the AKGT geophysical experiments has experienced multiple episodes of tectonism, involving accretion, reactivation and inversions which have occurred along zones of structural anisotropy within the crust. Regardless, or as a result of this, the BMA exists. Zones of structural anisotropy in this portion of the crust follow an east-west strike parallel to that of the BMA and appear to have influenced the evolution and position of the Neoproterozoic Kango and Kaaimans Group inliers within the Cape Fold Belt as well as the more recent Mesozoic-aged Uitenhage and Enon Basins (Dingle et al. 1983, de Wit & Ransome 1992, Rozendaal et al. 1999, Paton & Underhill 2004). Furthermore; rhealogical differences and lithospheric buckling within the crust hosting the BMA and the SCCB have been proposed as determining the axial depocentres of the Cape and Karoo Basins (Catuneanu 2004,

Cloetingh et al. 1992, Tankard et al 2009, Cole 1992). Further to the east the long wavelength magnetic anomalies that are considered by Thomas et al. (1992) as contemporaneous with the main the Beattie anomaly are parallel to tectonic sutures in the Natal sector of the NNMB which may indicate a structural relationship to the accretion of the Natal sector of the NNMB.

In addition the fact that the main limb of the BMA disappears below the Cape Syntaxis in the west may indicate the source was either buried beyond the Curie Isotherm along this orogenic front, or that the magnetic minerals were destroyed by the same tectonic event.

Models LC-1 and LC-2 propose that this collinear relationship between the BMA and major tectonic boundaries can be explained through thermoviscous remanent magnetisation (TVRM). TVRM can be acquired through tectonic uplift of a lower crustal model through the Curie Isotherm. Numerous features of the BMA support such an interpretation, the most significant of which is that it is arguable whether a single source lithology (rich in magnetite) can remain homogeneous across such a strike length. It is perhaps more likely that a tectonic event, most likely during the Kibaran, could have resulted in the uplift of a granulite terrane in both the Heimefrontfjella and across the southern margin of the Namaqua and Natal Mobile Belts. This uplift could have provided the granulite terrane an opportunity to obtain TVRM.

TVRM has been proposed as a source for long wavelength anomalies measured at both aeromagnetic as well as satellite altitudes (Pullaiah et al. 1975, Williams et al. 1985, Dunlop 1995, Kletetschka & Stout 1998, Yu & Tauxe 2006, McEnroe et al. 2009). Estimates on the potential additional contribution of this TVRM to a rock's net magnetisation vary between 20 % (Shive & Fountain 1988) to an order of magnitude higher than the natural remanent magnetisation itself (Kletetschka & Stout 1998). Recent studies have also shown that hematite-ilmenite intergrowths are particularly strong carriers of this remanent magnetisation and have a deeper Curie Isotherm associated with them, allowing for lower crustal sources as modeled (McEnroe et al. 2004, McEnroe et al. 2009, Puruker & Clark 2010).

Models LC-1 and LC-2 were generated to test whether a lower crustal model could fit the measured BMA response. In this respect the lower crustal interpretation by Lindeque and de Wit (2009) based on the NVR section provided an appropriate forward model geometry that satisfied this requirement very well.

5.7.2 Conclusions: Forward Models MC-1 and LC-1

In a recent publication; Lindeque et al. (2011) propose that two portions of elevated seismic reflectivity and adjacent anomalous conductivity located beneath the surface maximums of the BMA are the anomaly's source. In contrast to this; modelling completed for this thesis use two forward models to present alternate arguments regarding the potential source of the BMA. Model MC-1 utilizes a volumetrically large mid-crustal block of intermediate susceptibilities and LC-1 utilizes a thin lower crustal sliver of high susceptibilities, located between the Curie isotherms of magnetite and hematite.

The model MC-1 proposed here incorporates the reflectors identified by Lindeque et al. (2011) as the crustal source for the BMA. However; all modelling completed for this thesis has shown that a significantly larger and wider crustal volume is required. The crustal location of a source for a magnetic anomaly cannot be inferred from the position of the magnetic maximums at surface. This is in part due to the inclination of the regional field. Modelling completed for this thesis shows that a minimum width of the crustal source required to fit the measured BMA data must be 70 km and most likely extends southwards beneath the Cape Fold Belt. Model MC-1 includes the portions of high reflectivity identified by Lindeque et al. (2011) and also includes a larger portion of high reflectivity beneath the Cape Fold Belt, present at 10-30 km depth. This crustal unit correlates with a broad and diffuse zone of high electrical conductivity identified by Weckmann et al. (2007)[a].

Considering the size of the body modelled by the MC-1 unit; it is proposed that a large plutonic metamorphic protolith, extending south beneath the Cape Fold Belt, with a significant magnetite content, most probably concentrated along shear zones, is a more realistic lithology for the volume required by the forward model MC-1. This has been proposed previously for the Heimefrontfjella magnetic anomalies (Corner 1989).

In contrast to this; model LC-1 presents an alternative model source of magnetisation. It is understood that magnetic minerals can be created and then magnetised at different times. A lower crustal model is used to present two alternative sources for the BMA's magnetisation other than pure induced magnetisation. Proximity of the model LC-1 to the Curie Isotherm allows for the influence of the Hopkinson Effect. At temperatures approaching Curie both the number and mobility between domain walls within multidomain grains as well as thermal activation of single domain magnetite increases dramatically (up to 3x) leading up to the Curie temp and before randomization of the moments occur (Hunt et al 1995). This proximity to the Curie isotherm is met by the marginal location of the magnetic models NVR-i,-j to the Curie Isotherm and has been proposed as a source of long wavelength anomalies elsewhere (Dunlop 1995).

Alternatively; tectonism affecting the mid to lower crust and resulting in its uplift through the Curie Isotherm presents a significant opportunity for this crustal portion to obtain thermoviscous or burial magnetisation (Pullaiah et al. 1975, McEnroe et al. 2009, Puruker & Clark 2010). This uplift could have occurred along the unexposed southern portion of the NNMB, of which the Namaquan and Natal sectors share a common Kibaran tectonothermal history. Alternatively this uplift could have occurred during the Cape Orogeny. This argument is a unique explanation for the lateral continuity of the BMA

5.8 Recommendations

Modelling the lower limits of the forward models would have been aided by an updated calculation of the Curie Isotherm for the crustal portion modelled. This would allow the lower crustal model (LC-1) to be tested and would guide future modelling exercises and rule out portions of the MT, NVR or WRR vertical sections.

Future modelling should utilise a profile that captures the entire wavelength of the BMA including the magnetic lows. Also, additional filters (such as first vertical derivatives, upward continuation, analytical signal etc) would further characteristics of the BMA local field.

Any future forward models will remain unproven in the absence of direct borehole data. In this respect, deep drilling of the main limb of the BMA will remain a highly risky (if not impossible) enterprise, given the lack of constraint regarding the depth extent of its upper surface. It is recommended that the three component ground magnetic data be collected from the completed MT datasets completed across the Beattie anomaly (along profiles MT-1,2 and MT-4). This should help quantify the vectoral components of the anomaly and may assist in the calculation of depth-to-source estimates from the magnetic data (Abdelrahman & Sharafeldin 1996, Cooper 2006).

Additionally, a lower risk drill target would be to drill another limb of the Beattie set of anomalies which runs directly beneath Port St. Johns (Figure 1). Here the overlying Natal Group and Karoo sediments are at their thinnest and the Dwyka Group outcrops along the coast, this may represent a significantly thinner overburden to drill.

Another alternative project would be to undertake a program of detailed structural mapping in Natal with a primary focus on obtaining magnetic susceptibility readings from outcropping Tugela and Mzumbe and Margate Terrane units. This would provide direct observations and could shed some light on potential source lithologies for the BMA.

References

Abdelrahman, E.M. & Sharafeldin, S.M., 1996, An iterative least-squares approach to depth determination from residual magnetic anomalies due to thin dykes, Journal of Applied Geophysics, vol 34, pp 213-220

Aravamadhu, P.S., 1974, Certain aspects of magnetic studies of charnokites at Waltair, India, Field Investigations, Canadian Journal of Earth Science, Vol 11/4, pp 503 - 509

Arndt, N.T., Todt, W., Chauvel, M., Tapfer, M. & Weber, K., 1991, U-Pb zircon age and Nd isotopic composition of granitoids, charnockites and suprcrustal rocks from Heimefrontfjella, Antarctica, Geologische Rundschau, Vol 80, pp 759 - 777

Barsoukov, E, & Macdonald, J.R. (editors), 2005, Impedance Spectroscopy, Theory, Experiment and Applications, *John Wiley and Sons, New York, United States of America*.

Bauer, W., Thomas, R.J. & Jacobs, J., 2003, Proterozoic-Cambrian history of Dronning Maud Land in the context of Gondwana assembly. In: Proterozoic East Gondwana: Supercontinent Assembly and Breakup, eds: Yoshida, M., Windley, B.F. & Dasgupta, S., Geological Society of London, Special Publication, Vol 206, pp 247 - 269

Bauer, W., Jacobs, J., Thomas, R.J., Spaeth, G. & Weber, K., 2009, Geology of the Vardeklettane Terrane, Heimefrontfjella (East Antarctica), Polaforschung, Vol 79, pp 29 - 32

Beattie, J., 1909, Report of the magnetic survey of South Africa, Royal Society of London, Cambridge University Press, United Kingdom.

Borradaile, G.J. & Henry, B., 1997, Tectonic applications of magnetic susceptibility and its anisotropy, Earth Science Reviews, Vol 42, pp 49 - 93

Bowen, N.L. & Tuttle. O.F., 1949, The system MgO-SiO_2-H_2O. Geological Society of America, Bulletin 60, pp 439 - 460

Branch, T.C., Ritter, O., Weckmann, U., Sachsenhofer, R.F. & Schilling, F., 2007, The Whitehill Formation – a high conductivity marker horizon in the Karoo Basin, South African Journal of Geology, Vol 110 2/3, pp 465 - 476

Bräuer , B., Ryber, T. & Lindeque, A.S., 2007, Shallow seismic velocity structure of the Karoo Basin, South Africa, South African Journal of Geology, Vol 110, pp 439 - 448

Broquet, C.A.M., 1992, The sedimentary record of the Cape Supergroup: A review, In: Inversion tectonics of the Cape Fold Belt, Karoo and Cretaceous Basins of Southern Africa, de Wit & Ransome (eds), pp 159 - 184

Buffett, B.A., 2000, Earth's core and the geodynamo, Science, Vol 288, pp 2007-2012

Butler, R.F., 1992, Paleomagnetism, Magnetic Domains to Geological Terranes, Boston Blackwell Scientific Publications, 2004 edition available freely online: http://www.pmc.ucsc.edu/~njarboe/pmagresource/ButlerPaleomagnetismBook.pdf

Campbell, W.C., 1997, Introduction to geomagnetic fields, Cambridge University Press

Carte, A.E. & van Rooyen, A.I.M., 1969, Further measurements of heat flow in South Africa, Upper Mantle Project, Geological Society of South Africa, Special Publication, Vol 2, pp 445 - 448

Catuneanu, 2004, Basement control on flexural profiles and the distribution of the foreland facies: The Dwyka Group of the Karoo Basin, South Africa, Geology, Vol 32, pp 517 – 520

Catuneanu, O., Wopfner, H., Eriksson, P.G., Carirncross, B., Rubidge, B.S., Smith, R.M.H. and Hancox. P.J., 2005, The Karoo basins of South-central Africa, Journal of African Earth Sciences, Vol 43, pp 211-253

Chinnasamy, C.N., Narayanasamy, A., Ponpandian, N., Joseyphus, R.J., Jeyadevan, B., Tohji, K., Chattopadhyay, K., 2002, Grain size effect on the Neel temperature and magnetic properties of nanocrystlaline $NiFe_2O_4$ spinel, Journal of Magnetism and Magnetic Minerals, Vol, 238, pp 281-287

Clark, D.A., 1997, Magnetic petrophysics and magnetic petrology; aids to geological interpretation of magnetic surveys. AGSO Journal of Australian Geology and Geophysics, Vol 17, pp 83-103

Clark, D.A., 1999, Magnetic petrology of igneous intrusions: implications for exploration and magnetic interpretation, Exploration Geophysics, Vol 30, pp 5 - 26

Cloeting, S., Lankreijer, A., de Wit, M.J. & Martinez, I., 1992, Subsidence history analysis and forward modeling of the Cape and Karoo Supergroups. In: Inversion

tectonics of the Cape Fold Belt, Karoo and Cretaceous Basins of Southern Africa, de Wit & Ransome (eds), pp 239-248

Coetzee, 1981, Style and intensify of deformation in the Cape and Karoo rocks from Meirings Porrt to Beaufort West along 22.5degrees E, Abstract from Geocongress, South African Geodynamics Project

Cole, D.T., 1992, Evolution and development of the Karoo Basin, In: Inversion tectonics of the Cape Fold Belt, Karoo and Cretaceous Basins of Southern Africa, de Wit & Ransome (eds), pp 87 - 100

Cole, D.T. & McLachlan, I.R., 1991, Oil potential of the Permian Whitehill shale formation in the main Karoo basin, South Africa, Gonwana Seven Proceedings, pp 391 – 406, Sao Paolo, Brazil

Cole, D.T., & McLachlan, I.R., 1994, Oil shale potential and depositional environment of the Whitehill Formation in the main Karoo Basin, SOEKOR, now PASA, South African Petroleum Agency, Cape Town, Unpublished Report, No 1994-0213

Coles, R.L. & Currie, R.G., 1977, Magnetic anomalies and rock magnetisations in the southern Coast Mountains, British Columbia: possible relation to subduction, Canadian Journal of Earth Sciences, Vol 14/8, pp 1753 - 1770

Cooper, G.R.J., 1997, Forward modeling of magnetic data, Computers and Geosciences, Vol 23, pp 1125 – 1129

Cooper, G.R.J, 2006, Obtaining dip and susceptibility information from Euler deconvolution using the Hough transform, Computers and Geosceinces, Vol 32, pp 1592 -1599

Cornell, D.H., Thomas, R.J., Moen, H.F.G., Reid, D.L., Moore, J.M. & Gibson, R.L., 2006, The Namaqua Natal Province, In: Geology of South Africa, pp 325 - 379

Corner, B., 1989, The Beattie anomaly and its significance for crustal evolution within a Gondwana Framework, Congress of South African Geophysical Association, pp 15 – 17

Davis, A., 1978, The reflectance of coal, in C. Karr, Jr., ed., Analytical methods for coal and coal products, v. 1: New York, Academic Press, p. 27-81.

De Beer, J.H. & Gough, D.I., 1980, Conductive structures in the southernmost Africa, a magnetometer array study, Geophysical Journal of the Royal Astronomical Society, Vol 63, pp 470 – 495

De Beer, J.H. & Meyer, R., 1983, Geoelectrical and gravitational characteristics of the Namaqua-Natal Mobile Belt and its boundaries. Special Publication of the Geological Society of South Africa, Vo 10, pp 91 - 100

De Beer, J.H., 1983, Geophysical studies in the Southern Cape Province and models of the lithosphere in the Cape Fold Belt, In: Geodynamics of the Cape Fold Belt, eds: Sohnge, A.P.G. and Hälbich, I.W., a Special publication of the geological society of South Africa, pp 57-64

De Beer, J.H., van Zijl, J.S.V. & Gough, D.I., 1982, The Southern Cape Conductive Belt (South Africa): its composition, origin and tectonic significance, Tectonophysics, Vol 83, pp 205 - 225

De Wit, M.J., 1992, The Cape Fold Belt: A challenge for an integrated approach to inversion tectonics, In: Inversion tectonics of the Cape Fold Belt, Karoo and Cretaceous Basins of Southern Africa, de Wit & Ransome (eds), pp 3 - 14

De Wit, M.J. & Horsfield, B., 2007, Built on the shoulders of Alfred Wegener and Alex du Toit to apply German precision technology to the geological superlatives of South Africa, South African Journal of Geology, Vol 110 2/3, pp 165 - 174

Dingle, R.V., Siesser, W.G. & Newton, A.R. (1983) Mesozoic and Tertiary Geology of Southern Africa. Balkema, Rotterdam.

Dow, W.G., 1977, Kerogen studies and geological interpretations: Journal of geochemical exploration, Vol 7, pp 79-99

Duane, M.J., & Brown, R., 1992, Geochemical open-system behaviour related to fluid-flow and metamorphism in the Karoo, In M.J. de Wit and I.G.D. Ransome (editors), Inversion tectonics of the Cape Fold Belt, Karoo and Cretaceous Basins of South Africa, Balkema, Rotterdam, the Netherlands, pp 127-140

Duba, A., Huenges, E., Nover, G. and Will, G., 1988, Impedance of black shale from Munsterland 1 borehole: an anomalously good conductor, Geophysical Journal, Vol 94, pp 413-419

Duba, A., Heinkamp, S., Meurer, W., Nover, G. & Will, G., 1994, Evidence from borehole samples for the role of accessory minerals in lower crustal conductivity, Nature, 367, 59-61

Dunlop, D.J., 1995, Magnetism in Rocks, Journal of Geophysical Research, Vol 100, pp 2161 - 2174

Du Plessis, A., Thomas, R.J., 1991, Discussion on the causative bodies of the Beattie-set of magnetic anomalies. Ext. Abstr. South African Geophysical Association, Second Technical Meeting, Johannesburg: 57-59

Eglington, B.M., 2006, Evolution of the Namaqua-Natal Belt, southern Africa – A geochronological and isotope geochemical review. Journal of African Earth Sciences, Vol 46, pp 93 - 111

Eglington, B.M. & Armstrong, R.A., 2003, Geochronological and isotopic constrains on the Mesoproterozoic-Natal Belt; evidence from deep borehole intersections in South Africa, Precambrian Research, Vol 125, pp 179 – 189

Fatti, J.L. and Du Toit, J.J.L., 1970, A regional reflection-seismic line in the Karoo basin near Beaufort West. *Transactions of the Geological Society of South Africa*, Vol 73, pp 17-28.

Fouche, J., Bate, K.J. & van der Merwe, R., 1992, Plate tectonic setting of the Mesozoic Basins, southern offshore, South Africa: A review, In: Inversion tectonics of the Cape Fold Belt, Karoo and Cretaceous Basins of Southern Africa, de Wit & Ransome (eds), pp 33 – 48

Golynsky, A. & Jacobs, J., 2001, Grenville-agr versus Pan-African Magnetic Anomaly Imprints in Western Dronning Maud Land, East Antarctica, Journal of Geology, 2001, Vol 109, pp 136 - 142

Golynsky, A., Grikurov, G.E. & Kamenev, E.N., 2000, Geological significance of regional magnetic anomalies in Coats Land and Western Dronning Maud Land, Polarforschung, vol 67/3, pp 91 – 99

Golynsky, A., 2007, Magnetic anomalies in East Antarctica: a window on major tectonic provinces, USGS publication, 10th Internation Symposium on Antarctic Earth Sciences

Gough, D.I., 1963, Heat floe in the southern Karoo, Proceeds of the Royal Society of London, Vol A272, pp 207 - 230

Gose, W.A., Johnston, S.T. & Thomas, R.J., 2004, Age of magnetisation of Mesoproterozoic rocks from the Natal sector of the Namaqua-Natal belt, South Africa, Journal of African Earth Sciences, Vol 40, pp 137 - 145

Gough, D.I., 1973, Possible linear plume under southernmost Africa, Nature, Vol 245, pp 94 - 94

Gough, D.I., De Beer, J.H. & van Zijl, J.S.V., 1973, A magnetometer array study in Southern Africa, Gephysical Journal of Royal Astronomical Society, Vol 34, pp 421-433

Grantham, G.H., Thomas, R.J., & Mendonidis, P., 1994, Contrasting P-T-t loops from southern East Africa, Natal and East Antarctica, Journal of African Earth Sciences, Vol 19/3, pp 225 – 235

Grantham, G.H., Allen, A.R., Cornell, D.H. & Harris, C., 1996, Geology of Nicholson's Point granite, Natal Metamorphic Province, South Africa: the chemistry of charnokitic alteration and origin of the granite, Journal of African Earth Sciences, vol 23, pp 465 - 484

Gresse, P.G., Theron, J.N., Fitch, F.J. & Miller, J.A., 1992, Tectonic inversion and radiometric restting of the basement in the Cape Fold Belt, In: Inversion tectonics of the Cape Fold Belt, Karoo and Cretaceous Basins of Southern Africa, de Wit & Ransome (eds), pp 217-228

Groenewald, P.B., Grantham, G.H. & Watkeys, M.K., 1991, Geological evidence for a Proterozoic to Mesozoic link between southeastern Africa and Dronning Maud Land, Antarctica, Journal of the Geological Society, London, Vol 148, pp 1115 - 1123

Hälbich, I.W., 1983, A Tectonogenesis of the Cape Fold Belt (CFB), In: Geodynamics of the Cape Fold Belt, eds: Sohnge, A.P.G. and Hälbich, I.W., a Special publication of the geological society of South Africa, pp 165-176

Hälbich, I.W., 1993, Cape Fold Belt –Agulhas Bank Transect across Gondwana suture in Southern Africa, American Geophysical Union Special Publication, Vol 202, pp 18

Hälbich, I.W., 1992, The Cape Fold Belt Orogeny: State of the art 1970s-1980s, In: Inversion tectonics of the Cape Fold Belt, Karoo and Cretaceous Basins of Southern Africa, de Wit & Ransome (eds), pp 141 – 158

Hälbich, I.W., 1993, (Compiler) Global Geoscience Transect 9. The Cape Fold Belt – Agulhas Bank transect across Gondwana Suture, Southern Africa, American Geophysical Union Special Publication, 202, 18pp

Hälbich, I.W. & Swart, J., 1983, Structural zoning and dynamic history of the cover rocks of the Cape Fold Belt, In: Geodynamics of the Cape Fold Belt, eds: Sohnge, A.P.G. and Hälbich, I.W., a Special publication of the geological society of South Africa, pp 75 - 100

Hales, A.L. & Gough, D.I., 1960, Geophysical Journal of the Royal Astronomical Society, Vol 3 pp 225-236

Harrison, R.J., Dunin-Borkowski, R.E. & Putnis, A., 2002, Direct imaging of nanoscale magnetic interactions in minerals, Proceedings of the National Academy of Sciences, Vol 99/26, pp 16556-16561

Harvey, J.D., de Wit, M.J., Stankiewicz, J., Doucoure, C.M., 2001, Structural variations of the crust in the Southwestern Cape, deduced from seismic receiver functions, South African Journal of geology, C 104, pp 231-242

Hunt, C.P., Moskowitz, M. & Banerjee, S.K., 1995, Magnetic properties of rocks and minerals, In: Rock Physics and Phase Relations, A Handbook of physical constants, eds: Ahrens, T.J., AGU Reference Shelf 3

Jacobs, J. & Thomas, R.J., 1994, Oblique collision at about 1.1Ga along the southern margin of the Kaapvaal continent, south-east Africa, Geologiesche Rundschau, Vol.83, pp 322-333

Jacobs, J., Thomas, R.J. & Weber, K. 1993, Accretion and indentation tectonics at the southern edge of the Kaapvaal craton during the Kibaran (Grenville) orogeny, Geology, Col 21, pp 203-206

Jacobs, J., Hanse, B., Henjes-Kunst, F., Thomas, R.J., Weber, K., Armstrong, R.A. and Cornell, D., 1999, New age constraints on the Proterozoic/lower palaeozoic evolution of Heimefrontfjella, East Antarctica, and its bearing on Rodinia and Gondwana correlations, Terra Antarctica,Vol 6, pp 377 – 389

Jacobs, J., Fanning, C.M. & Bauer, W., 2003, Timing of Grenville-age vs Pan-African medium- to high grade metamorphism in western Dronning Maud Land (east Antarctica) and significance for correlations in Rodinia and Gondwana, Precambrian Research, Vol 125, pp 1 – 20

Johnson, M.R., 1991, Sandstone petrography, provenance and plate tectonic setting in Gondwana context of the southeastern Cape-Karoo Basin, South African Journal of Geology, Vol 94 2/3, pp 137 – 154

Johnson, M.R., van Vuuren, C.J., Visser, J.N.J., Cole, D.I., Wickens, H. De. V., Christie, A.D.M. and Roberts, D.L., 1997, The Foreland Karoo Basin, South Africa, in Sedimentary Basins of the World, Vol 3, pp 269-317

Jokat, W., Boebel, T., Konig, M. & Meyer, U., 2003, Timing and geometry of early Gondwana breakup, Journal of Geophysical Research Vol 108, pp 1 - 13

Juckes, L.M., 1968, The geology of Mannefallknausane and part of Vestfjella, Dronning Maud Land, British Antarctic Survey Bullentin, Vol 18, pp 65 - 78

Kletetschka, G. & Stout, J.H., 1998, The origin of magnetic anomalies in the lower crustal rocks, Labrador, Geophysical Research Letters, Vol 25, pp 199 - 202

Kribek, B., Hrabal, J., Landais, P., Hladikova, J. 1994. The association of poorly ordered graphite, coke and bitumens in greenschist facies rocks of the Ponikl Group, Lugicum, Czech Republic: the results of graphitization of various types of carbonaceous matter. J. metamorphic Geol., 12, 493-503.

Le Roux, J.P & Brynard, H.J., 1994, A strategy for uranium exploration in the Permo-Triassic Beaufort Group of the Main Karoo Basin, South Africa, Journal of Africa Earth Sciences, Vol 18/3, pp 245 - 253

Lindeque, A.S,, Ryberg, T., Stankiewicz, J., Weber, M.H. & de Wit, M.J., 2007, Deep crustal seismic reflection experiment across the Southern Karoo Basin, South Africa, South African Journal of Geology, Vol 110 2/3, pp 407-418

Lindeque, A.S. & de Wit, M.J., 2009, Revealing the Beattie Magnetic Anomaly and the anatomy of the crust of southernmost Africa: Geophysics and deep subsurface geology where the Cape Fold Belt and Karro Basin meet, 11th SAGA Biennial Technical Meeting and Exhibition, Swaziland, 16-18 September 2009, pp 490-499

Lindeque, A., de Wit, M.J., Ryber, T., Weber, M. & Chevallier, I., 2011, Deep crustal profile across the southern Karoo Basin and Beattie Magnetic Anomaly, South Africa: An intergrated interpretation with tectonic implications, South African Journal of Geology, Vol 114, pp 265-292

Macmillan, S. & Maus, S., 2005, International Geomagnetic Reference Field – The tenth generation, Earth Planets Space, Vol57, pp 1135 - 1140

McElhinney, M.W. & Senanayake, W.E., 1980, Palaeomagnetic evidence for the existence of the geomagnetic field 3.5Ga Ago, Journal of Geophysical Research, Vol 85, pp 3523.

McEnroe, S.A., Langenhorts, F., Falko, L., Robinson, P., Bromiley, G.D. & Shaw, C.S.J., 2004, What is magnetic in the lower crust, Earth and Planetary Science Letters, Vol 226, 1-2, pp 175-192

McEnroe, S.A., Fabian, K., Robinson, P. & Brown, L., 2009, Remanent Magnetisation in Crustal Rocks, ESA 2nd SWARM International Science Meeting Abstract, http://www.congrex.nl/09c24/S2_Posters/S2_P06_McEnroe_paper.pdf

Mougenot, D., Gennesseaux, M., Hernandez, J., Lepvrier, C., Malod, J.A., Raillrd, S., Vanney, J.R. & Villeneuve, M., 1991, La ride du Mozambique (Ocean Indien): un fragment continental individualise lors du coulissement de l'Amerique et de l'Antarctique le long de l'Afrique de l'Erst? – Geodynamics, 312/II; pp. 665-662

Nabighian, M.N., Grauch, V.J.S., Hansen, R.O., LaFehr, T.R., Li, Y., Peirce, J.W., Phillips, J.D. & Ruder, M.E., 2005, The historical development of the magnetic method in exploration, Geophysics, Vol 70/6, pp 33-61

Nakamura, N. & Borradaile, G.J., 2004, Metamorphic control of magnetic susceptibility and magnetic fabrics: a 3-D projection, In: Magnetic Fabri: Methods and Applications, Eds: Martin-Hernandez, F., Lunebürg, C.M., Aubourg, C. & Jackson, M., Geological Society of London, Special Publication, Vol 238, pp 61 - 68

Newton, A.R., 1992, Thrusting on the northern margin of the Cape Fold Belt, near Laingsburg, In: Inversion tectonics of the Cape Fold Belt, Karoo and Cretaceous Basins of Southern Africa, de Wit & Ransome (eds), pp 193 - 197

Nicolaysen, L.O. & Burger, A.J., 1965, Note on an extensive zone of 1,000 million year old metamorphic and igneous rocks in southern Africa, Sceinces Terre, Vol 10, pp 497 - 518

Parsiegla, N., Gohl, K. and Uenselmann-Neben, G., 2007, Deep Crustal structure of the sheared South African continental margin; first results of the Agulhas-Karoo Geoscience Transect, South African Journal of Geology, Vol 110 (2/3), pp. 393-406.

Paton, D.A. & Underhill, J.R., 2004, Role of crustal anisotropy in modifying the structural and sedimentological evolution of extensional basins: the Gamtoos Basin, South Africa, Basin Research, Vol 16, pp 339 - 359

Paton, D.A., Macdonald, D.I.M., and Underhill, J.R., 2006, Applicability of thin or thick skinned structural models in a region of multiple inversion episodes; southern South Africa, Journal of Structural Geology, Vol 28, pp 1933 - 1947

Pilkington, M., Percival, J.A., 1999, Crustal magnetisation and long-wavelength aeromagnetic anomalies of the Minto Block, Quebec, Journal of Geophysical Research, Vol 104, pp 7513 - 7526

Pitts, B.E., Maher, M.J., De Beer, J.H. & Gough, D.I., 1992, Interpretation of magnetic, gravity and magnetotelluric data across the Cape Fold Belt and Karoo Basin, In: Inversion tectonics of the Cape Fold Belt, Karoo and Cretaceous Basins of Southern Africa, de Wit & Ransome (eds), pp 27- 32

Popov, O., Sanchez, J.L., Rachev, P., Leccabue, F., Mikhov, M., 1991, The Hopkinson effect in $BaFe_{12}O_{19}$ fine particles, Journal of Applied Physics, Vol 69, Issue 8, pp5148-

Pous, J., Munoz, G., Heise, W., Melgarejo, J.C. and Quesada, C., 2004, Electromagnetic imaging of Variscan crustal structures in southwest Iberia: The role of interconnected graphite. Earth and Planetary Science Letters, Vol, 217, pp 435-450

Pullaiah, G.E., Irving, K.L., Buchan, & Dunlop, D.J., 1975, Magnetisation changes caused by burial and uplift, Earth Planet and Science Letters, Vol 28, pp 133-143

Puruker, M.E. & Clark D.A., 2010 in press, Interpretation of the lithospheric magnetic field, Geophysical Journal International

Quesnel, Y., Weckmann, U., Ritter, O., Stankiewicz, J., Lesur, V., Mandea, M., Langlais, B., Sotin, C. & Galdeano. A., 2009, Simple models for the Beattie Magnetic Anomaly in South Africa, Tectonophysics, Vol 478, pp 111-118

Rasmussen, P. and L.B. Pedersen, 1979. End correction in potential field modeling. Geophys. Prospecting, 27: 749-760

Reid, D.L., 1997, Sm-Nd age and REE geochemistry of Proterozoic arc-related igneous rocks in the Richtersveld Subprovince, Namaqua Mobile Belt, Southern Africa, Journal of African Earth Sciences, Vol 24, pp 621 - 633

Ritter, O., Haak, V., Rath, V., Stein, E. & Stiller, M., 1999, Very high electrical conductivity beneath the Munchberg Gneiss area in Southern Germany: implications for horizontal transport along shear planes, Geophysical Journal International, Vol 139, pp 161-170

Ritter, O., Weckmann, U. & Tietze, K., 2009, Electrical conducvity of the Cape Fold Belt, 11th SAGA Biennial Technical Meeting and Exhibition, Abstract, pp 481 - 485

Rozendaal, A., Gresse, P.G., Scheepers, R. & Le Roux, J.P., 1999, Neoproterozoic to Early Cambrian crustal evolution of the Pan-African Saldania Belt, South Africa, Precambrian Research, Vol 97, pp 303 - 323

Rudnick, R.L. & Fountain, D.M., 1995, The Nature and composition of the continental crust: a lower crustal perspective, Reviews of Geophysics, Vol 33, pp 267 - 309

Shive, P.N. & Fountain, D.M., 1988, Magnetic Mineralogy in an Archaean crustal cross section: implications for crustal magnetism, Journal of Geophysical Research, Vol 93, pp 12177 - 12186

Shive, P.N., Blakely, R.J., Frost, B.R. & Fountain, D.M., 1992, Magnetic properties of the lower continental crust, in Continental Lower Crust, edited by Fountain, D.M., Arculus, R. & Kay, R.W., pp 145-177, Elsevier, New York

Shone, R.W. & Booth, P.W.K., 2005, The Cape Basin, South Africa, A review, Journal of African Earth Sciences, Vol 43, pp 196-210

Simpson, F., and Bahr, K., 2004, *Practical Magnetotellurics*, Cambridge University Press

Sleep, N.H. & Fujita, K., 1997, Principles of Geophysics, Blackwell Science,

Smith, J., 1995, Understanding telluric distortion matrices, Geophysical Journal International, Vol 122, pp 219 - 226

SOEKOR (Southern Oil Exploration Corporation), 1966, Borehole Log KA1/66, from Council for Geoscience Library, Pretoria, South Africa

SOEKOR (Southern Oil Exploration Corporation), 1966, Borehole Log KW1/67, from Council for Geoscience Library, Pretoria, South Africa

SOEKOR (Southern Oil Exploration Corporation), 1966, Borehole Log CR1/68, from Council for Geoscience Library, Pretoria, South Africa

Stach, E., Taylor, G.H., Mackowsky, M.-Th., Cjamdra, D., Teichmuller, M. and Teichmuller, R., 1982, Stacj's Textbook of Coal Petrology, 3rd Edition, Gebruder Borntrager, Berlin, Germany, pp 535

Stankiewicz, J., Ryberg, T., Schulze, A., Lindeque, A., Weber, M.H. & de Wit, M.J., 2007, Initial results from wide-angle seismic refraction lines in the Southern Cape, South African Journal of Geology, Vol 110 2/3, pp 407-418

Stankiewicz, J., Parsiegla, N., Ryber, T., Gohl, K., Weckmann, U., Trumbull, R. & Weber, M., 2008, Crustal structure of the southern margin of the African continent:

Results from geophysical experiments, Journal of Geophysical Research, Vol 113, pp 1 - 15

Stesky, R.M. & Brace, W.F., 1973, Electrical conductivity of serpentinized rocks to 6 kilobars, Journal of Geophysical Research, Vol 78, pp 7614 - 7621

Tankard, A., Welsink, H., Aukes, P. & Stettler, E., 2009, Tectonic evolution of the Cape and Karoo basins of South Africa, Marine and Petroleum Geology, Vol 26, Issue 8, pp 1379-1412

Teichmüller, M., Teichmüller R and Weber, M., 1979, Inkohlung and Illit-Kristallinitat (Vergleichende Untersuchungen im Mesozoikum und Palaosoikum von Westfalen). Fortschirtte der Geologie Rheinland und Westfalen, 27, 201-276

Telford, W.M., Telfrod, L.P., Geldart, R.E., Sheriff, R.E. (1990), Cambridge University Press

Thomas, R.J., Du Plessis, A., Fitch, F.J., Marshall, C.G.A., Miller, J.A., von Brunn, V., & Watkeys, M.K., 1992, Geological studies in southern Natal and Transkey : implications for the Cape Orogeny, In: Inversion tectonics of the Cape Fold Belt, Karoo and Cretaceous Basins of Southern Africa, de Wit & Ransome (eds), pp 229 - 238

Thomas, R.J., Eglington, B.M., Bowring, S.A., Retief, E.A. and Walraven, F., 1993, New isotope data from a Neoproterozoic porphyritic granitoid-charnockite suite from Natal, South Africa, Precambrian Research, 62: 83-101.

Thomas, R.J., Agenbacht, A.L.D., Cornell, D.H. & Moore, J.M., 1994, The Late Kibaran of southern Africa; tectonic evolution and metallogeny, Ore Geology Reviews, Vol 9, pp 131 -160

Thomas, R.J., De Beer, C.H. & Bowring, S.A., 1996, A comparative study of the Mesoproterozoic late orogenic porphyritic granitoids of southwest Namaqualand and Natal, South Africa, Journal of African eEarth Sciences, Vol 23/3, pp 485 - 508

Toft, P.B., Scowen, P.A.H., Arkani-Hamed, J. & Francis, D., 1993, Demagnetisation by hydration in the Grenville province of Quebex, Canada: implications for magnetic anomalies of continental collision zones

Tomoquest.com, Magnetic surveying, Dr Marescot, Eidgenossische Technische Hochschule, Zurich, Online Manual, Magnetic Surveying, http://www.google.co.uk/url?sa=t&rct=j&q=&esrc=s&source=web&cd=4&ved=0CEYQFjAD&url=http%3A%2F%2Fwww.tomoquest.com%2Fattachments%2FFile%2FEEG_Mag

netic_Surveying.pdf&ei=XZtZUYMVhPvSBcDOgZAB&usg=AFQjCNH57FaFF9REhwK2p9SSONmlcY44wg&sig2=03laa7y2szNaLNTMA1tfcQ&bvm=bv.44442042,d.d2k&cad=rja

Van Zijl, J.S.V, 1979, A resistivity study of the Karoo basin (Abstract), Proceedings of the 18th Geological Congress, Geological Society of South Africa, Part1, pp 400 – 401

Van Zijl, J.S.V., 2006, A review of the resistivity structure of the Karoo Supergroup, South Africa, with emphasis on the dolerites: A study in anisotropy, South African Journal of Geology, Vol 109, pp 315-328

Visser, J.N.J., 1987, The palaeogeography of part of southwestern Gondwana during the Permo-Carbonigerous glaciations, Palaeogeography, Palaeoclimate, Palaeoecology, Vol 61, pp 205-219

Visser, J.N.J, 1992, Basin tectonics in southwestern Gondwana during the Carboniferous and Permian, In: Inversion tectonics of the Cape Fold Belt, Karoo and Cretaceous Basins of Southern Africa, de Wit & Ransome (eds), pp 109 - 116

Vozoff, K., 1991. *The magnetotelluric method*, In: Nabighian, M. N. (Ed.), Electromagnetic methods in applied geophysics, Volume 2, Application. SEG, Tulsa, pp. 641{711

[a] Weckmann, U., Ritter, O., Jung, A., Branch, T. & de Wit, M.J., 2007, Magnetotelluric measurements across the Beattie magnetic anomaly and the Southern Cape Conductive Belt, South Africa, Journal of Geophysical Research, Vol 112

[b] Weckmann, U., Jung, A., Branch, T. & Ritter, O., 2007, Comparison of electrical conductivity structures and 2D magnetic modeling along two profiles crossing the Beattie Magnetic Anomaly, South Africa, South African Journal of Geology, Vol 110 2/3, pp 449-464

Weckmann, U. & Branch, T.C., 2005, Comparing magnetic and magnetotellurics data for the Beattie Magnetic Anomaly, Conference Abstract; Electromagnetische Tiefe Forschung special publication

Williams, M.C., Shive, P.N., Fountain, D.M. & Frost, B.R., 1985, Magnetic properties of exposed deep crustal rocks from the Superior Province of Manitoba, Earth and Planetary Science Letters, Vol 76, pp 176 - 184

Yu, Y. & Tauxe, L., 2006, Acquisition of viscous remanent magnetisation, Physics of Earth and Planetary Interiors, Vol 159, pp 32 – 42.

Appendix 1 Vitrinite Reflectance

Results

Sample 1

Sample 1 contains very finely laminated sedimentary cycles down to sub-millimetre scales composed of fine and course grained laminations. Some of the course grained units may be a result of secondary recrystallization.

Certain layers are distinctly enriched in organic matter. Solid bitumen is commonly present along fractures and interstitially and around grain boundaries, particularly so within coarse grained units (See Figure 32). All reflectance values indicate a low metaanthracite stage for the visible organic carbon.

Sample 2

Sample 2 is a relatively poorly sorted shale with a unique population of organic matter composed of particles of variable size and bireflectance, ranging between metaanthracite to verging on graphitic. This spread of carbon rank is exhibited in Figure 10.

‘Graphitic’ particles are fine, anisotropic and distributed within a ‘peppery’ / disseminated mosaic texture and occasionally around sedimentary grains (See Figure 33). Large fragments of virtrinite and interstitial bitumen are also present, along with fine grained vitrinite particles from which true Rmax % were difficult to obtain. It is possible that carbon rank reaches true graphite.

Sample 3

Sample 3 contains sub-euhedral to euhedral pyritic crystals <0.1 mm in length. Organic components are rare and extremely fine grained inhibiting the accurate quantification of reflectance.

In Figure 35 the cubic pyrite is clearly visible, due to its high reflectance, while sub-micrometer bitumen is visible interstitially.

Sample 4

Sample 4 contains relatively coarse grained laminations with relatively large vitrinite particles. However; the Rmax and Rmin % are highly dependent on the orientation of the polished block and typically of a very low rank reaching only a low metaanthracite.

Summary

Samples 1 and 3 display solid bitumen that has been visible remobilized and deposited along coarser grain boundaries. Textures of the coarser grain units within Sample 1 may be indicative of some recrystallization. This is supported in Sample 3 by large cubic pyrite which is ubiquitous throughout the sample.

Samples 2 and 4 are relatively poorly sorted with grains and organic carbon of variable grain size. In some laminations, particularly in Sample 2, organic particles are orientated around grains. The highest rank carbon, approaching true graphite, is from Sample 2 from the Prince Albert Formation. Sample 4 is the most siliceous of samples, with a corresponding low carbon rank.

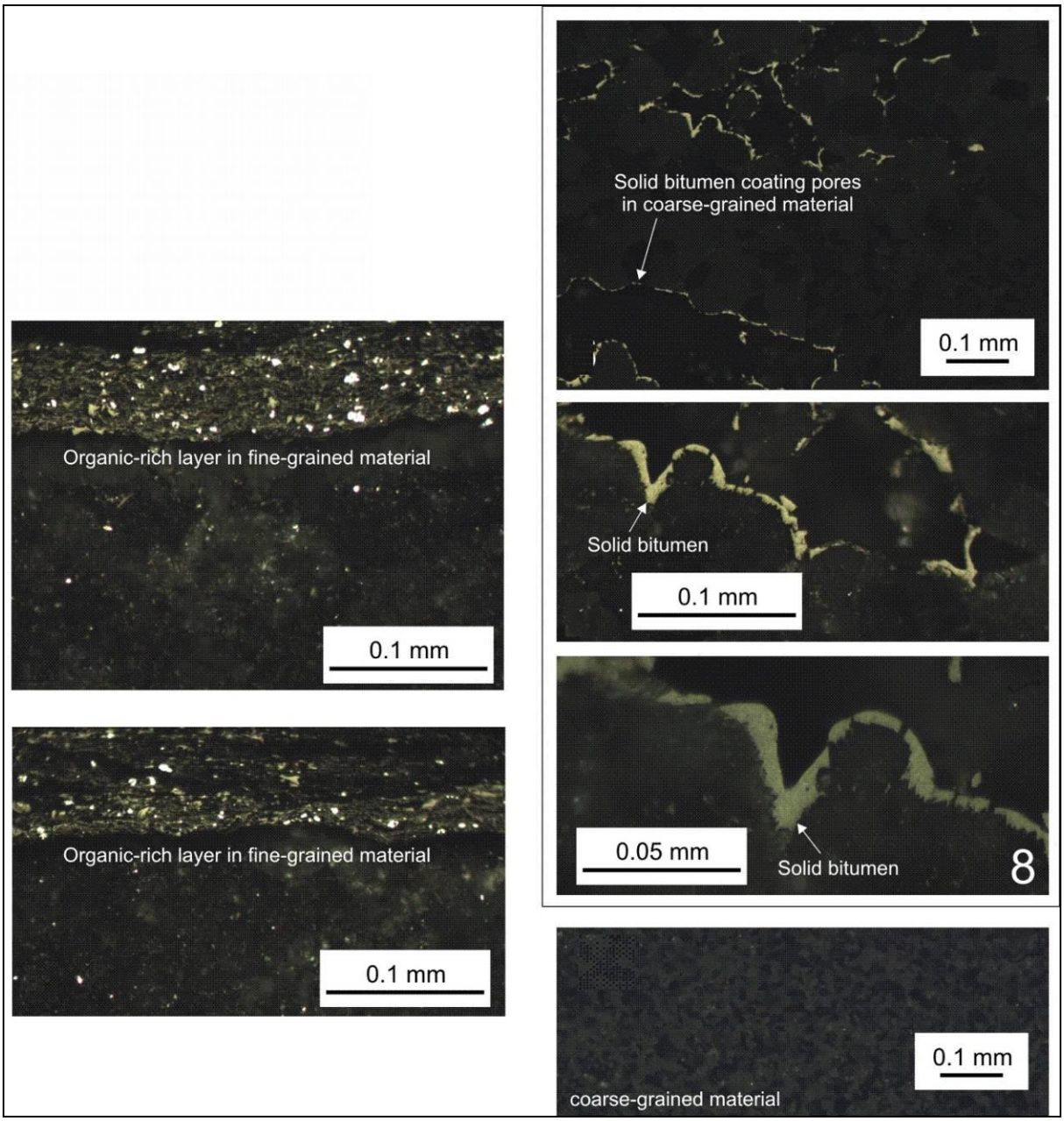

Figure 32: Microphotographs of Sample 1 (oil immersion, polarized light). Fine grained organic rich units are visible within left hand photos with coarse grained cycles within interstitial and grain boundary bitumen visible in right hand photos.

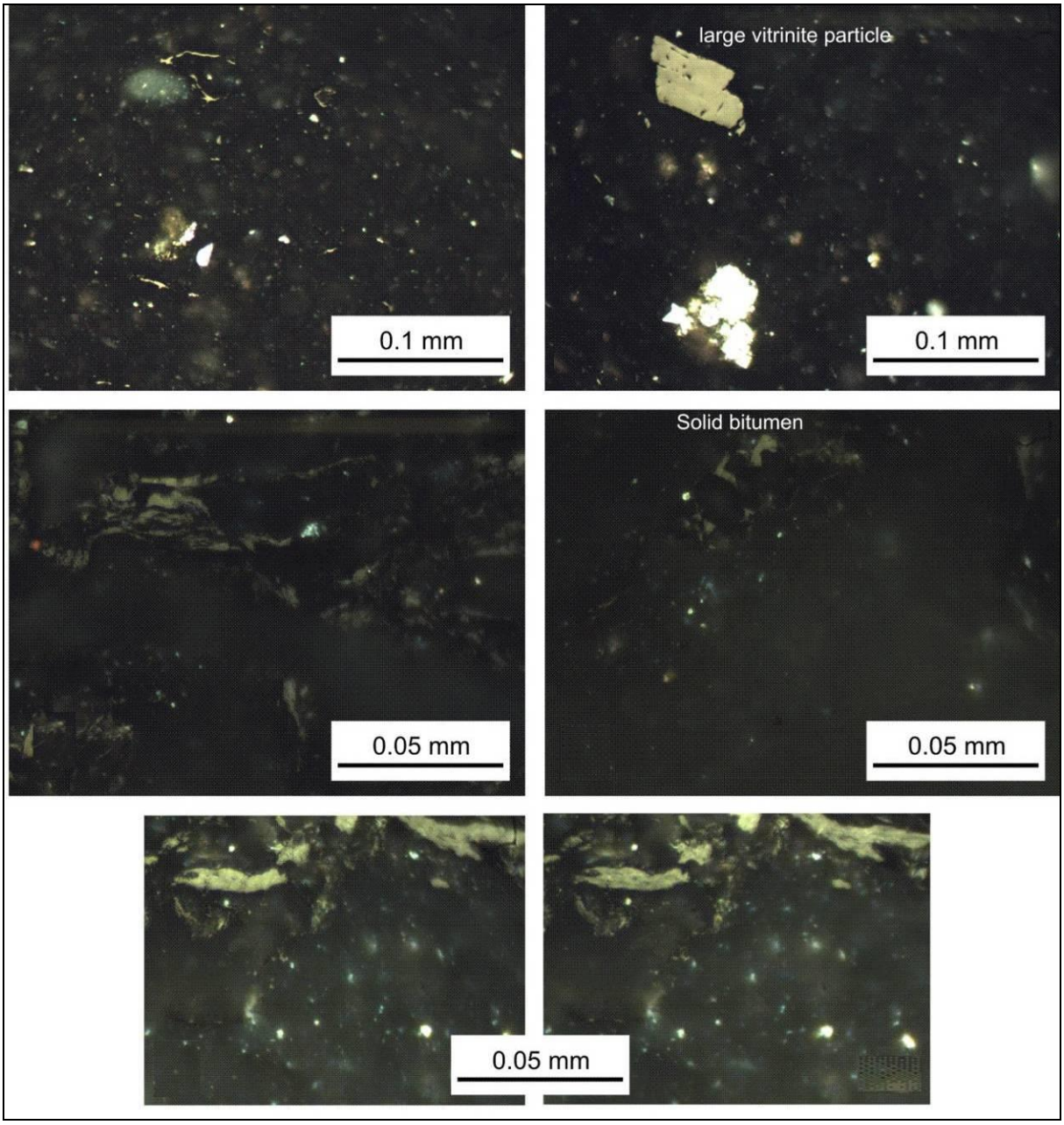

Figure 33. Microphotographs of Sample 2 (oil immersion, polarized light). Large vitrinite fragments are clearly visible in top right photo. Mosaic high rank carbon particles visible in top left image. Bottom two photos show "graphitic" particles with the polarizer in different positions. Note the distinct anisotropy of the organic matter, with high reflectivity of the horizontal vitrinite grains orientated along the same axis.

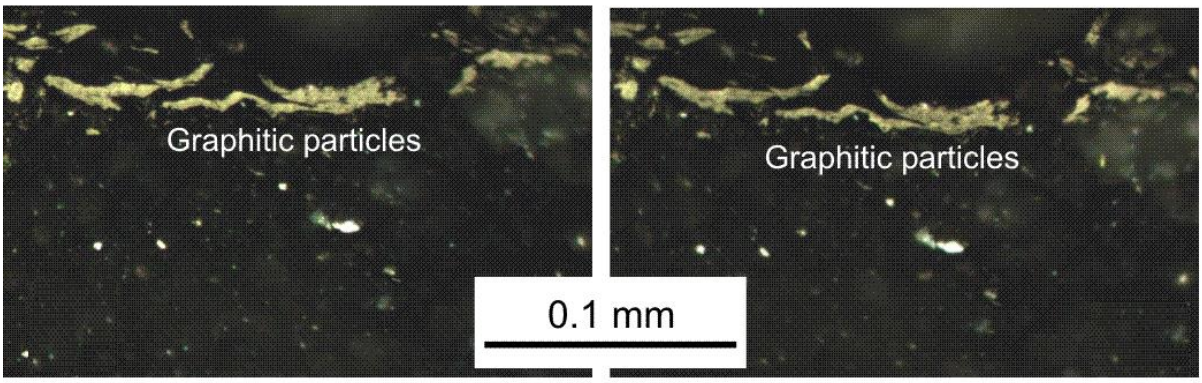

Figure 34. Microphotographs of Sample 2 (oil immersion, polarized light) showing accumulation of graphitic particles along grain boundaries.

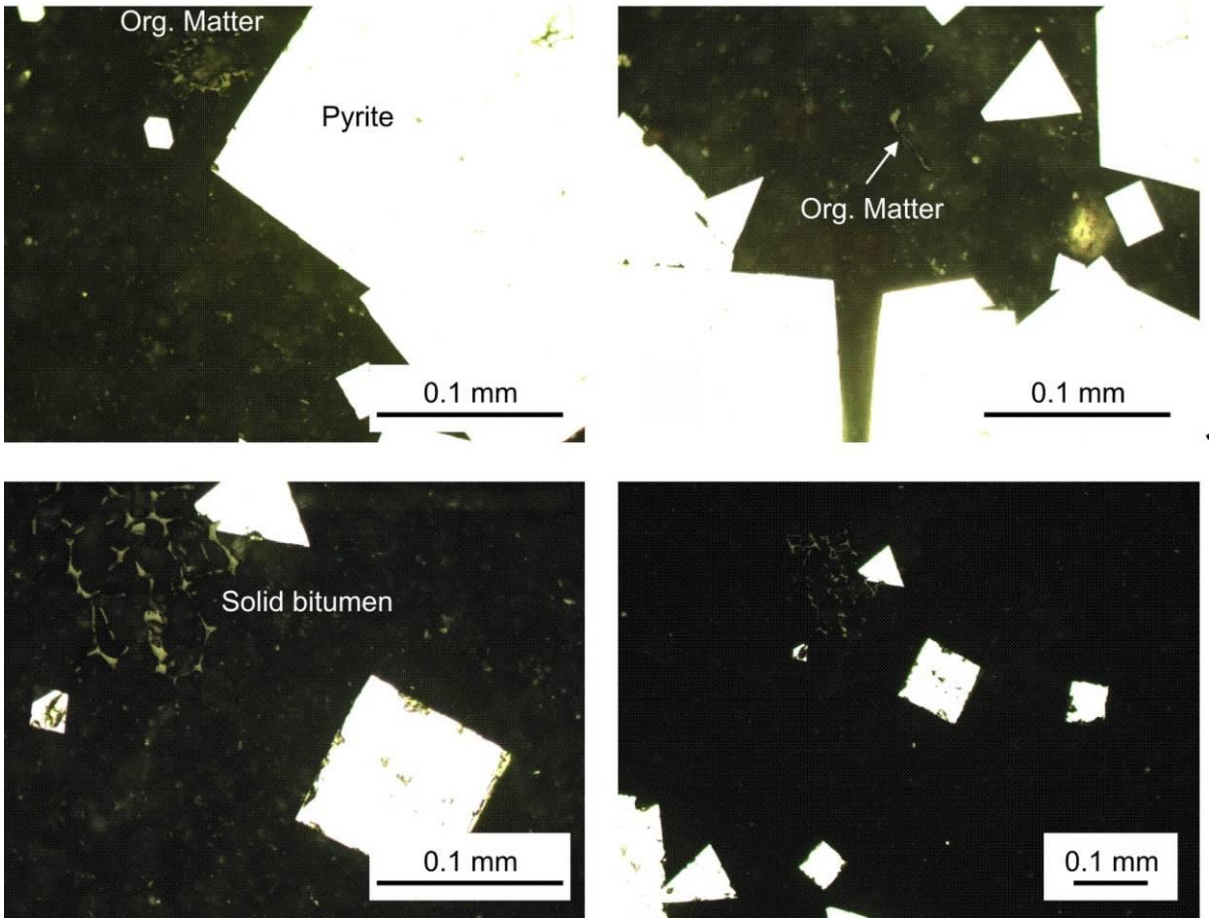

Figure 35: Microphotographs of sample 3 (oil immersion, polarized light). Photos were taken on blocks orientated perpendicular to the axis.

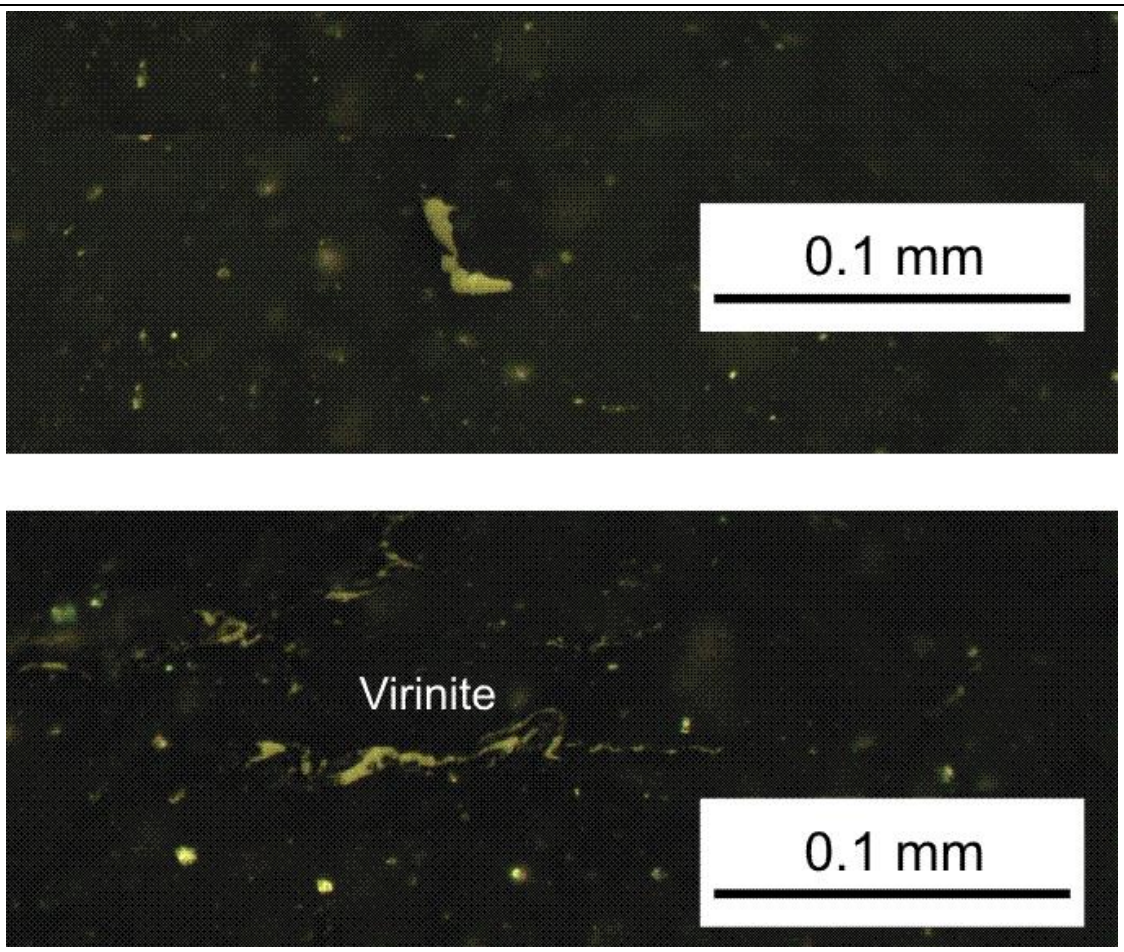

Figure 36: Microphotographs of Sample 4 showing very fine grained organic matter.

Appendix 2 Impedance Spectroscopy Graphs

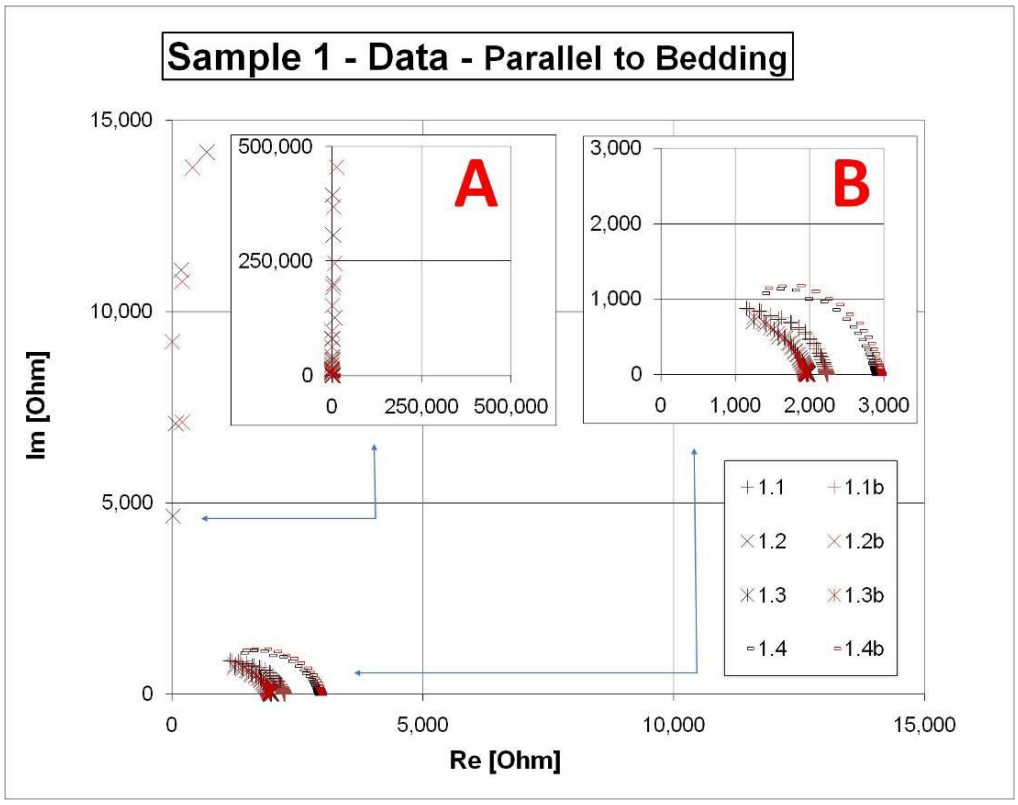

Figure 37: Measured Cole-Cole plot for Sample 1. Inset graph A displays the massive Z_{Im} component (Inset A) for reading 1_2 and 1_2b while Inset graph B 'zooms-in' to show the low resistivities recorded for readings 1_1, 1_3 and 1_4.

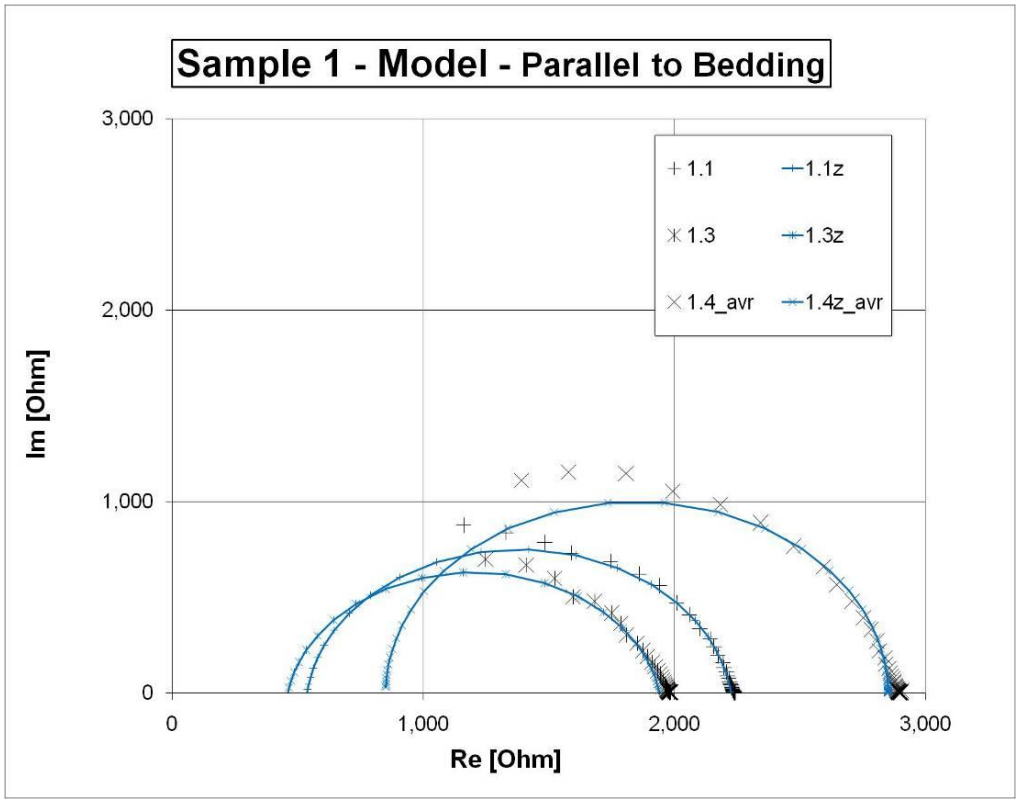

Figure 38: Theoretical/model curves (blue) fitted to measured data for readings 1_1, 1_3 and 1_4.

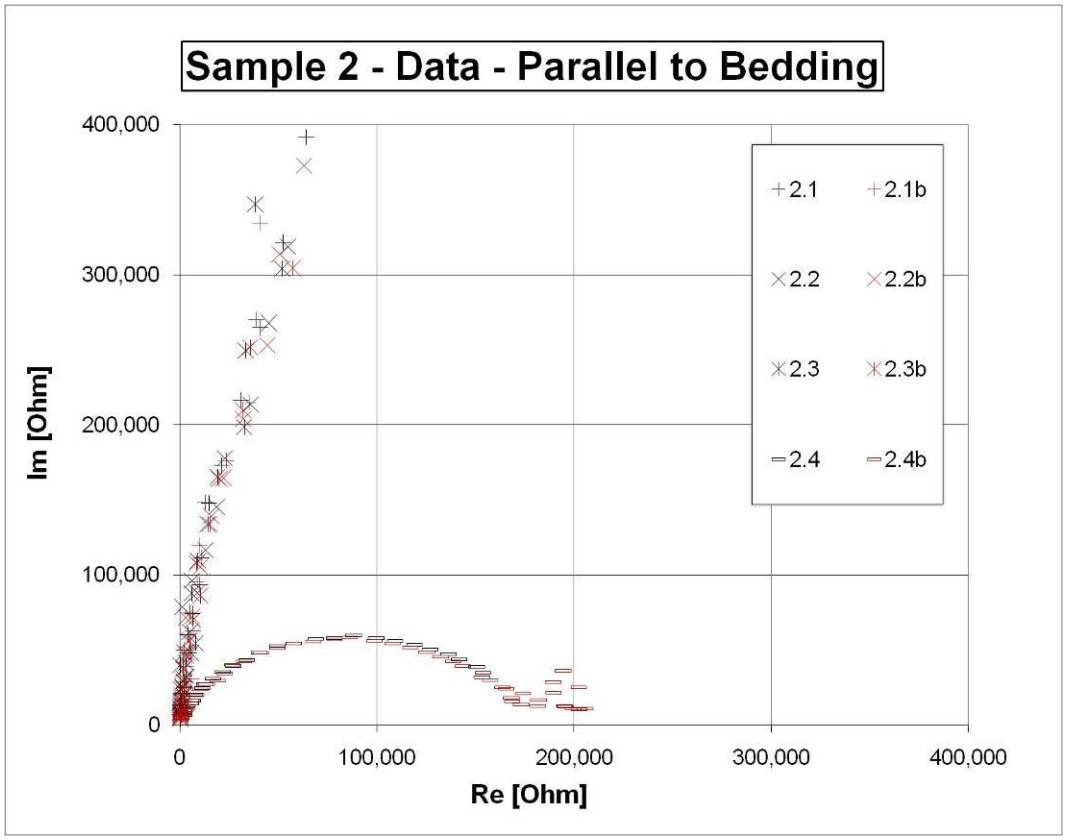

Figure 39: Measured curves showing heterogeneity within Sample 2.

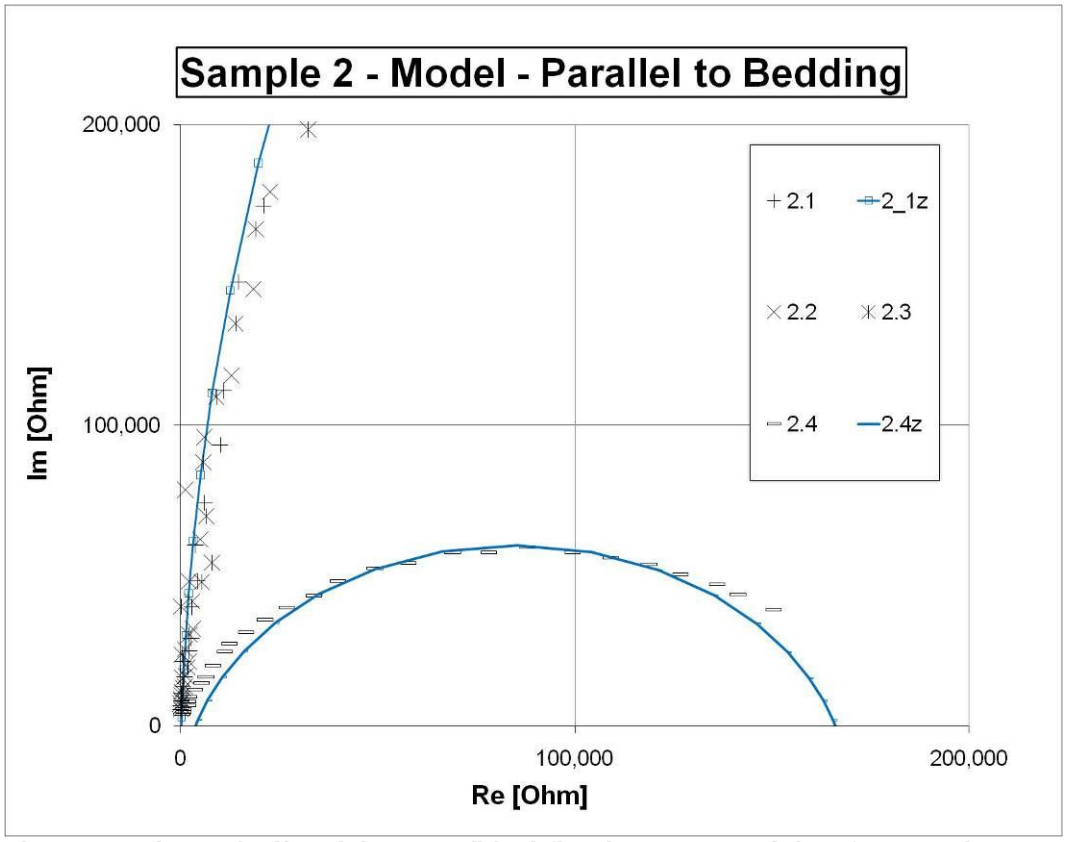

Figure 40: Theoretical/model curves (blue) fitted to measured data for Sample 2.

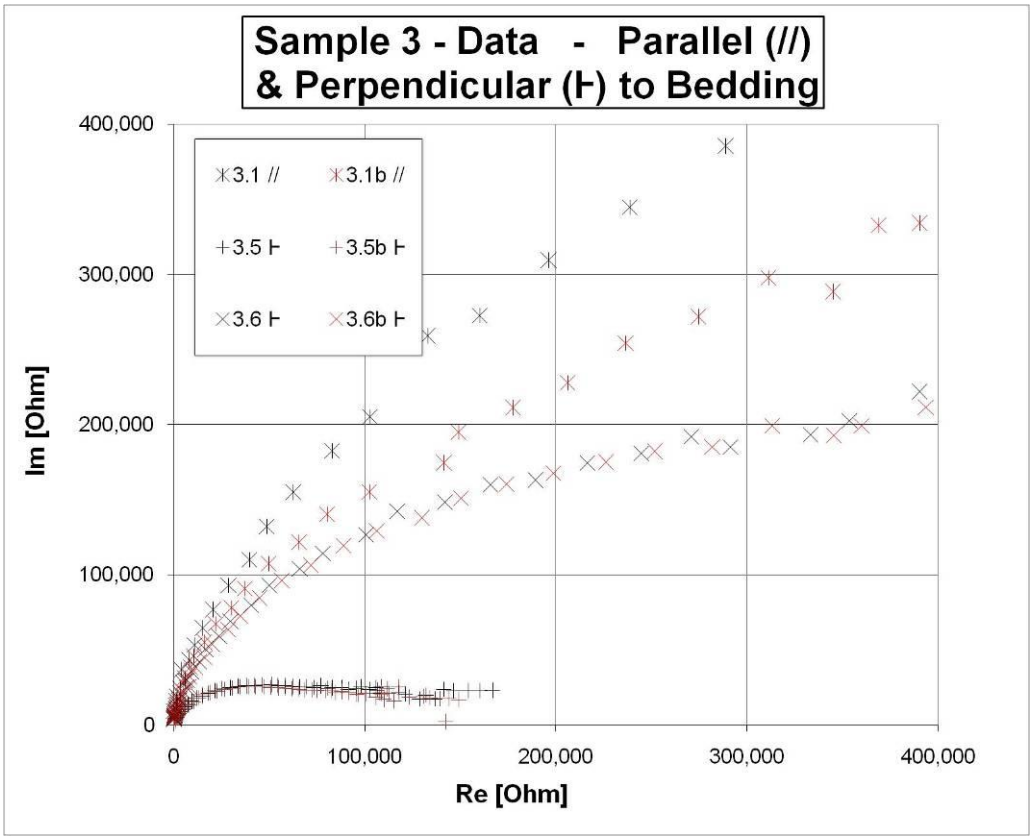

Figure 41: Measured curves for sites perpendicular to bedding for Sample 3. Readings 3_1 and 3_1b which were recorded parallel to bedding are included due to equivalent scale.

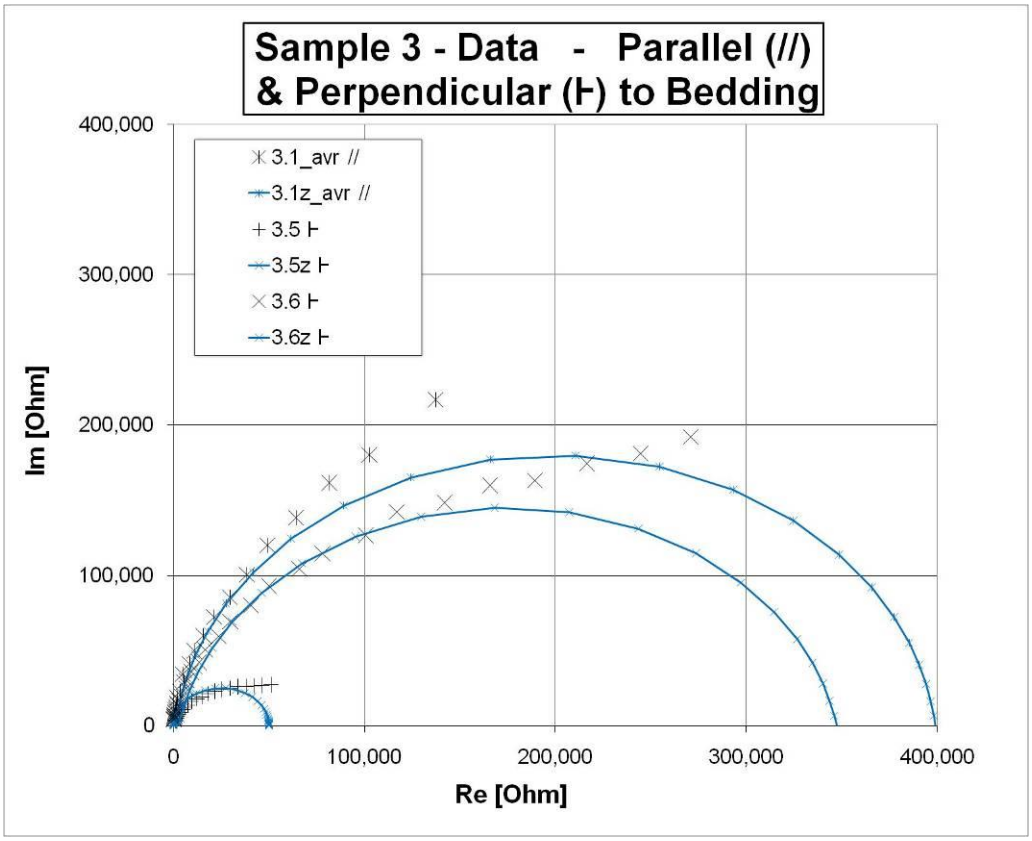

Figure 42: Theoretical/model curves (blue) fitted to measured data for Sample 3.

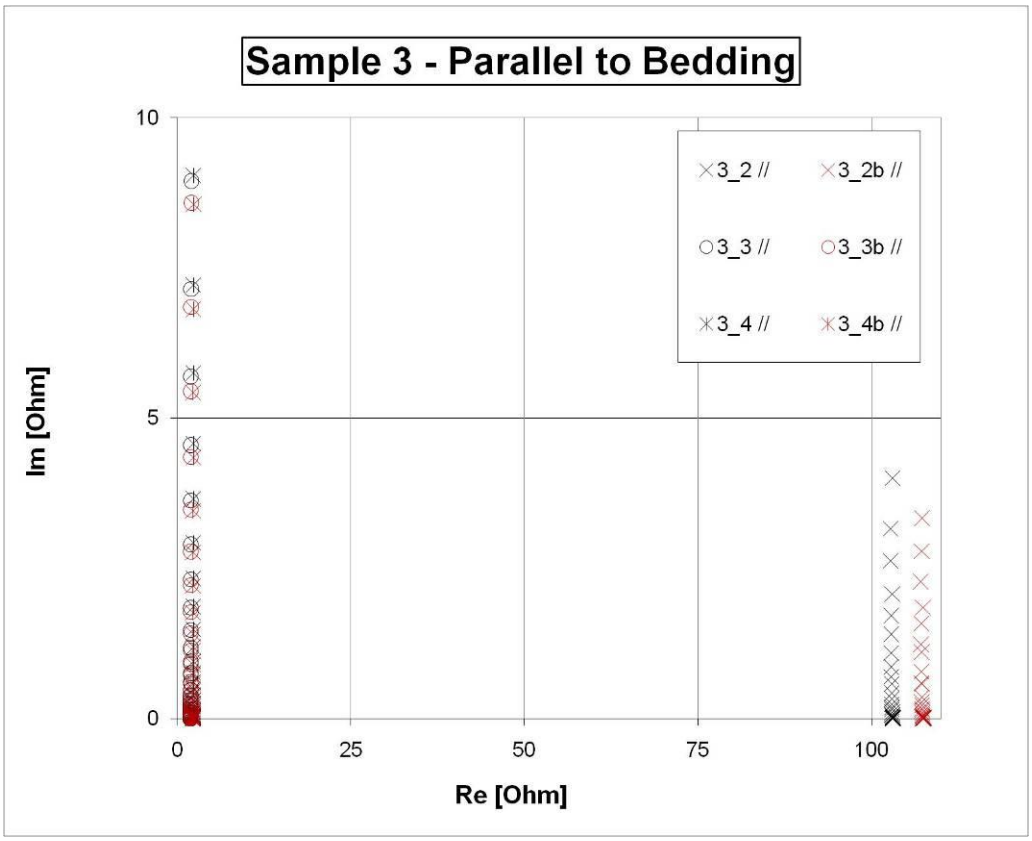

Figure 43: Measured curves for low resistivity sites on Sample 3, recorded parallel to bedding. Note dominance of quasi-metallic conduction and therfore lack of capacitive (dielectric) influence of Z_{Im} on the value of Z_{Re}.

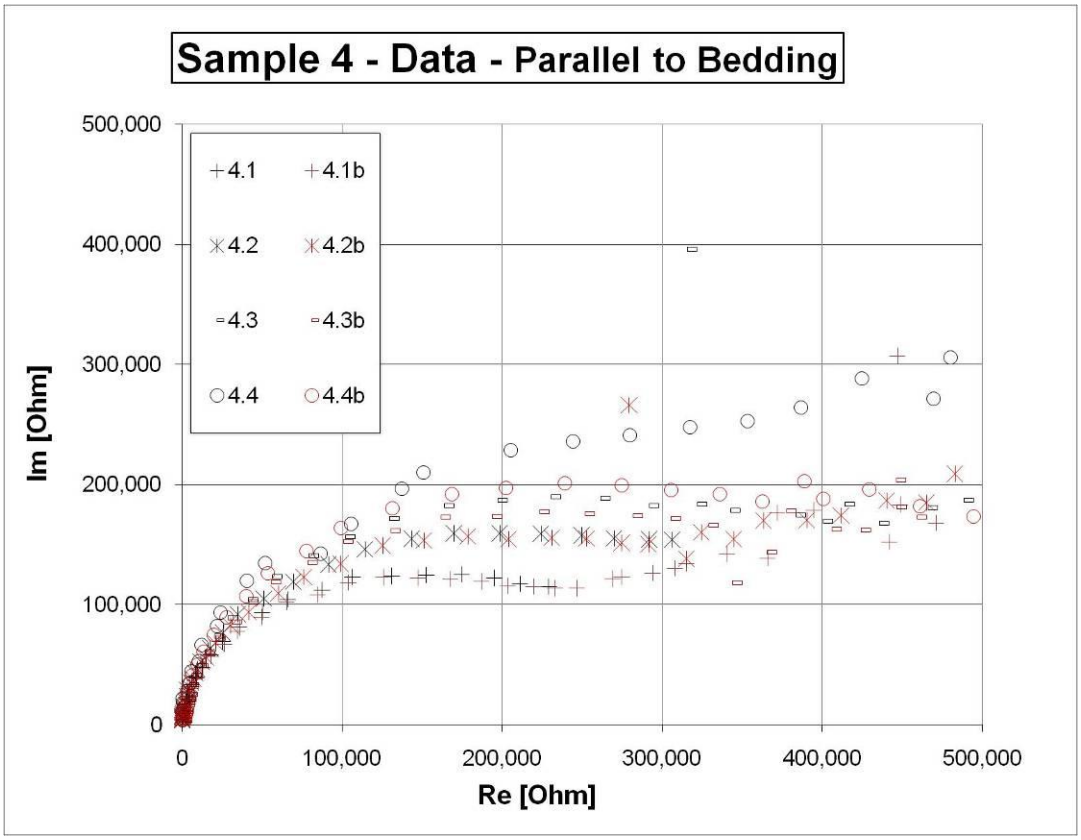

Figure 44: Measured curves for Sample 4 sites, parallel to bedding. Note relative homogeneity of the test curves.

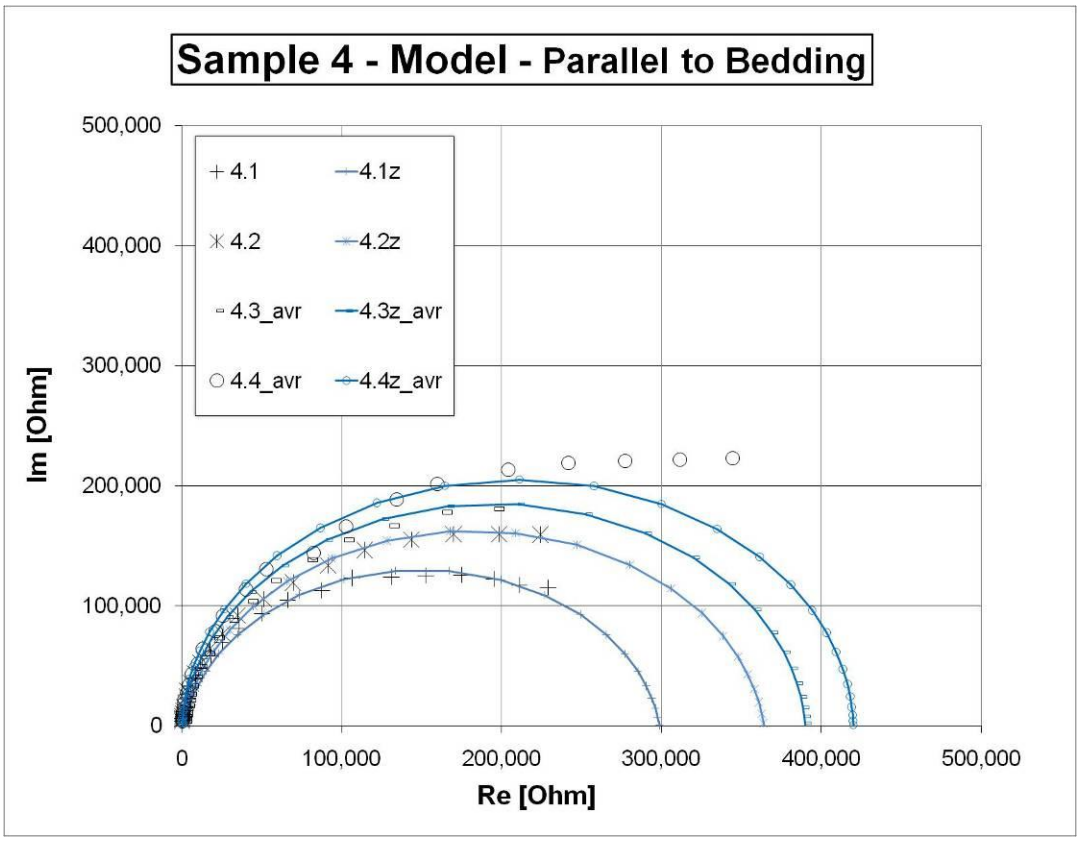

Figure 45: Theoretical/model curves (blue) fitted to the measured data for Sample 4, parallel to bedding.

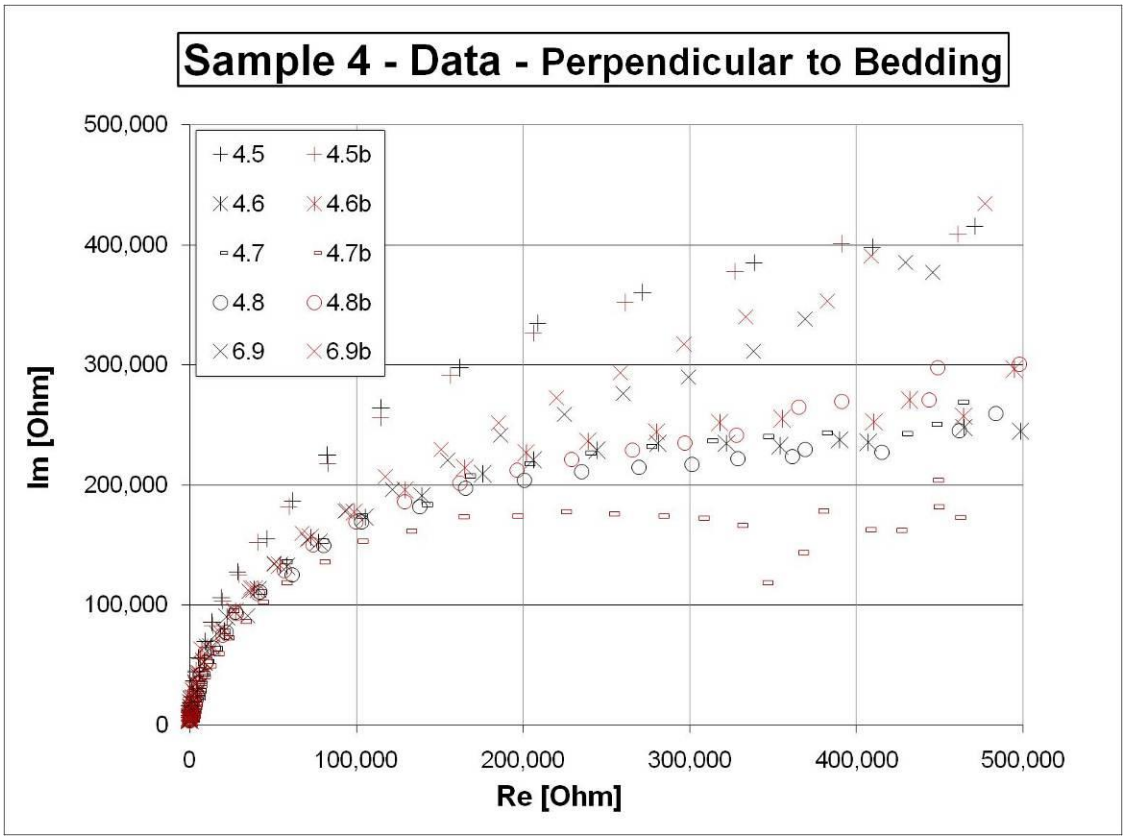

Figure 46: Measured curves for Sample 4 sites, perpendicular to bedding. Note relative homogeneity of the test curves.

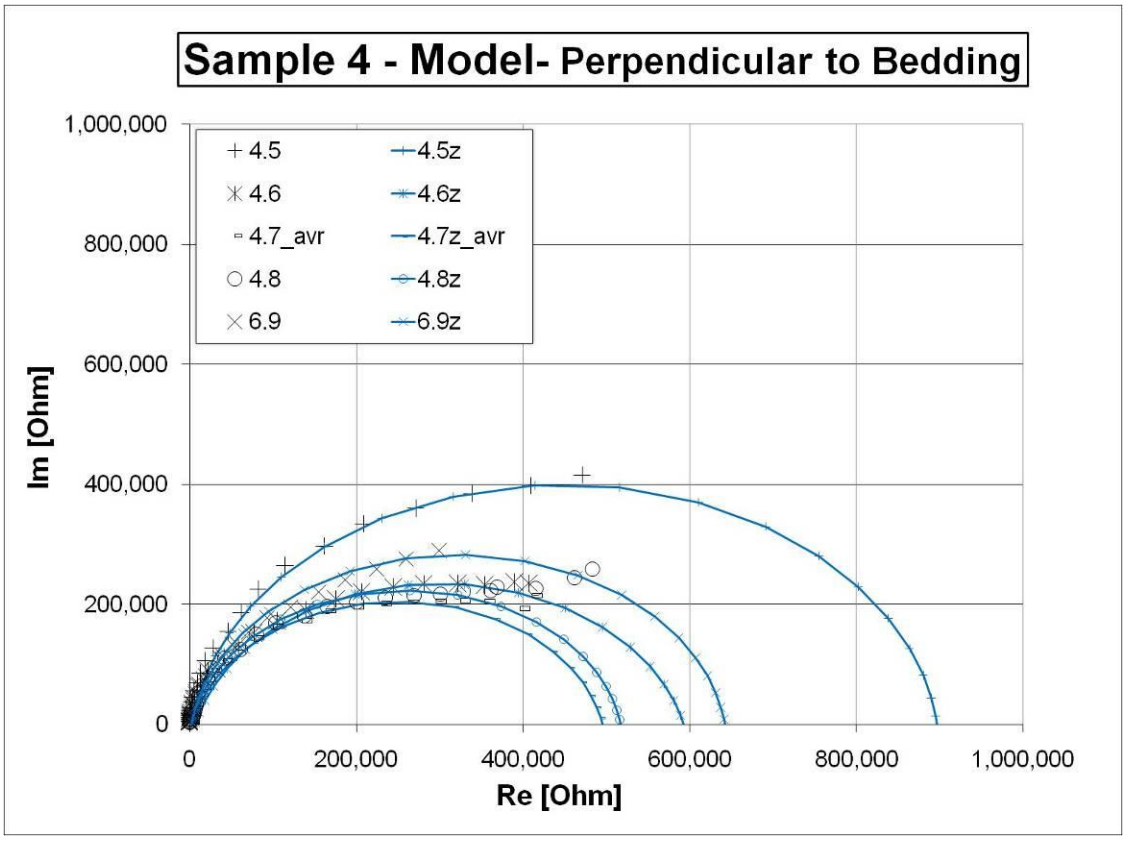

Figure 47: Theoretical/model curves (blue) fitted to the measured data for Sample 4, perpendicular to bedding.